PROCESSING MOFS INTO COMPLEX ARCHITECTURES

PROCESSING METAL-ORGANIC FRAMEWORK MATERIALS INTO COMPLEX ARCHITECTURES

By HE ZHU, B.Eng.

A Thesis Submitted to the School of Graduate Studies in Partial Fulfilment of the Requirements for the Degree Doctor of Philosophy

DOCTOR OF PHILOSOPHY (2016) McMaster University

(Chemical Engineering) Hamilton, Ontario

TITLE: Processing Metal-Organic Framework Materials into Complex Architectures

AUTHOR: He Zhu

B.Eng. (Zhejiang University, China)

SUPERVISOR: Dr. Shiping Zhu

NUMBER OF PAGES: xxvi, 161

LAY ABSTRACT

Porous materials are of great importance in modern life, from bottle cork to catalyst support, from sponge to oil-spill absorbate, these materials have been widely used in different areas. Since 1999, a new family of porous materials – metal-organic frameworks (MOFs) – has attracted great attentions from both academic researchers and industrial practitioners. Compared to conventional porous materials, they have unprecedented large surface areas, designable and tailorable pore structures, and possess excellent chemical and thermal stability. Furthermore, these materials can possess unconventional properties that traditional porous materials do not have, by tuning their structures, such as luminescence, electron conductivity, and structural flexibility. Despite all the benefits MOFs provide, they are difficult to be processed due to their crystalline particulate nature, while specially ordered shapes and morphologies are often required in many real-life applications. In this project, we developed several strategies to construct MOFs into different structures in order to overcome this challenge.

ABSTRACT

The metal-organic framework (MOF) research activities can be classified into MOF preparation, MOF processing, and MOF application. Processing MOFs into specially ordered shapes and morphologies is of great importance, since it bridges MOFs to real-life applications. Additionally, creating higher-order mesoscopic architectures with MOF particles as building blocks can introduce novel properties besides the inherent features of MOFs, thus opening a door to enhancing their performance in various applications. This thesis focused on the fabrication of MOFs into zero-dimensional and three-dimensional MOF architectures via various concepts inspired by polymerization and interfacial techniques.

- A raspberry-like MOF-polymer microsphere was prepared via dispersion polymerization. MOFs were found to be a good stabilizer and could be bound to polymer core with the help of polyvinylpyrrolidone. The prepared microsphere could be further developed into a polymer@MOF core-shell structure.
- A multilayered MOF colloidosome (MOFsome) was prepared through transient Pickering emulsion. The obtained MOFsome could be used as a stimulus-responsive carrier and as a general platform for construction of multicomponent colloidosomes.
- A porous MOF monolith was obtained using high internal phase emulsion template (HIPE). MOF particles were able to stabilize HIPE with internal phase up to 90 %

of the volume. The obtained monoliths were ultralight with density as low as 12 mg/cm^3.

- A flexible and porous nanocellulose aerogel with high MOF loadings was prepared through a straightforward sol-gel process, followed by freeze-drying. The hierarchical porous hybrid aerogel remained intact under compression and was demonstrated to be an ideal absorbents for water purification.
- A shapeable and versatile platform was demonstrated for *in situ* growth of MOF particles. The metal ion cross-linked alginate hydrogels were converted into MOF-alginate composites through a post-treatment of the hydrogels with MOF ligand solution. The macroscopic shape of the composite could be controlled and it was demonstrated to be an effective absorbent for water purification.

ACKNOWLEDGEMENTS

First of all, I would like to express my deepest gratitude to my supervisor, Dr. Shiping Zhu, for his constant help, endless patience, and inspiring guidance during my Ph.D. study. He does not tell me what to do, but teaches me how to do it, which is important not only in doing research, but also in living a life. He always tells me to jump out of the area and look at the big picture, which really inspires me and helps me become a better researcher. I treasure the advices and trainings from him, respect his dedication to work, and admire his positive attitude towards life. One thing he said that I will always remember is "keep going", encouraging me to continue moving on and do not stop. I simply could not wish for a better supervisor.

I also would like to thank my supervisory committee members, Dr. Igor Zhitomirsky and Dr. David Latulippe, for their valuable time in evaluating my research work and giving inspiring advices on my projects.

I would like to express my gratitude to Dr. Qi Zhang for his time in research guidance. His captiousness in research makes me grown up quickly, and makes me realize one important necessity to success, which is to be critical and strict to yourself. I would also like to extend my thanks to Dr. Emily D. Cranston for her time and patience in providing research guidance and constructive advices during the collaboration, and Dr. Heyang Liu for the useful discussion and advices.

I would like to thank Dr. Robert Pelton and Dr. Michael Thompson for providing generous access to their equipment, and Dr. Glynis de Silveira, Mr. Chris Butcher, Ms. Carmen Andrei, Ms. Victoria Jarvis, Dr. James F. Britten, Dr. Douglas Culley, Dr. Matiar Howlader, Dr. Leo Hsu for their assistance and training in different characterizations. My thanks also go to the entire Department of Chemical Engineering staffs, Ms. Kristina Trollip, Ms. Michelle Whalen, Ms. Linda Ellis, Ms. Kathy Goodram, Ms. Lynn Falkiner, Ms. Cathie Roberts, and Ms. Melissa Vasil for their administrative assistance, and Mr. Paul Gatt, Mrs. Justyna Derkach, Mr. Dan Wright, and Mr. Doug Keller for their technical assistance.

It was a great experience to work in PolyMac Zhu research group. I really enjoyed the time spent here with all the current and former members, who made the life lively and interesting. While I cannot list all their names individually here, they all have given me supports that I needed to complete this study. I would especially like to thank Erlita Mastan and Xuan Yang, who have always been supportive to me in research and daily life. I would also like to thank all my friends who shared my pain and happiness, without which I cannot survive from the Ph.D. study.

Last but definitely not least, I would like to express my deepest appreciation to my parents for their endless love and supports. I am really sorry for not being around for so many years, especially during the time bad things happened. Thank you for giving me enough freedom, understandings, and putting absolute faith in me. You have always been the most reliable backing and peaceful harbor for me. You are the reason I am where I am today. Thank you for being the best family one could ever asked for!

TABLE OF CONTENTS

LIST OF FIGURES

Figures in Supporting Information

LIST OF TABLES

Tables in Supporting Information

LIST OF ABBREVIATIONS AND SYMBOLS

Abbreviations

0D	zero-dimensional
1D	one-dimensional
2D	two-dimensional
3D	three-dimensional
AAO	anodized aluminum oxide
ADH	adipic acid dihydrazide
AIBN	2,2’-azobis(2-methylpropionitrile)
BDC	1, 4-benzenedicarboxylic acid
bim	benzimidazole
BTC	1, 3, 5-benzenetricarboxylic acid
CLSM	confocal laser scanning microscopy
CMC	carboxymethyl cellulose
CNC	cellulose nanocrystal
CNF	cellulose nanofibril
CNT	carbon nanotube
CTAB	cetyltrimethylammonium bromide
DLS	dynamic light scattering
DMF	dimethylformamide
DMSO	dimethyl sulfoxide

EDC	N’-ethyl-N-(3-dimethylaminopropyl)-carbodiimide
EDX	energy-dispersive X-ray spectroscopy
FCNF	functionalized cellulose nanofibril
FITC	fluorescein isothiocyanate
GO	graphene oxide
G block	α-L-guluronic acid residues
HIPE	high internal phase emulsion
HKUST	Hong Kong University of Science and Technology
HRTEM	high-resolution transmission electron microscopy
ICP-OES	inductively coupled plasma optical emission spectrometry
LB	Langmuir-Blodgett
LDH	layered double hydroxide
M block	1,4-linked β-D-mannuronic
MIL	Material Institute de Lavoisier
MMM	mixed-matrix membrane
MOF	metal-organic framework
MOFsome	metal-organic framework colloidosome
MOG	metal organic framework gel
MSN	molecular sieve nanosheet
NHS	N-hydroxysuccinimide
NP	nanoparticle
o/w	oil-in-water

PCNF	pristine cellulose nanofibril
PS	polystyrene
PVA	polyvinyl alcohol
PVP	polyvinylpyrrolidone
PXRD	powder X-ray diffraction
RB	Rhodiamine B
rGO	reduced graphene oxide
SDS	sodium dodecyl sulfate
SEM	scanning electron microscopy
SiNW	silicon nanowire
STEM	scanning transmission electron microscopy
TCPP	5,10,15,20-tetrakis(4-carboxyphenyl)porphyrin
TEM	transmission electron microscopy
TeNW	tellurium nanowire
TGA	thermogravimetric analysis
TMA	trimesic acid
UiO	University of Oslo
V50	2,2'-azobis(2-methylpropionamidine) dihydrochloride
ZIF	zeolitic imidazolate framework

Symbols

C	concentration
k_2	rate constant of pseudo-second-order kinetic model
m	mass
q	adsorptive capacity
t	time
T	temperature
V	volume
γ	surface tension
ΔA	change of surface area
ΔG^{form}	change of free energy
ΔS^{conf}	configurational entropy

DECLARATION OF ACADEMIC ACHIEVEMENT

This dissertation is used to fulfill the requirements of Ph.D. degree and is organized in a "sandwich" style consisting of five journal articles. The contributions from the authors of these articles are summarized below:

- He Zhu is the primary author of all five journal articles reproduced in this thesis.
- Dr. Shiping Zhu is the supervisor for all five articles.
- Dr. Emily D. Cranston and Xuan Yang are the co-authors for one article reproduced in Chapter 6.
- Dr. Qi Zhang is the co-author for four articles (Chapter 3, 4, 5, 7).

1 INTRODUCTION

In this chapter, the research background, the general research objectives, and the organization of this thesis are presented.

1.1 Research background

Porous materials have always been a research focus of both scientific studies and practical industrial applications due to their large surface area and high pore volume, which enable the materials to interact with molecules not only at their surface, but also in the bulk.[1] Since 1999, a new class of porous hybrid inorganic-organic frameworks, i.e. metal-organic frameworks (MOFs), has drawn great attention and become one of the most intensively studied research topics.[2-4] They are prepared from the self-assembly of metal ions or ion clusters with organic bridging ligands, leading to porous crystalline materials having highly ordered periodic porous structures with superior surface areas up to 7,000 $m^2 g^{-1}$.[5,6] In addition, MOFs have high thermal stability, tunable pore property, and various chemical reactive sites, which have great application potentials in many different areas, including gas storage,[7,8] gas separation,[9,10] chemical sensor,[11,12] catalysis,[13,14] proton conductor,[15,16] battery,[17,18] and drug delivery.[19,20]

Due to the various choices of metal center and the designability of bridging ligand, numerous types of MOFs have been designed, synthesized, and modified, since the two pioneering reports of MOF-5[2] and HKUST-1.[21] The commonly used methods for MOF synthesis include solvothermal/hydrothermal method, microwave/ultrasound assisted

method, electrochemical method, mechanochemical method, and so on. Researchers have also been working on scaling up MOFs to gram scale or even larger amount. To the best of my knowledge, there has been no successful commercialization of MOF materials to date. BASF and its collaborators are working on industrialization of these promising materials.

Although MOF particles are important and encouraging to study on, their particulate form limits their potential, since specially ordered shapes and morphologies are often required in many applications. Fabrication of MOF membranes has become one of the most critical areas in MOF research. Preparation of free-standing MOF membranes is dominated by interfacial or biphasic method,[22] where the metal ions and organic ligands are separately dissolved in two immiscible solvents and MOF membranes are formed at the interface upon placing one solution onto the other. On the other hand, significant efforts have been made to deposit MOFs onto chemically stable and cost effective shapeable substrates, such as synthetic polymers[23,24] and ceramics.[25,26] In addition, integrating MOF particles into polymer substrates through blending, i.e. mixed-matrix membranes (MMMs), has also been demonstrated as an alternative to prepare robust and flexible MOF-polymer composites.[27-30]

Recently, there has been a growing interest in fabricating MOF materials into complex architectures. Creating higher-order mesoscopic architectures with MOF crystals as building blocks can introduce novel properties, in addition to the inherent features of MOFs. This represents another approach in enhancing MOF performance in various applications. In this thesis, these complex architectures are classified into four categories: (1) zero-

dimensional (0D) architectures such as microspheres and hollow capsules, (2) one-dimensional (1D) architectures such as chains and fibers, (3) two-dimensional (2D) architectures such as nanosheets and patterns, and (4) three-dimensional (3D) architectures consisting of continuous and extended systems.[31] In general, the development of MOF complex architectures is still at its infancy, the main issue lies in the fact that spatial manipulation of the crystallization process or single crystals is considerably challenging. Therefore, it is of great importance to explore new methodologies to construct MOF-based complex architectures.

1.2 Research objectives

MOF is an enormous research area, which can be divided into three categories: (1) MOF design, preparation, and modification, (2) MOF processing, and (3) MOF application. This study focuses on the development of various processing methods to construct MOF 0D and 3D architectures. The overall objectives are: (1) to develop MOF complex architectures from interfacial techniques and (2) to develop MOF complex architectures assisted by polymers.

1.3 Thesis organization

This thesis is organized as a "sandwich thesis", which consists of several published articles in peer-reviewed journals, "sandwiched" between the chapters of Introduction and Literature Review (Chapter 1 & 2) and the chapter of Conclusion (Chapter 8). Chapter 3-7 can be grouped into two parts, with the first part centering on the fabrication of 0D MOF architectures and the second dealing with the fabrication of 3D MOF architectures.

Part 1 – Fabrication of zero-dimensional MOF architectures

In the first part of the thesis, two different approaches are developed to prepare 0D MOF architectures. The researchers borrowed the concepts from polymerization and interfacial processing and applied the techniques to the fabrication of 0D MOF architectures.

Chapter 3 reports a novel raspberry-like ZIF-8/PS composite spheres via dispersion polymerization of styrene with ZIF-8 and PVP as co-stabilizers. The ability of interfacial assembly of ZIF-8 nanoparticles made it possible to stabilize insoluble polymer particles formed in dispersion polymerization, thus achieving the hybrid organic-inorganic raspberry-like composite spheres. It was found that ZIF-8 itself was able to stabilize the polymerization, while PVP was crucial to bridge ZIF-8 and PS together. Moreover, the ZIF-8 nanoparticles decorated on the surface of PS could serve as seeds and further grow into a continuous MOF shell through subsequent solvothermal treatment. This paper was published in *Dalton Transactions* (DOI: 10.1039/C5DT02627J).

Chapter 4 demonstrates the fabrication of MOF colloidosomes (MOFsomes) via transient Pickering emulsion. Colloidosomes represent an interesting hollow spherical structure consisting of close-packed colloidal particles as shell. The assembly of MOF particles in MOFsomes introduces the periodical pores besides the regular interstices, as well as the intrinsic functionalities that single MOF particle possesses. In this work, we introduced a transient Pickering emulsion template, where the emulsion was stable at the beginning and became homogeneous eventually due to the partial solubility between oil

and water, to fabricate this hollow structure. This paper has been accepted for publication in *Advanced Materials Interfaces* (DOI: 10.1002/admi.201600294).

Part 2 – Fabrication of three-dimensional MOF architectures

In the second part of the thesis, 3D MOF architectures are realized either by applying the polymerization and interfacial processing techniques or by taking advantages of polymer properties.

Chapter 5 presents a 3D hierarchical porous MOF monolith prepared through an oil-in-water Pickering high internal phase emulsion (HIPE) template. UiO-66 was found to be able to stabilize Pickering HIPEs with an internal phase up to 90% of the volume. Upon adding polyvinyl alcohol (PVA) or polymerizing the continuous phase, two types of MOF-based 3D hierarchical porous monoliths were prepared with density as low as 12 mg cm^{-3}. This paper was published in *Chemistry - A European Journal* (DOI: 10.1002/chem.201600313).

Chapter 6 reports a MOF-cellulose nanocrystal (CNC) hybrid aerogel with micro, meso and macro pores, which was prepared through a straightforward water-based sol-gel process, followed by freeze-drying. Three different types of MOFs were successfully incorporated into the aerogel with up to 50 wt.% loading of uniformly distributed MOFs. The obtained hybrid aerogels were flexible, robust, and highly porous, which were investigated as convenient absorbents for removal of hazardous contaminants from water. This paper was published in *Advanced Materials* (DOI: 10.1002/adma.201601351).

Chapter 7 presents a general platform for *in-situ* fabrication of MOF materials into alginate substrate, whose macroscopic shape can be designed and controlled. The composite materials were prepared through the post-treatment of metal ion cross-linked alginate hydrogel with MOF ligand solution. MOF-alginate beads, fibers, and membranes were obtained by manipulating the shape of corresponding metal ion cross-linked hydrogels. This paper was published in *ACS Applied Materials & Interfaces* 2016 (DOI: 10.1021/acsami.6b04505).

1.4 Other works

I am the first author for all the above five publications. While the research ideas were generated through discussion with the supervisor and the team members, I was the major contributor, carrying out the actual experiments, providing breakthroughs, and writing the first drafts of these manuscripts. Other research contributions completed during my doctoral study, but not included in this thesis, are listed below.

The two first-authored papers report the development of two methods for preparation of two-dimensional (2D) MOF structures such as membrane and film. I am also the major contributor to these two publications, in terms of carrying out the experiment and analysing the data, as well as writing the first drafts for the manuscripts.

- **Zhu, H.**; Zhu, S., A versatile and facile surface modification route based on polydopamine for the growth of MOF films on different substrates. *The Canadian Journal of Chemical Engineering* **2015**, 93, (1), 63-67.

- **Zhu, H.**; Liu, H.; Zhitomirsky, I.; Zhu, S., Preparation of metal–organic framework films by electrophoretic deposition method. *Materials Letters* **2015**, 142, 19-22.

In the following two papers, I am the second author. I played a supporting role in the MOF preparation and data analysis.

- Liu, H.; **Zhu, H.**; Zhu, S., Reversibly dispersible/collectable metal-organic frameworks prepared by grafting thermally responsive and switchable polymers. *Macromolecular Materials and Engineering* **2015,** 300, (2), 191-197.
- Lu, Y.; **Zhu, H.**; Wang W.; Li B.; Zhu, S., Rapid collection and re-dispersion of MOF particles by a simple and versatile method using thermo-responsive polymer. *RSC Advances* **2016**, 6, 63398-63402.

1.5 References

[1] M. E. Davis, *Nature* **2002**, *417*, 813-821.

[2] H. Li, M. Eddaoudi, M. O'Keeffe, O. M. Yaghi, *Nature* **1999**, *402*, 276-279.

[3] M. Eddaoudi, J. Kim, N. Rosi, D. Vodak, J. Wachter, M. O'Keeffe, O. M. Yaghi, *Science* **2002**, *295*, 469-472.

[4] O. M. Yaghi, M. O'Keeffe, N. W. Ockwig, H. K. Chae, M. Eddaoudi, J. Kim, *Nature* **2003**, *423*, 705-714.

[5] O. K. Farha, I. Eryazici, N. C. Jeong, B. G. Hauser, C. E. Wilmer, A. A. Sarjeant, R. Q. Snurr, S. T. Nguyen, A. O. z. r. Yazaydın, J. T. Hupp, *Journal of the American Chemical Society* **2012**, *134*, 15016-15021.

[6] I. Senkovska, S. Kaskel, *Chemical Communications* **2014**, *50*, 7089-7098.

[7] A. R. Millward, O. M. Yaghi, *Journal of the American Chemical Society* **2005**, *127*, 17998-17999.

[8] D. Gygi, E. D. Bloch, J. A. Mason, M. R. Hudson, M. I. Gonzalez, R. L. Siegelman, T. A. Darwish, W. L. Queen, C. M. Brown, J. R. Long, *Chemistry of Materials* **2016**, *28*, 1128-1138.

[9] Y. Peng, Y. Li, Y. Ban, H. Jin, W. Jiao, X. Liu, W. Yang, *Science* **2014**, *346*, 1356-1359.

[10] Y. Hu, J. Wei, Y. Liang, H. Zhang, X. Zhang, W. Shen, H. Wang, *Angewandte Chemie International Edition* **2016**, *55*, 2048-2052.

[11] M. Tu, S. Wannapaiboon, K. Khaletskaya, R. A. Fischer, *Advanced Functional Materials* **2015**, *25*, 4470-4479.

[12] V. Stavila, C. Schneider, C. Mowry, T. R. Zeitler, J. A. Greathouse, A. L. Robinson, J. M. Denning, J. Volponi, K. Leong, W. Quan, M. Tu, R. A. Fischer, M. D. Allendorf, *Advanced Functional Materials* **2016**, *26*, 1699-1707.

[13] J. E. Mondloch, M. J. Katz, W. C. Isley III, P. Ghosh, P. Liao, W. Bury, G. W. Wagner, M. G. Hall, J. B. DeCoste, G. W. Peterson, *Nature materials* **2015**, *14*, 512-516.

[14] E. D. Metzger, C. K. Brozek, R. J. Comito, M. Dincă, *ACS central science* **2016**, *2*, 148-153.

[15] G. K. Shimizu, J. M. Taylor, S. Kim, *Science* **2013**, *341*, 354-355.

[16] P. Ramaswamy, N. E. Wong, B. S. Gelfand, G. K. Shimizu, *Journal of the American Chemical Society* **2015**, *137*, 7640-7643.

[17] Z. Wang, B. Wang, Y. Yang, Y. Cui, Z. Wang, B. Chen, G. Qian, *ACS applied materials & interfaces* **2015**, *7*, 20999-21004.

[18] G. Huang, F. Zhang, X. Du, Y. Qin, D. Yin, L. Wang, *ACS nano* **2015**, *9*, 1592-1599.

[19] P. Horcajada, T. Chalati, C. Serre, B. Gillet, C. Sebrie, T. Baati, J. F. Eubank, D. Heurtaux, P. Clayette, C. Kreuz, *Nature materials* **2010**, *9*, 172-178.

[20] S. Li, K. Wang, Y. Shi, Y. Cui, B. Chen, B. He, W. Dai, H. Zhang, X. Wang, C. Zhong, *Advanced Functional Materials* **2016**, *26*, 2715-2727.

[21] S. S.-Y. Chui, S. M.-F. Lo, J. P. Charmant, A. G. Orpen, I. D. Williams, *Science* **1999**, *283*, 1148-1150.

[22] R. Ameloot, F. Vermoortele, W. Vanhove, M. B. Roeffaers, B. F. Sels, D. E. De Vos, *Nature chemistry* **2011**, *3*, 382-387.

[23] H. Zhu, S. Zhu, *The Canadian Journal of Chemical Engineering* **2015**, *93*, 63-67.

[24] M. Zhou, J. Li, M. Zhang, H. Wang, Y. Lan, Y.-n. Wu, F. Li, G. Li, *Chemical Communications* **2015**, *51*, 2706-2709.

[25]H. Bux, C. Chmelik, J. M. van Baten, R. Krishna, J. Caro, *Advanced materials* **2010**, *22*, 4741-4743.

[26] D. Liu, X. Ma, H. Xi, Y. Lin, *Journal of Membrane Science* **2014**, *451*, 85-93.

[27] T. Yang, Y. Xiao, T.-S. Chung, *Energy & Environmental Science* **2011**, *4*, 4171-4180.

[28] T. Rodenas, I. Luz, G. Prieto, B. Seoane, H. Miro, A. Corma, F. Kapteijn, F. X. L. i Xamena, J. Gascon, *Nature materials* **2015**, *14*, 48-55.

[29] M. S. Denny, S. M. Cohen, *Angewandte Chemie International Edition* **2015**, *54*, 9029-9032.

[30] N. C. Su, D. T. Sun, C. M. Beavers, D. K. Britt, W. L. Queen, J. J. Urban, *Energy & Environmental Science* **2016**, *9*, 922-931.

[31] Here we consider microspheres and microcapules as 0D architectures for the consistency with most MOF related articles. But it should be noted that those architectures are also reported as 3D in many literatures.

2 LITERATURE REVIEW

In this chapter, a thorough literature review of the recently developed methods to fabricate MOF complex architectures is given. The literatures are summarized according to the dimension of MOF architectures, namely 0D, 1D, 2D, and 3D architectures. Each subcategory is organized based on the processing approach, either bottom-up or top-down method.

2.1 Zero-dimensional architectures

The 0D structures refer to microspheres and hollow capsules, which are different from 3D structures that possess extended architectures.

2.1.1 Bottom-up methods

Spherical templates are usually involved in order to construct 0D structures. Large ceramic beads having sizes in millimeter or micrometer scale, such as alumina[1] and silica[2,3] beads, have been used to prepare ceramic-core MOF-shell composite spheres. These inorganic templates are difficult to remove after the MOF shell preparation. Thus, these composites must be used of as a whole in applications. Tsung and coworkers found that by using Cu_2O as sacrificial template, hollow ZIF-8 capsules could be obtained.[4] Cu_2O assisted the nucleation of ZIF-8 coating and it was etched off simultaneously during the growth process. A yolk-shell structure was also obtained when Pd nanocrystal was embedded within Cu_2O prior to the growth of ZIF-8 shell. In contrast to the previous work, Huo and coworkers utilized Cu_2O as the metal sources for MOF shell formation.[5]

Recently, a yolk-shell template was used for the preparation of copper hydroxysulfates@MOF yolk-shell structure.[6]

Another option is to use polymer as template. Carboxylate-terminated PS spheres have been widely used to grow PS@MOF core-shell structures. The first report was studied by Oh et al.[7] The surface-functionalized PS spheres were placed into a ZIF-8 precursor solution followed by solvothermal reaction. ZIF-8 hollow microspheres were obtained after etching the polymer cores, shown in Figure 2-1. Similar results have been shown by Li and coworkers using mono-dispersed PS nanoparticles through a step-by-step self-assembly strategy.[8] Since then, these ZIF-8 based core-shell microspheres have been explored for various applications, from catalysis to gas separation.[9-11]

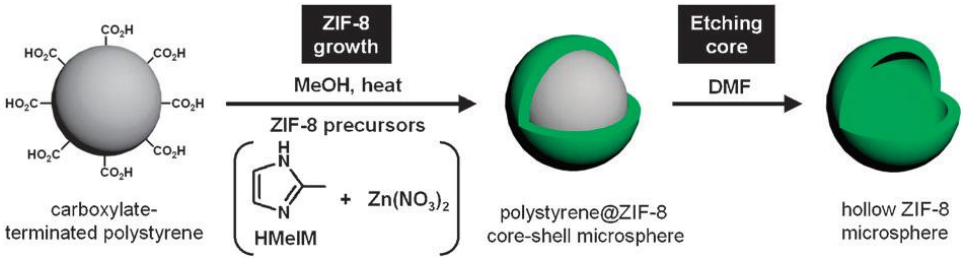

Figure 2-1. Schematic preparation of polystyrene@ZIF-8 and hollow ZIF-8 microspheres from carboxylate-terminated polystyrene spheres. Reprinted with permission from [7].

Besides using template to grow MOF particles, assembling MOFs at the droplet interface represents another strategy to prepare 0D MOF architectures. The first example of MOF hollow capsule was achieved with the help of interfacial approach.[12] Metal ions and bridging ligands were separately dissolved in two immiscible solvents, followed by injection of one solution into the other through syringe under continuous flow (Figure 2-

2). Aside of using micro-fluidic devices,[12,13] conventional emulsions have also been applied to prepare MOF hollow capsules. Similar to these systems, an inverse emulsion based interfacial synthesis of ZIF-8 nano-spheres with controllable shell thickness has also been reported.[14] PVP was used as stabilizer and functional nanoparticles were encapsulated during the process of emulsification. Another one-step synthesis of hollow MOF architectures based on Fe-soc-MOF was also demonstrated via an emulsion process.[15] Tween-85, as specific emulsifier, was found to be the key factor in realizing the hollow MOF capsules. In addition to the liquid-liquid interface, liquid-air interface was also proven to be useful in assisting fabrication of hollow MOF architectures.[16,17] A series of MOFs have been shaped into hollow superstructures through the spray-drying method (Figure 2-3).

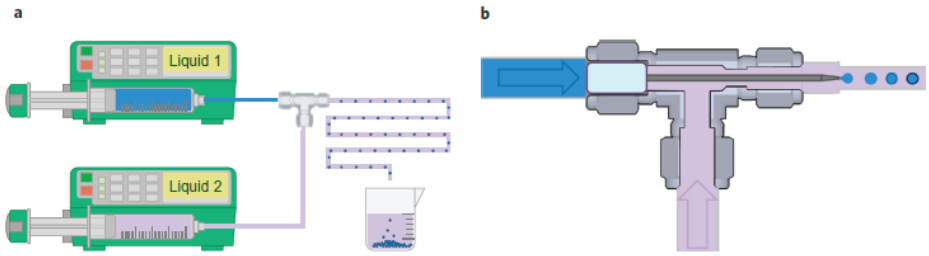

Figure 2-2. Preparation of hollow MOF capsules. a) Overview of the process. Both immiscible liquids are supplied by syringe pumps to a T-junction, where the formation of aqueous solution droplets in the continuous organic phase takes place. b) Cut-away view of the T-junction showing details of the emulsification step. Reprinted with permission from [12].

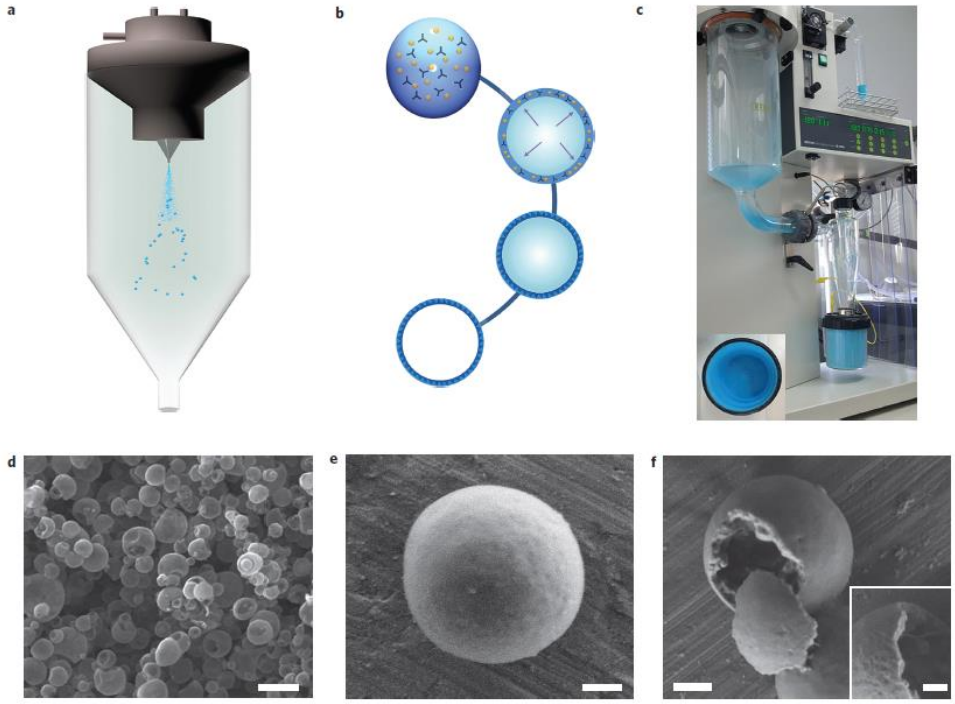

Figure 2-3. Spray-drying synthesis of hollow spherical HKUST-1 superstructures. a) Schematic showing the spray-drying process used to synthesize HKUST-1 superstructures. b) Proposed formation process. c) Photograph of the spray-dryer. d–f) Representative FESEM images showing a general view of the spherical HKUST-1 superstructures. Scale bars: 5 mm (d), 500 nm (e,f), 200 nm (f, inset). Reprinted with permission from [16].

2.1.2 Top-down methods

Similar to the above-mentioned strategies, templates are required to facilitate the assembly of pre-synthesized MOF particles. However, precisely manipulating MOF particles is much more difficult than controlling MOF precursor solutions, thus only a few attempts have been reported so far on the top-down methods.

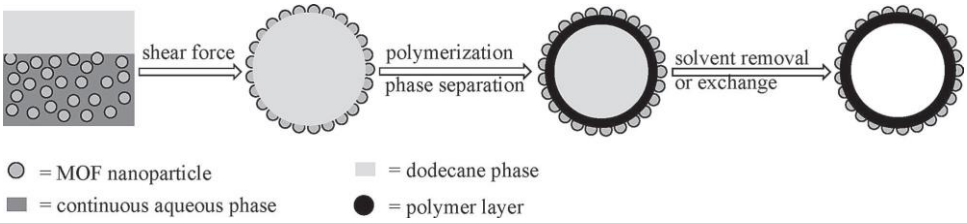

Figure 2-4. Schematic illustration of MOF-polymer composite capsule formation. Reprinted with permission from [18].

Pickering emulsion as a powerful tool was first introduced to prepare MOF hollow spheres by Bradshaw and co-workers.[18] MOF particles, including ZIF-8, MIL-101(Cr), and UiO-66, were used as Pickering emulsifier to stabilize an oil-in-water emulsion. By careful design of the oil internal phase, they were able to obtain hollow MOF-PS composite, since dodecane in the oil phase is a poor solvent for cross-linked PS, leading to phase separation and precipitation at the interface (Figure 2-4). The same group further applied this strategy to encapsulate functional biomolecules within MOF-based hollow capsules.[19] The agarose hydrogel droplet was stabilized by UiO-66 and magnetic iron oxide nanoparticles, followed by the deposition of ZIF-8 shell. The obtained hollow capsules presented an excellent size-selective catalytic behavior. Our group also developed two interfacial approaches based on dispersion polymerization and transient Pickering emulsion template to assemble MOF particles into 0D architectures, which is discussed in Chapter 3 & 4 in detail, respectively.

2.2 One-dimensional architectures

Alignment of colloid particles into 1D architectures has become an emerging research area, since these assemblies may present interesting properties different from single

particles. However, despite the enormous amount of efforts in developing MOFs, very few reports have been related to the 1D MOF architectures.

2.2.1 Bottom-up methods

In order to prepare 1D architecture, MOF nucleation must be confined along one single direction. The template can be classified into rod-like nano-fiber and template possessing cylindrical channels.

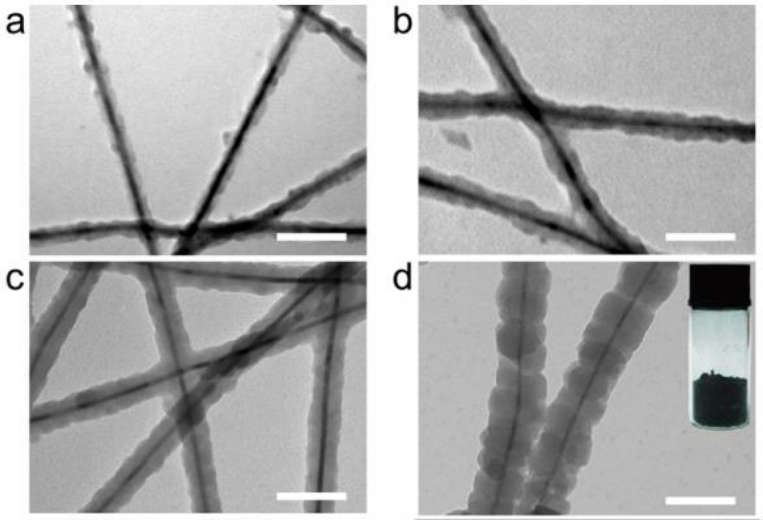

Figure 2-5. TEM images of as-prepared Te@ZIF-8 by regulating the amounts of precursors. Reprinted with permission from [20].

Silicon nanowires (SiNWs) have been used to direct the growth of MOFs.[21] SiNWs were functionalized with –COOH group, followed by a layer-by-layer growth of HKUST-1. The researchers were able to control the MOF morphology by tuning the soaking time, synthesis temperature, and precursor solution concentration. Ultrathin tellurium nanowires (TeNWs) with excellent dispersivity can also act as templates for directed growth and

assembly of ZIF-8 nanocrystals, resulting in the formation of uniform ZIF-8 nanofibers (Figure 2-5).[20]

Metal oxide nanorods are another type of good candidates for templating, and as metal source for MOF growth. ZnO has been widely used to facilitate the growth of ZIFs, mainly ZIF-8 and ZIF-8/ZIF-67. Zheng et al. reported the fabrication of free-standing ZnO@ZIF-8 nanorods, as well as vertically standing arrays.[22] They found that solvent composition and reaction temperature are two crucial factors for successfully fabricating well-defined ZnO@ZIF-8 heterostructures. They demonstrated that the prepared ZnO@ZIF-8 nanorod arrays could be applied to the detection of hydrogen peroxide in the presence of serous buffer solution. The ZnO@ZIF-8 nanorod arrays were also deposited onto flexible carbon cloth, followed by an annealing process in order to get ZnO@ZnO quantum dots/C core–shell nanorod arrays, which showed great potential as lithium-ion battery anode.[23] Fan and co-workers demonstrated the potential application of ZnO@ZIF-8 nanorods as a type of size-selective sensing materials, which were generated by a limitation effect of the pore aperture of ZIF-8 shell.[24] Most recently, ZnO@ZIF-CoZn core–sheath nanowire array was successfully created as chemiresistor gas sensor with improved selectivity, response, recovery behavior, and working temperature (Figure 2-6).[25] Similarly, TiO_2 nanorod arrays were used as template to prepare TiO_2@MIL-125-NH_2 core-shell materials as promising photosensitizers for photoelectrochemical water splitting.[26]

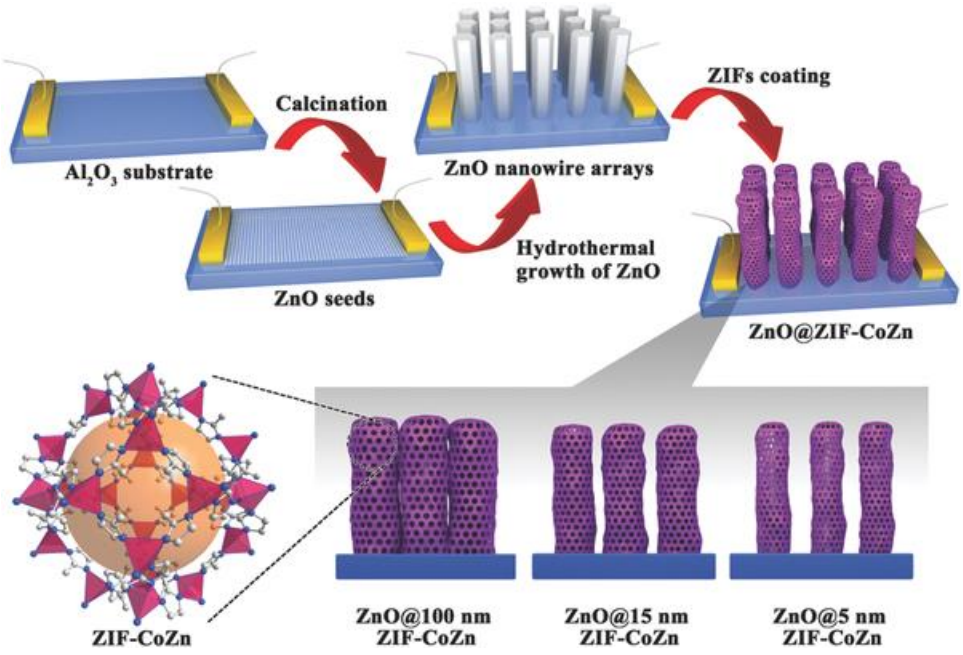

Figure 2-6. Schematic illustration of the preparation of ZnO@ZIF-CoZn gas sensors. Reprinted with permission from [25].

On the contrary to the solid metal oxide templates, hollow carbon nanofibers were used to direct the growth of MOFs.[27] MOF crystals were strictly confined in the cavity, as well as the outer wall of the carbon nanofibers (Figure 2-7). The hybrid material showed improved thermal stability and gas uptake over FCNF and MOF-2. Chitin hollow fibers were also used as a nontoxic, biodegradable, and low-weight support material for MOF deposition.[28] The abundant functional groups inside chitin favored predominant nucleation of MOF crystallites inside of the hollow fibers, and the prepared composite showed high potential for filtration applications for toxic industrial gases.

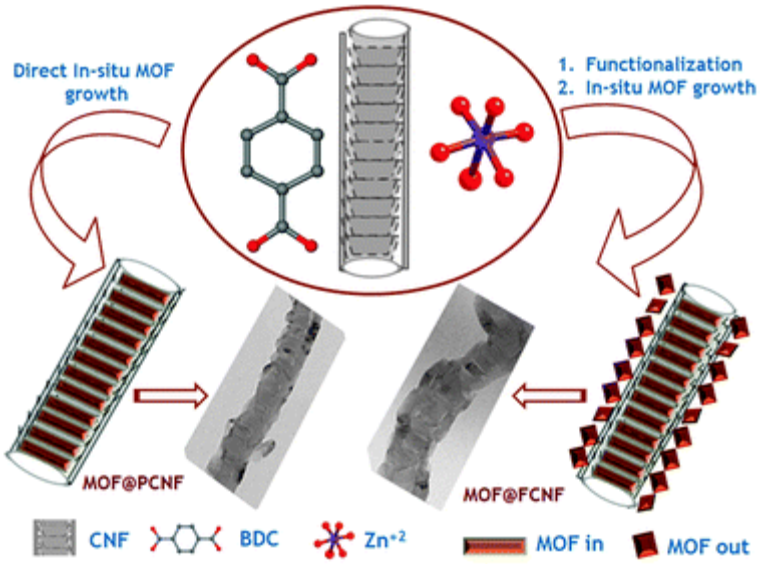

Figure 2-7. Scheme illustrating the synthesis for hybrid MOF@PCNF and MOF@FCNF using pristine CNFs (PCNF) and functionalized CNFs (FCNF), respectively. Reprinted with permission from [27].

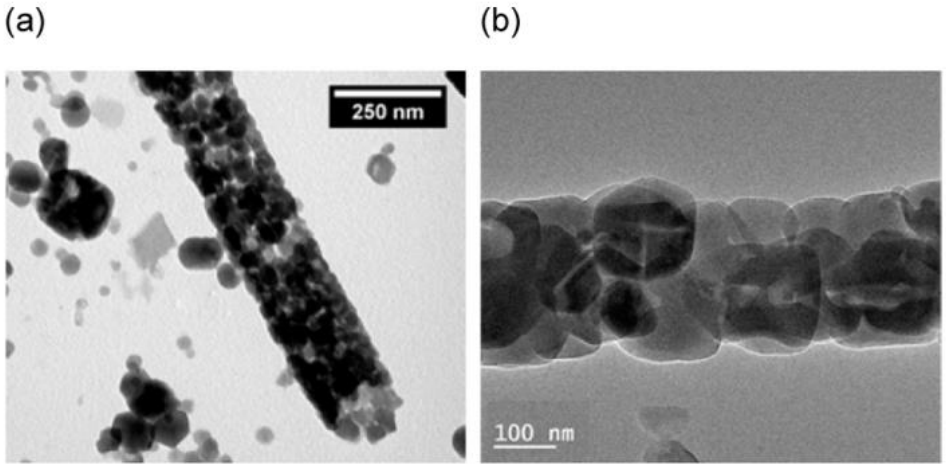

Figure 2-8. HRTEM images (a,b) for single free-standing ZIF-8 superstructures. Reprinted with permission from [30].

Similar to carbon nanofibers, anodized aluminium oxide (AAO) membranes are also useful as template for the confinement of 1D MOF architectures. The first study was

performed by Sutter and co-workers.[29] An efficient crystal growth was achieved by forcing synthetic solutions through AAO membrane in a step-by-step manner. They further reported self-supported ZIF-8 chains by etching ZIF-8 embedded AAO membranes prepared from the same protocol (Figure 2-8).[30]

2.2.2 Top-down methods

Electrospinning was first introduced by Smarsly's group to construct hierarchical porous nanofibers consisting of MOF nanoparticles and polymers (Figure 2-9).[31] Up to 56 wt.% ZIF-8 nanoparticles were incorporated and well distributed within the nanofibers. Since then, different MOF particles and polymers have been electrospun for different applications.[32-35] Most recently, Wang et al. thoroughly studied fiber morphologies, surface functionalities, and porosity of the filters, and investigated the compatibility between MOFs and polymers.[36] With careful design, they were able to apply the composite material as efficient air filters.

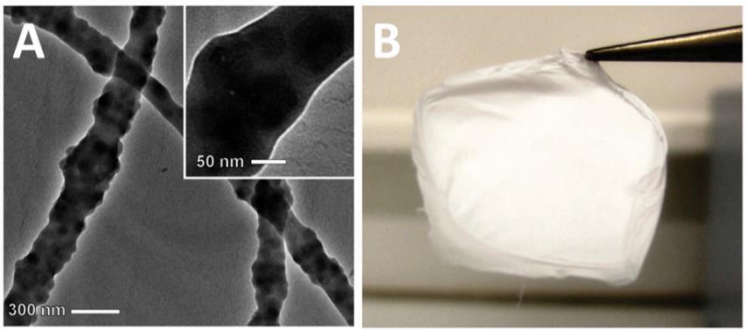

Figure 2-9. (A) TEM of ZIF-8 nanoparticles in PVP. (B) Photograph of a non-woven ZIF-8–PVP fiber mat. The diameter is ca. 1.5 cm. Reprinted with permission from [31].

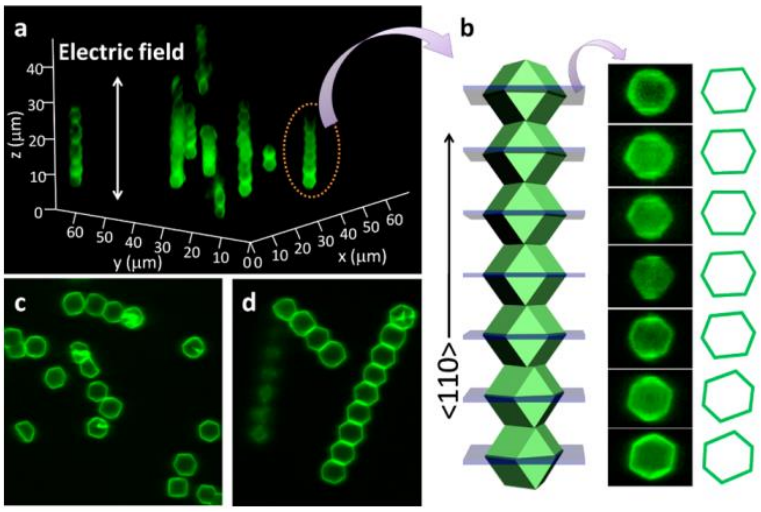

Figure 2-10. Electric field assembly of rhombic dodecahedra. (a) Typical in situ observation of 1-D chains of rhombic dodecahedra (Figure 2d) along the direction of electric field (1 MHz, 200 V/mm) by confocal microscopy. (b) Confocal cross sections perpendicular to the electric field, along with schematic representations of contour. Elongated hexagonal outlines indicate the ⟨110⟩ orientation of crystals along the direction of electric field. (c) Disconnected chains of rhombic dodecahedra after turning off the AC field (1 MHz, 200 V/mm). (d) Stably locked chains of rhombic dodecahedra after turning off the AC field (1 kHz, 200 V/mm). Reprinted with permission from [37].

Another plausible work was reported by Granick and co-workers, and it was based on a template-free electric field induced method.[37] Mono-dispersed ZIF-8 particles were first prepared by simultaneously adding two capping ligands. Upon dispersion in ethylene glycol and application of AC electric field, the particles facets linked to form linear chains (Figure 2-10). The MOF chains remained locked to each other even after removal of the electric field, if the MOF particle facets were planar.

2.3 Two-dimensional architectures

The preparation of 2D MOF architectures, namely MOF membranes/films, has been intensively studied over the past decades. The reason of increasing interest in MOF membrane fabrication lies in its great potential in various applications, including separations and sensors. Compared to other dimensional MOF architectures, the development of MOF membranes/films is much faster due to the easiness of planar systems.

2.3.1 Bottom-up methods

An impressive number of works has been done to prepare MOF membranes/films onto different macrostructural planar templates. Different strategies have been applied, such as solvothermal growth method, seeded secondary growth method, and layer-by-layer growth method. The details of these works are not discussed in this thesis due to the maturity of these approaches. In this section, we focused on the fabrication of MOF nanosheets supported on 2D template, such as graphene and MoS_2, or as free standing nanomaterials.

Graphene oxide (GO) nanosheets are a type of widely studied 2D materials, which provide good templates for the construction of 2D MOF architectures. ZIF-8 and its cobalt analogue ZIF-67 are the most studied MOF type grown on the GO nanosheets. The strong interactions between metal ions from ZIF and GO lead to the preference of surface nucleation. Many reports have demonstrated the combination of ZIF and GO, however, most of them lacked a uniform ZIF particle distribution.[38-42] In 2014, Zhang and co-workers reported a facile procedure to coat ZIF-8 on various 2D templates, including MoS_2, GO, and reduced GO (rGO) (Figure 2-11).[43] This hybrid material showed write-once-

read-many-times memory effect with high ON/OFF ratio and long operating lifetime, which was promising in fabricating memory devices. Wang's group adopted a two-step approach to coat uniform ZIFs on GO nanosheets.[44] ZIF clusters were first deposited onto GO due to their strong coordination interaction, followed by a confined growth on the GO nanosheets. The prepared composite was carbonized and the ZIF coating acted as a spacer, which prevented the severe agglomeration of rGO. They further used these materials as seeds to construct a defect-free ZIF/GO membrane, which exhibited excellent molecular sieving gas separation properties.[44] Recently, Zheng and co-workers coated a Fe-based MOF on GO functionalized with magnetic particles through a stepwise procedure.[45] The obtained materials were highly selective in extraction and separation of biomolecules from biological samples.

Recently, another type of excellent templates, layered double hydroxide (LDH), was studied for preparation of MOF 2D architectures.[46] The existence of unsaturated metal ions on the surface of LDH nanoplate provides active nucleation sites for MOF growth. ZIF-67 was grown onto CoAl-LDH, followed by a pyrolysis treatment to get a porous carbon-based framework, which showed a superior electrocatalytic oxygen reduction performance. In addition, sodium ion exchanged zirconium phosphate (NaZrP) nanoplatelets were also reported as a 2D template for MOF growth through a layer-by-layer process.[47] The amount of assembled HKUST-1 could be readily controlled by varying the number of growth cycles and the prepared hybrid nanoplates were tested as catalyst for cyclohexene oxidation.

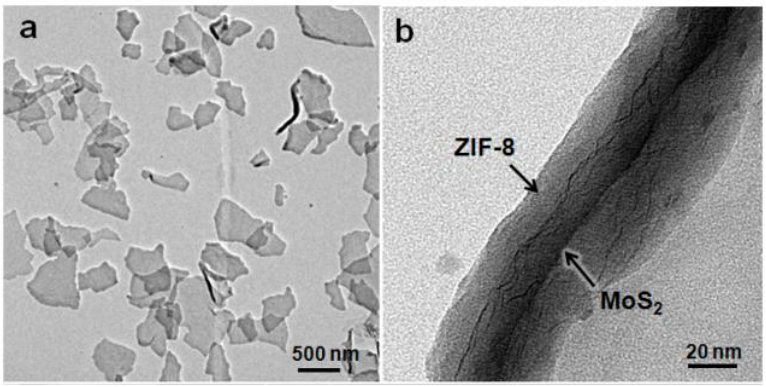

Figure 2-11. (a) TEM image of MoS2@ZIF-8 hybrid structures. (b) TEM image of a curled MoS2@ZIF-8 structure, showing the MoS2 nanosheet and ZIF-8 coating. Reprinted with permission from [43].

Confined growth of MOFs was also explored as a powerful tool to grow 2D MOF nanoplates. A superhydrophobic-superhydrophilic micropattern was first fabricated on a polymer surface using an appropriate quartz photomask.[48] Then the aqueous droplets containing copper acetate were placed on the superhydrophilic regions, which were covered by a water immiscible 1-octanol solution of trimesic acid (Figure 2-12). The MOF formed at the interface resembled the shape of droplet surface. Similar to this report, Kim's group reported a mold membrane with desired shapes of open windows, which preferred to stay at the interface of the two immiscible solvents due to its intermediate density.[49] Since the interfacial reaction was confined within the open windows of the mold, the desired morphology of MOF 2D structure could be obtained by designing the shapes of the open windows.

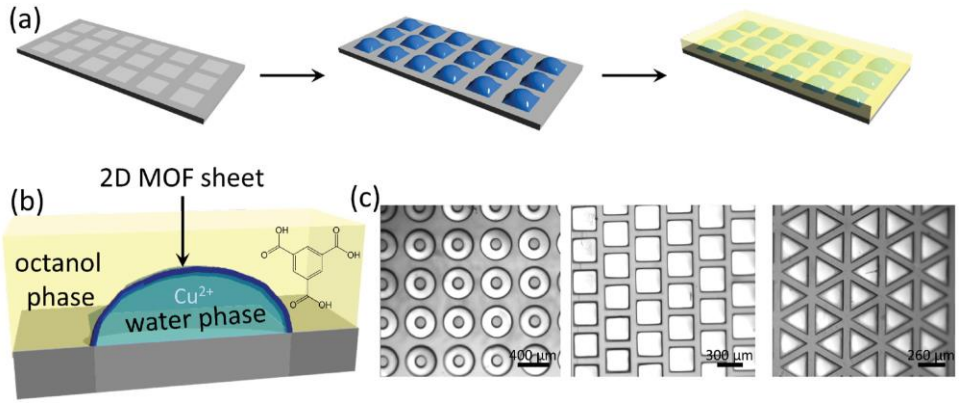

Figure 2-12. a) Schematic illustration of the process for the formation of MOF superstructures at the superhydrophobic–superhydrophilic micropatterned substrate; b) basic unit of interfacial HKUST-1 growth on an individual water droplet formed on the hydrophilic pattern; c) photographs of microdroplets with ring, square, and triangular shapes formed on the corresponding superhydrophobic–superhydrophilic microarrays. Reprinted with permission from [48].

2.3.2 Top-down methods

Exfoliation of bulk materials into single or multi-layers has also been applied to prepare 2D MOF nanosheets. The delamination of MOFs into nanosheets was first reported by Xu's group in 2011.[50] A zinc-based MOF, MOF-2, was delaminated and exhibited remarkable amine intercalation property and reversible amine exchangeability. Since this pioneering work, different MOFs have been delaminated and studied for various applications.[51-55] However, most of the reported delaminated MOF nanosheets suffered from structural deterioration and morphological damage, which hindered their potential applications. In 2014, Yang and co-workers reported a 1-nm-thick MOF nanosheet with a large lateral area and high crystallinity, which was used to fabricate ultrapermeable membranes with excellent molecular sieving properties for H_2/CO_2 separation.[56] The MOF nanosheets were prepared through a two-step strategy, where pristine MOF crystals

were first wet ball-milled at low speed, followed by exfoliation in volatile solvent with the aid of ultrasonication (Figure 2-13).

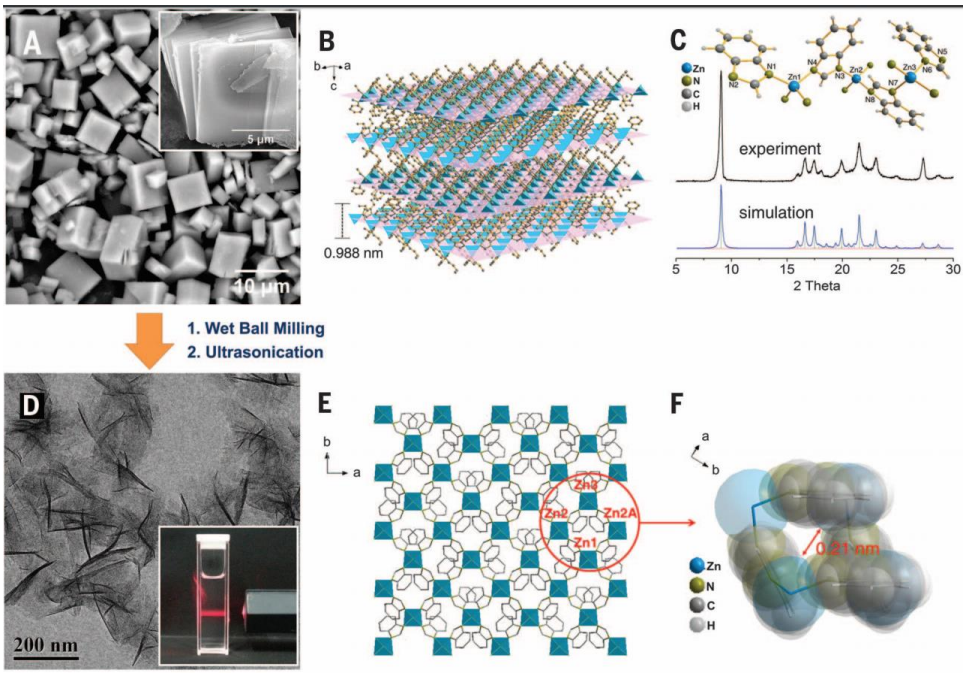

Figure 2-13. (A) SEM image of as-synthesized $Zn_2(bim)_4$ crystals. The inset image shows the typical flake-like morphology of $Zn_2(bim)_4$ crystals. (B) Architecture of the layered MOF precursor. (C) PXRD patterns of $Zn_2(bim)_4$. (D) TEM image of $Zn_2(bim)_4$ MSNs. The inset shows the Tyndall effect of a colloidal suspension. (E) Illustration of the grid-like structure of the $Zn_2(bim)_4$ MSN. (F) Space-filling representation of a four-membered ring of the $Zn_2(bim)_4$ MSN. Reprinted with permission from [56].

Another powerful tool to assemble MOFs into 2D materials is Langmuir-Blodgett (LB) technique, which was first introduced by Kitagawa's group.[57] A layer of MOF particles was first spread on the top of water surface, which was then compressed by the mobile barriers and deposited on the desired substrate via dip coating. This method required no chemical functionalization of MOF particles and the substrates, and it also showed possibility of control over the orientation of deposited crystals. There were several other

studies reporting the possibility of assembling other MOFs as well as their potential applications.[58-60]

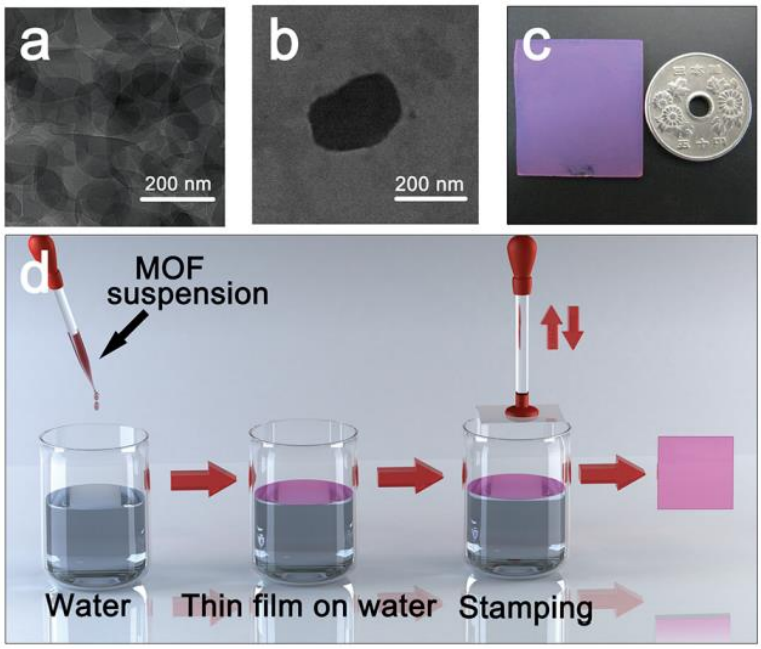

Figure 2-14. (a, b) TEM images of the synthesized Cu−TCPP nanosheets. (c) Photograph of the MOF thin film after 15 deposition cycles on a quartz substrate. (d) Illustration of the assembly process of this MOF thin film. Reprinted with permission from [61].

A so-called 'modular assembly' strategy for fast construction of MOF nanofilms was developed by Kitagawa's group (Figure 2-14).[61,62] They first prepared a hydrophobic MOF nanosheet module, which was then suspended in ethanol under sonication. The suspension was placed onto water, which served as a flat surface. MOF particles spread on the surface automatically due to their hydrophobic nature, thus forming a uniform film. Finally, the film was easily transferred to a substrate through stamping. They further studied electrical properties of the prepared oriented MOF thin film and found that the

nanofilm had low activation energy and a proton conductivity that was among the highest reported for MOF materials.

An unique solvent evaporation-induced assembly of MOF particles was also reported by Granick and co-workers.[63] By choosing proper solvent and salt concentration, ZIF-8 can self-assemble into close-packed hexagonal arrangements due to the directional capillary force or van der Waals attractions.

Electrophoretic deposition was another technique used for the assembly of 2D MOF architectures.[64,65] Pre-synthesized MOF particles were first dispersed into a proper solvent, then an electric field was applied to the suspension. MOF particles moved towards anode or cathode according to their surface charge, thus depositing on the electrode.

2.4 Three-dimensional architectures

Integration of MOFs into 3D structures can enhance and expand the potential applications of MOF materials. For instance, introducing macro- or meso-pores into MOFs by combining MOFs and 3D porous materials can enhance the diffusion rate of molecules, leading to fast interactions between MOFs and targeted molecules, which could be of benefit in applications for gas adsorption, molecular separations, chemical sensing, and heterogeneous catalysis.

2.4.1 Bottom-up methods

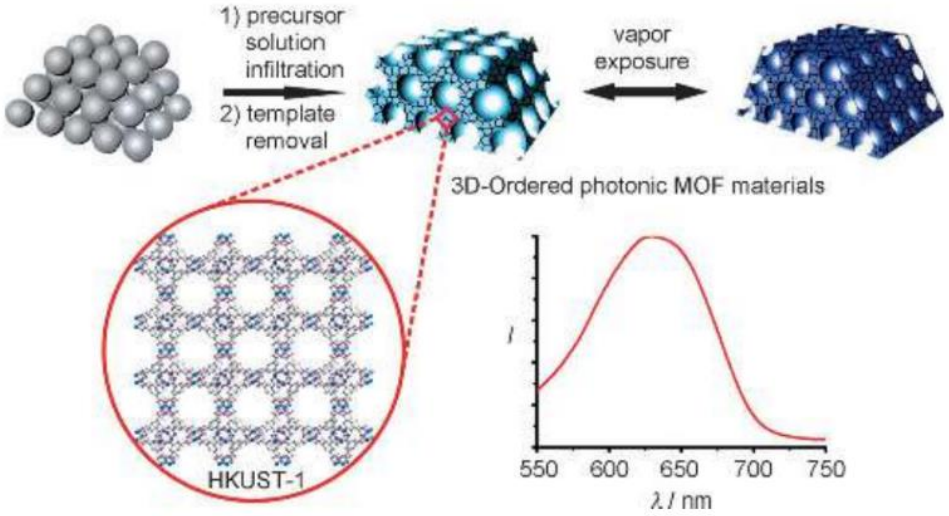

Figure 2-15. Schematic illustration of the preparation of metal-organic frameworks with three-dimensional ordered macroporous structure, which can be served as dynamic photonic materials. Reprinted with permission from [66].

Inverse-opal structures were usually applied as macroporous templates to fabricate 3D MOF architectures.[66,67] The colloidal particles first self-assembled into 3D periodic arrays, followed by MOF growth at the interstices of these particles (Figure 2-15). The integration of this macroporous array endowed additional optical properties to the MOFs, which could be used as signal transducers. The same idea was used to fabricate asymmetric 3D MOF architectures.[68] The prepared colloidal crystal arrays were partially immersed into a MOF precursor solution, leading to an interesting 3D structure, which showed potential in vapor sensing, size-screening, and dye removal. Kitagawa and co-workers also developed a two-step method to prepare 3D MOF architectures.[69] Colloidal crystal superstructure was used to prepare aluminum oxide template through a sol-gel process, followed by the treatment

of ligand solution under microwave condition. The prepared 3D MOF materials possessed the micropores of the MOF, as well as the mesopores and macropores inherited from the parent alumina aerogel. This hierarchical porous structure synergistically enhanced the selectivity and mass transfer for water-ethanol separation.

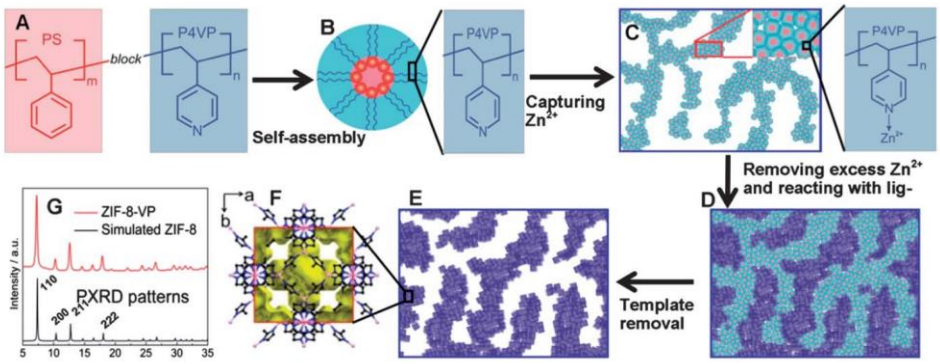

Figure 2-16. Synthesis of hierarchical ZIF-8-VP templated from PSty14-b-P4VP19 block co-oligomer micelles. Reprinted with permission from [70].

Two functional co-oligomer templates were used to grow 3D MOF architectures by Cheetham's group.[70] The synthesized co-oligomer was first self-assembled into micelles and protonated in order to increase the affinity to metal ions. The micelles then reacted with metal ions, followed by immersion in ligand solution to prepare MOFs. The micelle template was finally etched to get the intergrown hierarchical porous MOF architectures (Figure 2-16). Organic−inorganic hybrid electrospun fibrous mats were investigated as supporting template to grow various MOFs *in-situ*.[71] The prepared fibrous mats showed good affinity to MOF particles, thus no pre-modification was needed. The loading of MOFs could be controlled by repeating the growth procedure. The obtained MOF-containing mats were used as fibrous sorbents with enhanced adsorption capacity and removal rate. A

gelatin hydrogel matrix was also used as a template to grow MOF *in-situ*.[72] The gelatin hydrogel doped with metal ion was prepared either by soaking pure gelatin in a metal ion solution or by *in-situ* preparation of gelatin together with metal ion. The metal-ion@gelatin hydrogel was treated with a ligand solution to get the MOF@gelatin composite. Our group introduced another biopolymer, which is alginate, as a general and shapeable platform to prepare MOF-polymer hierarchical structure, which is described in detail in Chapter 7.

Another template-free sol-gel process was also reported to prepare 3D MOF architectures. The combination of metal ions and organic ligands leads to gelation under certain conditions, which can be further dried (usually supercritical dried in order to reduce volume shrinkage) to get free-standing MOF aerogels. An early example was reported by Kaskel and co-workers, which demonstrated the preparation of Fe-BTC (BTC = 1, 3, 5-benzenetricarboxylic acid) aerogel.[73] Gelation happened within seconds upon the combination of ethanolic solutions of iron(III) nitrate and trimesic acid. The obtained aerogel dried under supercritical condition showed high permanent porosity and pore volumes. Other examples include Al-BDC (BDC = 1, 4-benzenedicarboxylic acid),[74] Fe-Al-BTC,[75] HKUST-1,[76] and so on.

2.4.2 Top-down methods

Compared to the bottom-up methods, very few top-down strategies have been developed to assemble MOF particles into 3D architectures. This is mainly due to the difficulty of manipulating MOF particles in a 3D space.

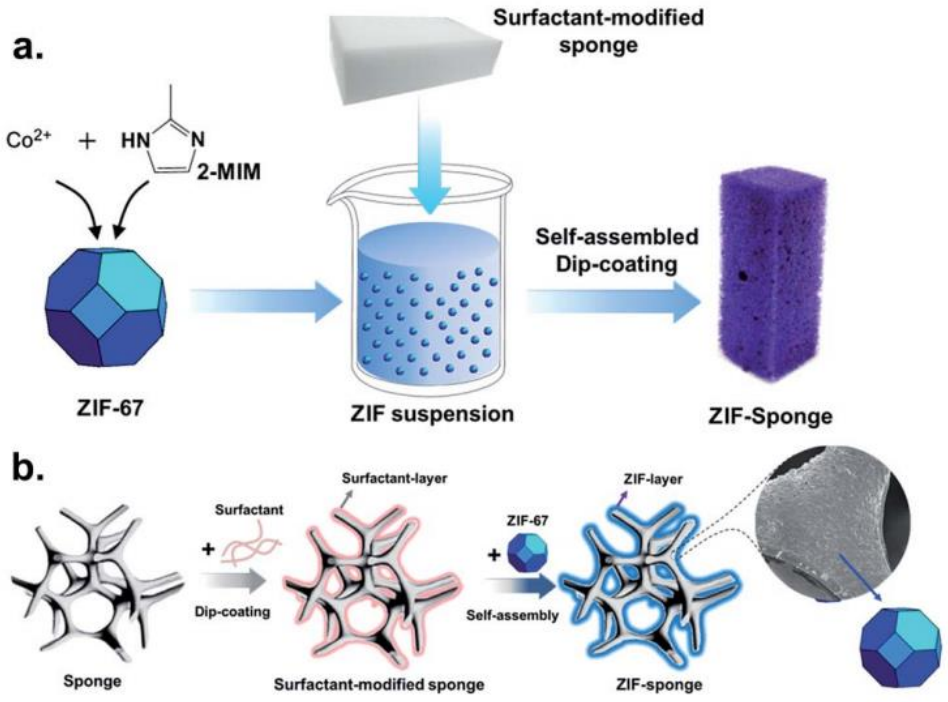

Figure 2-17. Schematic illustrations showing the preparation of ZIF–sponge: (a) surfactant-assisted dip-coating self-assembling process and (b) surface-modification of the sponge skeleton first with a surfactant and then ZIF-67. Reprinted with permission from [77].

Lin and Chang developed a rapid, simple and inexpensive dip-coating approach to prepare ZIF-67 onto a melamine sponge template.[77] The sponge was first modified with surfactant to improve the affinity towards MOF nanocrystals, which then facilitated the self-assembly of MOFs on sponge skeletons via electrostatic attraction and possibly π-π stacking interactions (Figure 2-17). The obtained ZIF–sponge showed a remarkably high adsorption capacity for malachite green dye. Cerdà and co-workers further applied this method to prepare a Co-Ni LDH@sponge composite, which showed fast and efficient extraction of phenolic acids from fruit juices.[78]

Pickering high internal phase emulsion (HIPE) is another option to assemble MOF particles into 3D hierarchical structures. MIL-100(Fe) and a non-ionic surfactant were used to stabilize oil-in-water HIPEs.[79] The oil phase was then polymerized to prepare a free-standing, fully-open, hierarchically porous polyHIPEs. MOF particles were decorated on the surface. It was found that up to 14% of MIL-100(Fe) was incorporated into the monolith. The prepared monolith showed an appealing catalytic activity in Friedel–Crafts alkylation in a batch mode, as well as in a flow-through mode. Recently, our group developed an emulsifier-free MOF-based Pickering HIPE template to assemble MOF particles into 3D hierarchically porous architectures, which is described in detail in Chapter 5. Our group also developed a sol-gel process to prepare free-standing MOF-CNC aerogels with combined properties of structural CNCs and functional MOFs, which is described in detail in Chapter 6.

2.5 Concluding remarks

MOFs have been intensively studied for almost two decades, and it is now one of the hottest research areas in both academia and industry. MOFs possess many useful properties, yet they are difficult to process. Developing novel strategies to assemble MOF particles into architectures with various dimensions can improve the performance beyond that of the bulk crystal powders. As described above, 2D MOF architectures have been primarily studied, while the development of 0D, 1D, and 3D architectures is an emerging area. More efforts and focuses are expected to be targeted in this important area in the coming years.

2.6 References

[1] S. Aguado, J. Canivet, D. Farrusseng, *Chemical Communications* **2010**, *46*, 7999-8001.

[2] S. Sorribas, B. Zornoza, C. Téllez, J. Coronas, *Chemical Communications* **2012**, *48*, 9388-9390.

[3] Y.-Y. Fu, C.-X. Yang, X.-P. Yan, *Chemistry – A European Journal* **2013**, *19*, 13484-13491.

[4] C.-H. Kuo, Y. Tang, L.-Y. Chou, B. T. Sneed, C. N. Brodsky, Z. Zhao, C.-K. Tsung, *Journal of the American Chemical Society* **2012**, *134*, 14345-14348.

[5] Y. Liu, W. Zhang, S. Li, C. Cui, J. Wu, H. Chen, F. Huo, *Chemistry of Materials* **2014**, *26*, 1119-1125.

[6] H. Gao, Y. Luan, K. Chaikittikul, W. Dong, J. Li, X. Zhang, D. Jia, M. Yang, G. Wang, *ACS applied materials & interfaces* **2015**, *7*, 4667-4674.

[7] H. J. Lee, W. Cho, M. Oh, *Chemical Communications* **2012**, *48*, 221-223.

[8] A.-L. Li, F. Ke, L.-G. Qiu, X. Jiang, Y.-M. Wang, X.-Y. Tian, *CrystEngComm* **2013**, *15*, 3554-3559.

[9] F. Zhang, Y. Wei, X. Wu, H. Jiang, W. Wang, H. Li, *Journal of the American Chemical Society* **2014**, *136*, 13963-13966.

[10] H. J. Lee, S. Choi, M. Oh, *Chemical Communications* **2014**, *50*, 4492-4495.

[11] S. Hwang, W. S. Chi, S. J. Lee, S. H. Im, J. H. Kim, J. Kim, *Journal of Membrane Science* **2015**, *480*, 11-19.

[12] R. Ameloot, F. Vermoortele, W. Vanhove, M. B. Roeffaers, B. F. Sels, D. E. De Vos, *Nature chemistry* **2011**, *3*, 382-387.

[13] G.-Y. Jeong, R. Ricco, K. Liang, J. Ludwig, J.-O. Kim, P. Falcaro, D.-P. Kim, *Chemistry of Materials* **2015**, *27*, 7903-7909.

[14] Y. Yang, F. Wang, Q. Yang, Y. Hu, H. Yan, Y.-Z. Chen, H. Liu, G. Zhang, J. Lu, H.-L. Jiang, *ACS applied materials & interfaces* **2014**, *6*, 18163-18171.

[15] M. Pang, A. J. Cairns, Y. Liu, Y. Belmabkhout, H. C. Zeng, M. Eddaoudi, *Journal of the American Chemical Society* **2013**, *135*, 10234-10237.

[16] A. Carné-Sánchez, I. Imaz, M. Cano-Sarabia, D. Maspoch, *Nature chemistry* **2013**, *5*, 203-211.

[17] Z. Wang, D. Ananias, A. Carné-Sánchez, C. D. Brites, I. Imaz, D. Maspoch, J. Rocha, L. D. Carlos, *Advanced Functional Materials* **2015**, *25*, 2824-2830.

[18] J. Huo, M. Marcello, A. Garai, D. Bradshaw, *Advanced Materials* **2013**, *25*, 2717-2722.

[19] J. Huo, J. Aguilera-Sigalat, S. El-Hankari, D. Bradshaw, *Chemical Science* **2015**, *6*, 1938-1943.

[20] W. Zhang, Z.-Y. Wu, H.-L. Jiang, S.-H. Yu, *Journal of the American Chemical Society* **2014**, *136*, 14385-14388.

[21] N. Liu, Y. Yao, J. J. Cha, M. T. McDowell, Y. Han, Y. Cui, *Nano Research* **2012**, *5*, 109-116.

[22] W.-w. Zhan, Q. Kuang, J.-z. Zhou, X.-j. Kong, Z.-x. Xie, L.-s. Zheng, *Journal of the American Chemical Society* **2013**, *135*, 1926-1933.

[23] G. Zhang, S. Hou, H. Zhang, W. Zeng, F. Yan, C. C. Li, H. Duan, *Advanced Materials* **2015**, *27*, 2400-2405.

[24] H. Tian, H. Fan, M. Li, L. Ma, *ACS Sensors* **2016**, *1*, 243-250.

[25] M.-S. Yao, W.-X. Tang, G.-E. Wang, B. Nath, G. Xu, *Advanced Materials* **2016**, 28, 5229-5234.

[26] L. Zhang, P. Cui, H. Yang, J. Chen, F. Xiao, Y. Guo, Y. Liu, W. Zhang, F. Huo, B. Liu, *Advanced Science* **2016**, *3*.

[27] P. Pachfule, B. K. Balan, S. Kurungot, R. Banerjee, *Chemical Communications* **2012**, *48*, 2009-2011.

[28] D. Wisser, F. M. Wisser, S. Raschke, N. Klein, M. Leistner, J. Grothe, E. Brunner, S. Kaskel, *Angewandte Chemie International Edition* **2015**, *54*, 12588-12591.

[29] M. Maksoud, N. Roques, S. Brandès, L. Arurault, J.-P. Sutter, *Journal of Materials Chemistry A* **2013**, *1*, 3688-3693.

[30] M. Gualino, N. Roques, S. Brandès, L. Arurault, J.-P. Sutter, *Crystal Growth & Design* **2015**, *15*, 3552-3555.

[31] R. Ostermann, J. Cravillon, C. Weidmann, M. Wiebcke, B. M. Smarsly, *Chemical Communications* **2011**, *47*, 442-444.

[32] Y.-n. Wu, F. Li, H. Liu, W. Zhu, M. Teng, Y. Jiang, W. Li, D. Xu, D. He, P. Hannam, *Journal of Materials Chemistry* **2012**, *22*, 16971-16978.

[33] E. F. de Melo, N. d. C. Santana, K. G. B. Alves, G. F. de Sá, C. P. de Melo, M. O. Rodrigues, S. A. Júnior, *Journal of Materials Chemistry C* **2013**, *1*, 7574-7581.

[34] J. Quirós, K. Boltes, S. Aguado, R. G. de Villoria, J. J. Vilatela, R. Rosal, *Chemical Engineering Journal* **2015**, *262*, 189-197.

[35] J. Ren, N. M. Musyoka, P. Annamalai, H. W. Langmi, B. C. North, M. Mathe, *International Journal of Hydrogen Energy* **2015**, *40*, 9382-9387.

[36] Y. Zhang, S. Yuan, X. Feng, H. Li, J. Zhou, B. Wang, *Journal of the American Chemical Society* **2016**, *138*, 5785-5788.

[37] N. Yanai, M. Sindoro, J. Yan, S. Granick, *Journal of the American Chemical Society* **2012**, *135*, 34-37.

[38] R. Kumar, K. Jayaramulu, T. K. Maji, C. Rao, *Chemical Communications* **2013**, *49*, 4947-4949.

[39] H. x. Zhong, J. Wang, Y. w. Zhang, W. l. Xu, W. Xing, D. Xu, Y. f. Zhang, X. b. Zhang, *Angewandte Chemie International Edition* **2014**, *53*, 14235-14239.

[40] X. Cao, B. Zheng, X. Rui, W. Shi, Q. Yan, H. Zhang, *Angewandte Chemie* **2014**, *126*, 1428-1433.

[41] X. Qiu, X. Wang, Y. Li, *Chemical Communications* **2015**, *51*, 3874-3877.

[42] J. Wei, Y. Hu, Z. Wu, Y. Liang, S. Leong, B. Kong, X. Zhang, D. Zhao, G. P. Simon, H. Wang, *Journal of Materials Chemistry A* **2015**, *3*, 16867-16873.

[43] X. Huang, B. Zheng, Z. Liu, C. Tan, J. Liu, B. Chen, H. Li, J. Chen, X. Zhang, Z. Fan, W. Zhang, Z. Guo, F. Huo, Y. Yang, L.-H. Xie, W. Huang, H. Zhang, *ACS Nano* **2014**, *8*, 8695-8701.

[44] J. Wei, Y. Hu, Y. Liang, B. Kong, J. Zhang, J. Song, Q. Bao, G. P. Simon, S. P. Jiang, H. Wang, *Advanced Functional Materials* **2015**, *25*, 5768-5777.

[45] G. Cheng, Z.-G. Wang, S. Denagamage, S.-Y. Zheng, *ACS applied materials & interfaces* **2016**, *8*, 10234-10242.

[46] Z. Li, M. Shao, L. Zhou, R. Zhang, C. Zhang, M. Wei, D. G. Evans, X. Duan, *Advanced Materials* **2016**, *28*, 2337-2344.

[47] Y. Kan, A. Clearfield, *Inorganic Chemistry* **2016**, *55*, 5634-5639.

[48] M. Tsotsalas, H. Maheshwari, S. Schmitt, S. Heißler, W. Feng, P. A. Levkin, *Advanced Materials Interfaces* **2016**, *3*, doi: 10.1002/admi.201500392.

[49] J.-O. Kim, K.-I. Min, H. Noh, D.-H. Kim, S.-Y. Park, D.-P. Kim, *Angewandte Chemie International Edition* **2016**, 55, 7116-7120.

[50] P.-Z. Li, Y. Maeda, Q. Xu, *Chemical Communications* **2011**, *47*, 8436-8438.

[51] A. Kondo, C. C. Tiew, F. Moriguchi, K. Maeda, *Dalton Transactions* **2013**, *42*, 15267-15270.

[52] S. C. Junggeburth, L. Diehl, S. Werner, V. Duppel, W. Sigle, B. V. Lotsch, *Journal of the American Chemical Society* **2013**, *135*, 6157-6164.

[53] A. Gallego, C. Hermosa, O. Castillo, I. Berlanga, C. J. Gómez-García, E. Mateo-Martí, J. I. Martínez, F. Flores, C. Gómez-Navarro, J. Gómez-Herrero, *Advanced Materials* **2013**, *25*, 2141-2146.

[54] P. Beldon, S. Tominaka, P. Singh, T. S. Dasgupta, E. Bithell, A. Cheetham, *Chemical Communications* **2014**, *50*, 3955-3957.

[55]C. Hermosa, B. R. Horrocks, J. I. Martínez, F. Liscio, J. Gómez-Herrero, F. Zamora, *Chemical Science* **2015**, *6*, 2553-2558.

[56] Y. Peng, Y. Li, Y. Ban, H. Jin, W. Jiao, X. Liu, W. Yang, *Science* **2014**, *346*, 1356-1359.

[57]M. Tsotsalas, A. Umemura, F. Kim, Y. Sakata, J. Reboul, S. Kitagawa, S. Furukawa, *Journal of Materials Chemistry* **2012**, *22*, 10159-10165.

[58] G. Lu, C. Cui, W. Zhang, Y. Liu, F. Huo, *Chemistry–An Asian Journal* **2013**, *8*, 69-72.

[59] C. Cui, Y. Liu, H. Xu, S. Li, W. Zhang, P. Cui, F. Huo, *Small* **2014**, *10*, 3672-3676.

[60] J. Benito, M. Fenero, S. Sorribas, B. Zornoza, K. J. Msayib, N. B. McKeown, C. Téllez, J. Coronas, I. Gascón, *Colloids and Surfaces A: Physicochemical and Engineering Aspects* **2015**, *470*, 161-170.

[61] G. Xu, T. Yamada, K. Otsubo, S. Sakaida, H. Kitagawa, *Journal of the American Chemical Society* **2012**, *134*, 16524-16527.

[62] G. Xu, K. Otsubo, T. Yamada, S. Sakaida, H. Kitagawa, *Journal of the American Chemical Society* **2013**, *135*, 7438-7441.

[63] N. Yanai, S. Granick, *Angewandte Chemie International Edition* **2012**, *51*, 5638-5641.

[64] I. Hod, W. Bury, D. M. Karlin, P. Deria, C. W. Kung, M. J. Katz, M. So, B. Klahr, D. Jin, Y. W. Chung, *Advanced Materials* **2014**, *26*, 6295-6300.

[65] H. Zhu, H. Liu, I. Zhitomirsky, S. Zhu, *Materials Letters* **2015**, *142*, 19-22.

[66] Y. n. Wu, F. Li, W. Zhu, J. Cui, C. a. Tao, C. Lin, P. M. Hannam, G. Li, *Angewandte Chemie International Edition* **2011**, *50*, 12518-12522.

[67] J. Cui, N. Gao, C. Wang, W. Zhu, J. Li, H. Wang, P. Seidel, B. J. Ravoo, G. Li, *Nanoscale* **2014**, *6*, 11995-12001.

[68] L. Li, X. Jiao, D. Chen, C. Li, *Crystal Growth & Design* **2016**, *16*, 2700-2707.

[69] J. Reboul, S. Furukawa, N. Horike, M. Tsotsalas, K. Hirai, H. Uehara, M. Kondo, N. Louvain, O. Sakata, S. Kitagawa, *Nature materials* **2012**, *11*, 717-723.

[70] S. Cao, G. Gody, W. Zhao, S. Perrier, X. Peng, C. Ducati, D. Zhao, A. K. Cheetham, *Chemical Science* **2013**, *4*, 3573-3577.

[71] C. Liu, Y.-n. Wu, C. Morlay, Y. Gu, B. Gebremariam, X. Yuan, F. Li, *ACS Applied Materials & Interfaces* **2016**, *8*, 2552-2561.

[72] A. Garai, W. Shepherd, J. Huo, D. Bradshaw, *Journal of Materials Chemistry B* **2013**, *1*, 3678-3684.

[73] M. R. Lohe, M. Rose, S. Kaskel, *Chemical Communications* **2009**, 6056-6058.

[74] L. Li, S. Xiang, S. Cao, J. Zhang, G. Ouyang, L. Chen, C.-Y. Su, *Nature communications* **2013**, *4*, 1774.

[75] A. Mahmood, W. Xia, N. Mahmood, Q. Wang, R. Zou, *Scientific reports* **2015**, *5*.

[76] A. K. Chaudhari, I. Han, J. C. Tan, *Advanced Materials* **2015**, *27*, 4438-4446.

[77] K.-Y. A. Lin, H.-A. Chang, *Journal of Materials Chemistry A* **2015**, *3*, 20060-20064.

[78] M. Ghani, R. M. Frizzarin, F. Maya, V. Cerdà, *Journal of Chromatography A* **2016**, *1453*, 1-9.

[79] S. Kovačič, M. Mazaj, M. Ješelnik, D. Pahovnik, E. Žagar, C. Slugovc, N. Z. Logar, *Macromolecular rapid communications* **2015**, *36*, 1605-1611.

3 PREPARATION OF RASPBERRY-LIKE ZIF-8/PS COMPOSITE SPHERES VIA DISPERSION POLYMERIZATION

This chapter is reprinted with permission from the paper published in *Dalton Transactions* (DOI: 10.1039/C5DT02627J) by *He Zhu, Qi Zhang, and Shiping Zhu.*

The idea was generated through discussion with the supervisor and the team members. He Zhu performed experiments, provided breakthroughs, and prepared the first draft, which was then revised by Dr. Qi Zhang and Dr. Shiping Zhu.

3.1 Abstract

Raspberry-like ZIF-8/PS composite spheres are prepared via dispersion polymerization of styrene with ZIF-8 and PVP as co-stabilizers. PVP is found to be crucial in determining morphology of the final product. It helps adherence of ZIF-8 nanoparticles to PS spheres. It is found that ZIF-8 nanoparticles thus prepared are partially embedded into PS sphere surfaces, resulting in a stable raspberry-like structure. Surface coverage of ZIF-8 can reach up to ~32%. The effects of ZIF-8 content and PVP concentration on the particle size and morphology are examined in detail with the mechanisms elucidated. The raspberry-like

spheres can be used as a template to grow thick ZIF-8 layers on the PS spheres through subsequent solvothermal treatment, leading to the formation of polymer-core MOF-shell structure.

3.2 Introduction

Organic-inorganic hybrid composites represent an emerging research area and attract rapidly growing interest. Silica and titanium dioxide are the most studied inorganic nanoparticles and have been incorporated with various polymers, resulting in different morphologies.[1-3] Dispersion polymerization is an important technique for single step fabrication of micrometer-sized particles and it is usually employed to prepare desired composite structures.[4,5] In the dispersion polymerization, monomer can be dissolved in solvent, while the resulting polymer is insoluble. As the reaction proceeds, polymer particles start to form and are stabilized by a stabilizer. If inorganic particles are used as the stabilizer, an organic-inorganic composite can thus be achieved.

Metal-organic frameworks (MOFs) are a class of porous crystalline materials, consisting of metal ions (or ion clusters) and organic bridging ligands. They have drawn great attention in the recent years due to their high porosity and tunable pore structure, superior surface area, and thermal stability, which have potential applications, such as gas separation,[6,7] gas storage,[8,9] chemical sensor,[10,11] catalysis,[12,13] and drug delivery.[14,15] An examination of the literatures reveals that most works focused on design and preparation of new MOFs with interesting chemical properties,[15-19] post-modification of existing MOFs,[20,21] and fabrication of MOF membranes.[7,22-27]

Recently, studies on the preparation of MOF-based organic-inorganic composites have drawn more and more attention. This represents a new approach to improve MOF performance rather than altering MOF chemical components. MOF/polymer composites are indeed of great interest but much less studied. Among the literature works, carboxylate-terminated polystyrene (PS) spheres were used to grow PS@ZIF-8 core-shell and ZIF-8 hollow microspheres through etching the polymer core.[28] Similar results were reported by Li and coworkers using monodispersed PS nanoparticles through a step-by-step self-assembly method.[29] Emulsion-based fabrication of MOF microcapsules was studied by Huo et al.. MOF/PS composite microcapsules were prepared through Pickering emulsion with MOF particles as the surfactant.[30]

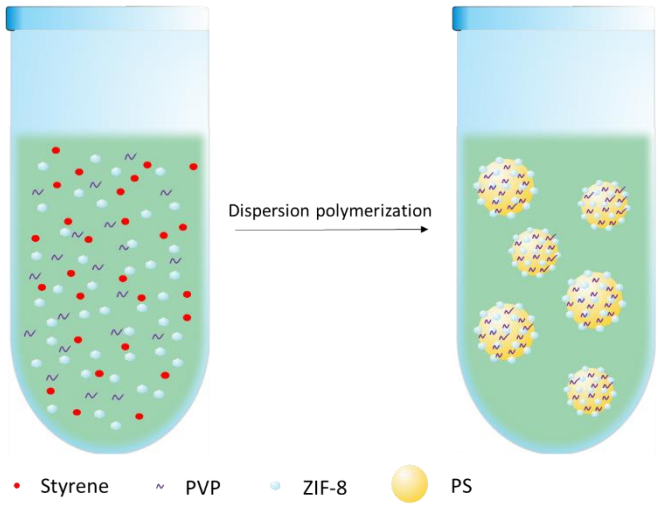

Figure 3-1. Schematic illustration for preparation of ZIF-8/PS composite spheres through dispersion polymerization of styrene with ZIF-8 and PVP as co-stabilizers.

Zeolitic imidazolate frameworks (ZIFs) are a family of MOFs with excellent thermal and chemical stabilities.[31] ZIF-8, as a prototype ZIF, has been prepared with different

sizes,[32] assembled into various structures,[33-35] and applied in many fields.[10,36,37] And recently, it has been used as Pickering surfactant to prepare ZIF-8/Polymer composite microcapsules,[30] which showed interfacial assembly potential of ZIF-8. In this paper, we report a facile method for the preparation of raspberry-like ZIF-8/PS organic-inorganic composite spheres through dispersion polymerization, using ZIF-8 and poly(vinylpyrrolidone) (PVP) as co-stabilizers. ZIF-8 nanoparticles stabilize PS particles when PS chains precipitate out from the dispersion polymerization, resulting in the final products having raspberry-like structure (**Figure 3-1**).

3.3 Experimental

Zinc nitrate hexahydrate (98 %), 2-methylimidazole (99 %), and poly(vinylpyrrolidone) (PVP) were purchased from Sigma-Aldrich and used without further purification. PVP has an average molecular weight of 10,000 g/mol. Styrene (99.9 %, Sigma) was passed through an inhibitor remover column and stored under freeze prior to use. Initiator 2,2'-azobis(2-methylpropionitrile) (AIBN) was purified by recrystallization. Other chemicals were commercially available and used as received.

ZIF-8 nanoparticles were synthesized using the precipitation method reported by Pan.[38] In brief, 1.17 g zinc nitrate hexahydrate and 22.7 g 2-methylimidazole were dissolved in 8 g and 80 g deionized water, respectively. The zinc nitrate solution was then slowly dropped into 2-methylimidazole solution under stirring. After 10 minutes, ZIF-8 crystals were collected by ultracentrifugation and washed 3 times with deionized water.

PS spheres were prepared via dispersion polymerization of styrene in methanol with PVP as the sole stabilizer. 0.01 g PVP and 0.1 g styrene were dissolved in 2 mL methanol. The mixture was bubbled with N2 under stirring for 30 minutes. AIBN (2.5 mg in 0.5 mL of methanol) was added. The reaction was conducted at 70 ℃ for 24 hours and the product was then mixed with 0.03 g ZIF-8 nanoparticles for 24 hours under shaking before SEM characterization.

ZIF-8/PS composite spheres were also prepared via the dispersion polymerization of styrene in methanol using a similar protocol. A typical procedure was as follows (Run #2 in **Table 3-1** as an example): 0.03 g ZIF-8 was dispersed in 2 ml methanol containing 0.01 g PVP by sonication for 20 minutes. 0.1 g styrene was then added. The mixture was bubbled with N2 under stirring for 30 minutes. AIBN (2.5 mg in 0.5 ml methanol) was added afterwards, the polymerization was then conducted at 70 ℃ for 24 hours. The crude product was centrifuged, the supernatant was decanted, and the precipitate was washed with methanol and water for 3 cycles. ZIF-8/PS composite spheres were soaked in a mixture of 1 M HCl aqueous solution and methanol (4/1, v/v) under stirring for 2 days to remove ZIF-8 nanoparticles from the raspberry-like composite spheres.

The solvothermal growth of raspberry-like composite spheres followed the reported protocol[39] with some modification: 0.0269 g zinc chloride, 0.0324 g 2-methylimidazole, and 0.0134 g sodium formate were dissolved in 10 ml methanol. Sample R #6 (see details in **Table 3-1**) was re-dispersed into the solution by sonication, which was heated up to 85 ℃ for a preset time period. The product was centrifuged and washed with methanol.

MOF particles and composite spheres were characterized by JEOL JSM 7000 Scanning Electron Microscopy (SEM) and JEOL-1200ex Transmission Electron Microscopy (TEM). Their particle sizes were analyzed by Nano Measure. Particle surface coverage was estimated using ImageJ. Powder X-ray diffraction was conducted on a Bruker SMART 6000 area detector. Thermogravimetric analyze (TGA) was performed on a TA Q5000 thermogravimetric analyzer with a ramp rate of 10 ℃/min.

3.4 Results and discussion

ZIF-8 nanoparticles with an average size of 50-100 nm were prepared using a previously reported precipitation method.[38] As a first try for the composite spheres in this work, ZIF-8 nanoparticles were simply mixed with PS spheres, which were pre-prepared by dispersion polymerization with PVP as the sole stabilizer. It was found that almost no ZIF-8 nanoparticles were attached to PS surface (**Figure 3-2A**). The dispersion polymerization of styrene was then carried out with ZIF-8 as the sole stabilizer (no PVP added). The reaction temperature was 70 ℃. AIBN of 2.5 wt.% with respect to the monomer was used as the initiator. SEM analysis of the dispersion product also showed bare PS particles with only a few ZIF-8 nanoparticles stuck to the surface (**Figure 3-2B**). This suggested that ZIF-8 did not favor adhesion to the PS particle surface. Finally, PVP was employed as a co-stabilizer to assist bridging ZIF-8 particles to PS sphere. PVP has been widely used as stabilizer for dispersion polymerization of styrene.[40,41] It has also been used in MOF synthesis via interfacial methods.[36] A quick run of the dispersion polymerization was then conducted, in the presence of both ZIF-8 and PVP (Sample R #2 in **Table 3-1**). The

raspberry-like PS spheres with ZIF-8 nanoparticles evenly distributed on the surface were finally observed, as shown in **Figure 3-2C**. TEM was also used to characterize the raspberry-like structure. The PS inner core and ZIF-8 outer seed were clearly evident (**Figure 3-2D**). Finally, XRD showed that the crystallinity of ZIF-8 particles was well maintained after the dispersion polymerization (**Figure 3-2E**). This experiment thus demonstrated feasibility of the method for preparation of raspberry-like ZIF-8/PS composite spheres via dispersion polymerization of styrene with ZIF-8 and PVP as co-stabilizers.

Table 3-1. Experimental conditions and results from the dispersion polymerization of styrene with ZIF-8 and PVP as stabilizer [a]

	ZIF-8 g	PVP g	Mean Diameter/μm [b]	Surface Coverage [c] %	MOF content [d] %
R #1	0.02	0.01	0.84 ± 0.32	28	24
R #2	0.03	0.01	0.98 ± 0.34	32	37
R #3	0.04	0.01	1.1 ± 0.4	32	44
R #4	0.05	0.01	1.1 ± 0.4	32	54
R #5	0.03	0.02	1.2 ± 0.4	31	35
R #6	0.03	0.03	1.2 ± 0.3	31	28
R #7	0.03	0.04	1.1 ± 0.4	30	27
R #8	0.03	0.05	0.98 ± 0.30	31	23

a) All runs were carried out with 0.1 g styrene, 2.5 mg AIBN and the required amount of stabilizer in the table in 2.5 mL methanol for 24 hours at 70 ℃; b) The mean diameter was calculated based on 100 randomly selected composite spheres using Nano Measure. c) The surface coverage was estimated by ImageJ based on 3 randomly selected areas (assuming flat surface). d) MOF content was estimated using TGA.

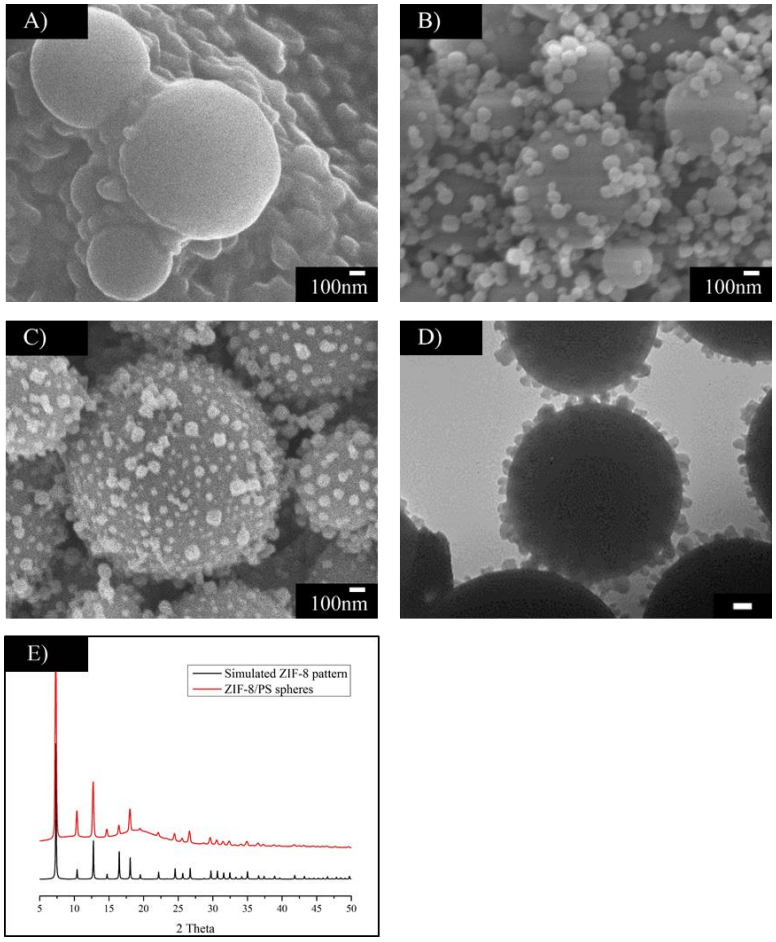

Figure 3-2. SEM and TEM images (scale bar: 100 nm) of PS spheres prepared by (A) simply mixing PS spheres with ZIF-8 particles; (B) dispersion polymerization of styrene with ZIF-8 (0.03 g) as stabilizer; (C, D) dispersion polymerization of styrene with ZIF-8 (0.03 g) and PVP (0.01 g) as co-stabilizers (R #2). (E) XRD pattern of the ZIF-8/PS sphere and simulated ZIF-8 particles.

Stability of the raspberry-like composite spheres was tested by sonication. **Figure 3-3A** shows the SEM image of sample R #2 after 1 hour sonication. The raspberry-like structure remained untouched, no obvious detachment of ZIF-8 nanoparticles was observed. It was found that ZIF-8 nanoparticles were partially embedded into PS spheres, which contributed to the stability. At an early stage of the dispersion polymerization, ZIF-8 nanoparticles

moved to PS sphere surfaces. When the sphere surface was soft, ZIF-8 nanoparticles partially penetrated into the surface (**Figure 3-3C**). As the reaction proceeded, PS spheres grew and became glassy, which made ZIF-8 nanoparticles difficult to attach. This was also the reason for the failed experiment of simply mixing ZIF-8 particles and PS spheres. There were no interactions between ZIF-8 nanoparticles and PS spheres. The penetration of ZIF-8 nanoparticles was confirmed by dissolution of ZIF-8 with a mixture of 1 M HCl and methanol solution (4/1, v/v). **Figure 3-3B** shows the bare PS surface with small pits where ZIF-8 nanoparticles resided.

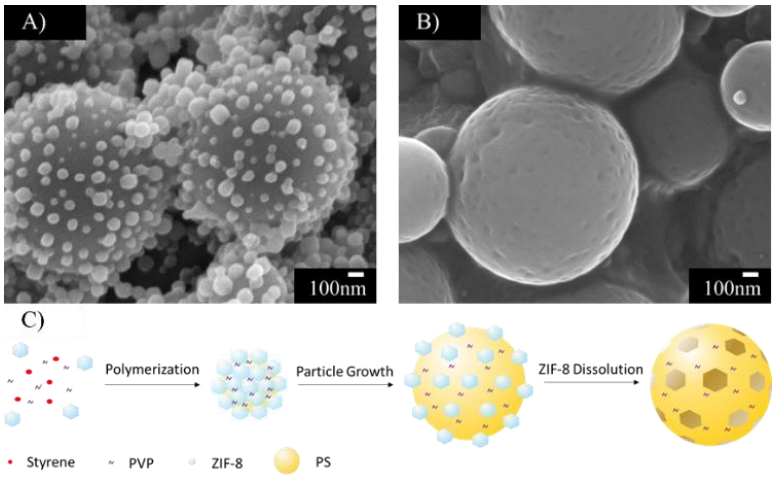

Figure 3-3. SEM images of sample R #2 after (A) 1 hour sonication; (B) dissolution of ZIF-8 nanoparticles. (C) Scheme of composite sphere growth and dissolution.

After proof of the concept, we studied the effects of ZIF-8 and PVP amounts on the composite preparation, as well as the resulting particle structures. In the first series of experiments, the polymerization runs were conducted with different amounts of ZIF-8 at a fixed amount of PVP (R #1-4 in **Table 3-1**), with the objective to find the influence of ZIF-

8 on composite spheres. **Figure 3-4** shows the SEM images of sample R #1-4 with their higher magnification images inserted at the top right corner. It could be clearly observed that all the four runs yielded the raspberry-like ZIF/PS composite spheres and the ZIF-8 nanoparticles were evenly distributed on the surface of PS spheres. The sizes of 100 randomly selected composite spheres were analyzed by Nano Measure. Meanwhile, ImageJ was used to estimate the surface coverage of MOF particles on PS surface, assuming flat the surface. The mean particle diameter and average surface coverage were then estimated from the measurements, as shown in **Table 3-1**. It was found that with the increase of ZIF-8 amount, the mean diameter of the spheres increased from 0.84 μm to 1.1 μm. This was probably because ZIF-8 nanoparticles took much PVP and thus reduced the PVP concentration in solution. Typically, lowering stabilizer concentration in dispersion polymerization would result in large polymer particles. With the increase of ZIF-8 amount, the surface coverage increased at the beginning from 28 % to 32 % (R #1 and R #2), followed by a level-off around 32 % (R #2 ~ R #4). The supernatant from centrifugation after the polymerization became turbid when the ZIF-8 amount reached 0.03 g, suggesting not all ZIF-8 nanoparticles attached to the surface. The ZIF-8 content was analyzed by TGA, which increased as the initial ZIF-8 ratio increased. The data were higher than the theoretical values, which was probably due to the incomplete conversion of styrene.

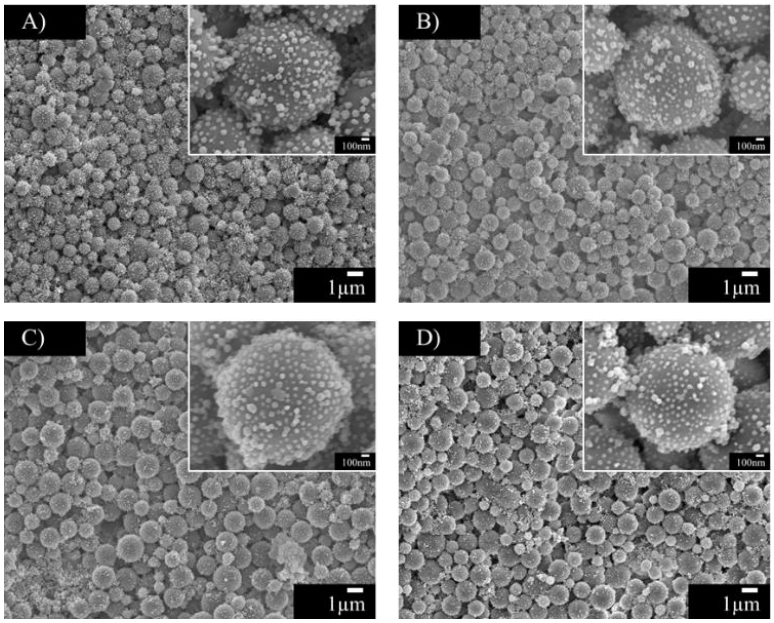

Figure 3-4. SEM images (scale bar: 1μm and 100 nm) of ZIF-8/PS composite particles with 0.01 g of PVP and different amount of ZIF-8. (A) 0.02 g (R #1); (B) 0.03 g (R #2); (C) 0.04 g (R #4); (D) 0.05 g (R #4).

Polymerization runs were also conducted with varying the PVP amount at a fixed ZIF-8 amount (R #2, 5-8 in **Table 3-1**), to investigate the influence of PVP on composite spheres. **Figure 3-5** shows SEM images of sample R #5-8 with their higher magnification images inserted at the top right corner. Similar results could be seen from the SEM images with varying ZIF-8 amount. The raspberry-like structures were clear and the distributions of ZIF-8 on the surface were uniform. The estimated average particle size and surface coverage data are included in **Table 3-1**. The mean diameter of the particles increased from 0.98 μm to 1.2 μm, and then gradually decreased to 0.98 μm. With the increased PVP amount, more and more ZIF-8 nanoparticles were wrapped by PVP molecules, which reduced the concentration of ZIF-8 nanoparticles as the stabilizer. An excess amount of

PVP would increase the concentration of PVP as the stabilizer in the system, leading to smaller PS spheres. However, the surface coverage changed little and remained around 32 % because of the fixed ZIF-8 amount. Similar to the first set of experiments, the ZIF-8 content was analyzed by TGA and decreased as the initial PVP content increased since more PVP was attached to the composite spheres.

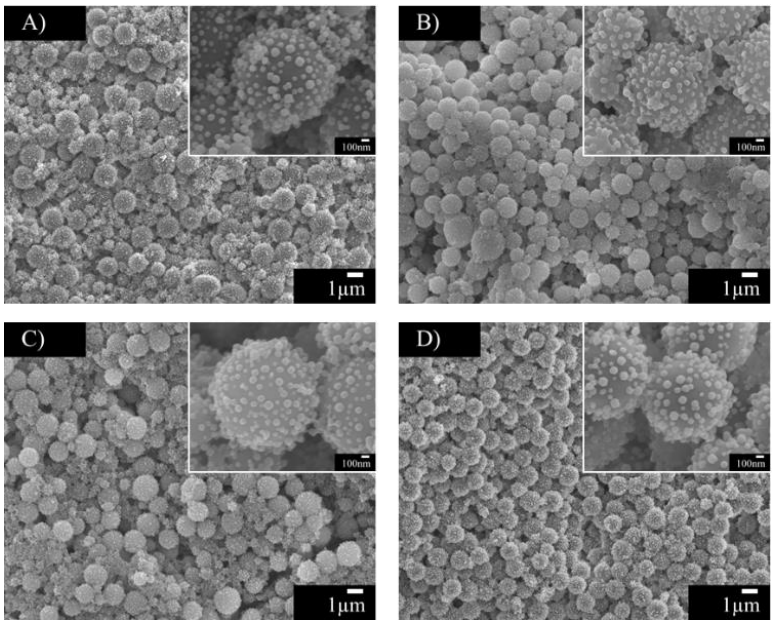

Figure 3-5. SEM images (scale bar: 1μm and 100 nm) of ZIF-8/PS composite particles with 0.03 g ZIF-8 and different amounts of PVP (A) 0.02 g (R #5); (B) 0.03 g (R #6); (C) 0.04 g (R #7); (D) 0.05 g (R #8).

The use of the PVP polymer and ZIF-8 nanoparticle as co-stabilizers in the dispersion polymerization of styrene made the mechanisms of stabilization very complex and interesting. PVP chains would first adsorb to ZIF-8 nanoparticles. From the above experimental observations, it appeared that free PVP, free ZIF-8 nanoparticle and ZIF-8/PVP nanoparticle could all act as stabilizer for PS precipitates from the dispersion

polymerization. The stabilization ability of the three was in the order of free PVP, free ZIF-8 and ZIF-8/PVP. ZIF-8/PVP nanoparticles were not as good as free PVP and free ZIF-8 in terms of stabilizing PS spheres. However, PVP chains adhered to ZIF-8 nanoparticles clearly helped bridging the ZIF-8 nanoparticle to PS spheres.

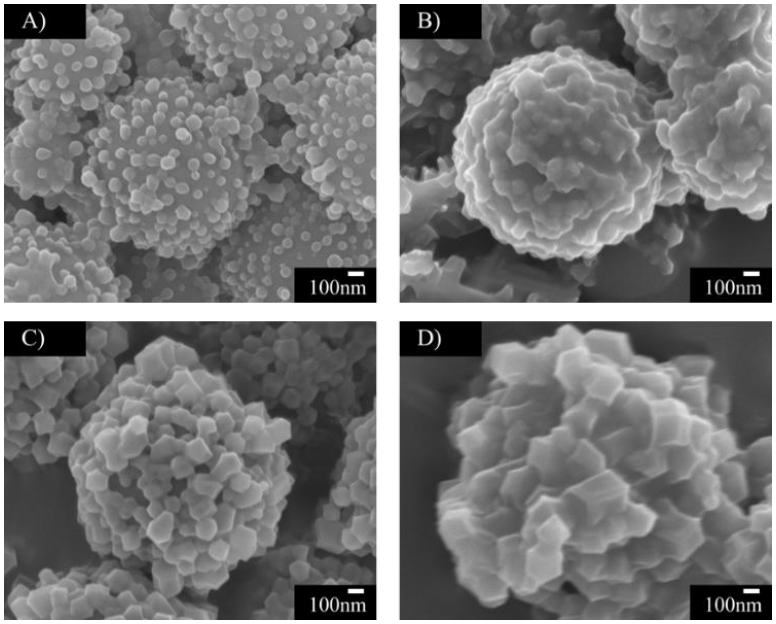

Figure 3-6. SEM images of PS/ZIF-8 core/shell particles prepared from Sample Run #6 via solvothermal reaction for (A) 0 minute; (B) 10 minutes; (C) 30 minutes; (D) 60 minutes.

The raspberry-like composite spheres could be used as a template for further MOF growing to form PS/ZIF-8 core/shell structures with a solvothermal method. ZIF-8 nanoparticles on PS surface served as seeds, growing into bigger sizes and finally forming intergrown ZIF-8 shell under certain conditions. Sample R #6 was taken as an example. SEM images obtained after certain period of time are shown in **Figure 3-6**. After 10 minutes of the reaction, the PS sphere surfaces were almost fully covered by ZIF-8 nanoparticles, forming the core-shell structure. With the reaction proceeded, ZIF-8 grains

grew bigger and the shell thickness increased. The inner PS cores could be removed after the seeded solvothermal growth to give ZIF-8 hollow spheres. Such hollow MOF particles have many potential applications.[42]

3.5 Conclusions

Raspberry-like ZIF-8/PS composite spheres have been successfully prepared by the dispersion polymerization of styrene in methanol, with ZIF-8 and PVP as co-stabilizers. The composite spheres are stable due to the partial impregnation of ZIF-8 nanoparticles into the PS spheres. The composite sphere size is influenced by the added ZIF-8 and PVP amounts. Increasing ZIF-8 content at a fixed PVP level increases the sphere size. Increasing PVP concentration at a fixed ZIF-8 content also increases the sphere size but excessive PVP would also decrease the size. This is because free PVP chains, free ZIF-8 nanoparticles and combined ZIF-8/PVP nanoparticles could all act as stabilizer for PS precipitates from the dispersion polymerization of styrene. The free PVP and free ZIF-8 are more effective than ZIF-8/PVP in stabilizing PS spheres. However, the combined PVP help adherence of ZIF-8 nanoparticles to PS spheres. The maximum PS sphere surface coverage with ZIF-8 nanoparticles is around 31-32%. The raspberry-like composite spheres thus prepared could be used as a template for further growth of the MOF material from PS spheres, facilitating preparation of PS/ZIF-8 core/shell structure with the solvothermal method.

3.6 Acknowledgements

We sincerely thank the Natural Sciences and Engineering Research Council (NSERC) of Canada and the Canada Research Chair (CRC) program of the Federal Government for supporting this research work.

3.7 References

[1] M. Chen, L. Wu, S. Zhou, B. You, *Macromolecules* **2004**, *37*, 9613-9619.

[2] T. Chen, P. J. Colver, S. A. Bon, *Advanced Materials* **2007**, *19*, 2286-2289.

[3] L. A. Fielding, O. O. Mykhaylyk, A. Schmid, D. Pontoni, S. P. Armes, P. W. Fowler, *Chemistry of Materials* **2014**, *26*, 1270-1277.

[4] S.-W. Zhang, S.-X. Zhou, Y.-M. Weng, L.-M. Wu, *Langmuir* **2005**, *21*, 2124-2128.

[5] A. Schmid, S. Fujii, S. P. Armes, C. A. Leite, F. Galembeck, H. Minami, N. Saito, M. Okubo, *Chemistry of materials* **2007**, *19*, 2435-2445.

[6] H. T. Kwon, H.-K. Jeong, *Journal of the American Chemical Society* **2013**, *135*, 10763-10768.

[7] Q. Liu, N. Wang, J. r. Caro, A. Huang, *Journal of the American Chemical Society* **2013**, *135*, 17679-17682.

[8] A. R. Millward, O. M. Yaghi, *Journal of the American Chemical Society* **2005**, *127*, 17998-17999.

[9] R. Sabouni, H. Kazemian, S. Rohani, *Microporous and Mesoporous Materials* **2013**, *175*, 85-91.

[10]G. Lu, J. T. Hupp, *Journal of the American Chemical Society* **2010**, *132*, 7832-7833.

[11] J. Liu, F. Sun, F. Zhang, Z. Wang, R. Zhang, C. Wang, S. Qiu, *Journal of Materials Chemistry* **2011**, *21*, 3775-3778.

[12] Y. Lee, S. Kim, J. K. Kang, S. M. Cohen, *Chemical Communications* **2015**, 51, 5735-5738.

[13] M. J. Katz, S.-Y. Moon, J. E. Mondloch, M. H. Beyzavi, C. J. Stephenson, J. T. Hupp, O. K. Farha, *Chemical Science* **2015**, 6, 2286-2291.

[14] P. Horcajada, T. Chalati, C. Serre, B. Gillet, C. Sebrie, T. Baati, J. F. Eubank, D. Heurtaux, P. Clayette, C. Kreuz, *Nature materials* **2010**, *9*, 172-178.

[15] L. Cooper, T. Hidalgo, M. Gorman, T. Lozano-Fernández, R. Simón-Vázquez, C. Olivier, N. Guillou, C. Serre, C. Martineau, F. Taulelle, *Chemical Communications* **2015**, 51, 5848-5851.

[16] E.-L. Zhou, C. Qin, K.-Z. Shao, Z.-M. Su, *Journal of Materials Chemistry A* **2015**, 3, 7224-7228.

[17] A. K. Crane, N. G. White, M. J. MacLachlan, *CrystEngComm* **2015**, *17*, 4912-4918.

[18] B. D. Chandler, D. T. Cramb, G. K. Shimizu, *Journal of the American Chemical Society* **2006**, *128*, 10403-10412.

[19] K. Liu, B. Li, Y. Li, X. Li, F. Yang, G. Zeng, Y. Peng, Z. Zhang, G. Li, Z. Shi, S. Feng, D. Song, *Chemical Communications* **2014**, *50*, 5031-5033.

[20] M. Kim, J. F. Cahill, Y. Su, K. A. Prather, S. M. Cohen, *Chemical Science* **2012**, *3*, 126-130.

[21] H. Liu, H. Zhu, S. Zhu, *Macromolecular Materials and Engineering* **2015**, 300, 191-197.

[22] R. Ameloot, F. Vermoortele, W. Vanhove, M. B. Roeffaers, B. F. Sels, D. E. De Vos, *Nature chemistry* **2011**, *3*, 382-387.

[23] H. Lu, S. Zhu, *European Journal of Inorganic Chemistry* **2013**, *2013*, 1294-1300.

[24] I. Hod, W. Bury, D. M. Karlin, P. Deria, C. W. Kung, M. J. Katz, M. So, B. Klahr, D. Jin, Y. W. Chung, *Advanced Materials* **2014**, *26*, 6295-6300.

[25] H. Zhu, S. Zhu, *The Canadian Journal of Chemical Engineering* **2015**, *93*, 63-67.

[26] H. Zhu, H. Liu, I. Zhitomirsky, S. Zhu, *Materials Letters* **2015**, *142*, 19-22.

[27] O. Shekhah, H. Wang, S. Kowarik, F. Schreiber, M. Paulus, M. Tolan, C. Sternemann, F. Evers, D. Zacher, R. A. Fischer, *Journal of the American Chemical Society* **2007**, *129*, 15118-15119.

[28] H. J. Lee, W. Cho, M. Oh, *Chemical Communications* **2012**, *48*, 221-223.

[29] A.-L. Li, F. Ke, L.-G. Qiu, X. Jiang, Y.-M. Wang, X.-Y. Tian, *CrystEngComm* **2013**, *15*, 3554-3559.

[30] J. Huo, M. Marcello, A. Garai, D. Bradshaw, *Advanced Materials* **2013**, *25*, 2717-2722.

[31] K. S. Park, Z. Ni, A. P. Côté, J. Y. Choi, R. Huang, F. J. Uribe-Romo, H. K. Chae, M. O'Keeffe, O. M. Yaghi, *Proceedings of the National Academy of Sciences* **2006**, *103*, 10186-10191.

[32] J. Cravillon, R. Nayuk, S. Springer, A. Feldhoff, K. Huber, M. Wiebcke, *Chemistry of Materials* **2011**, *23*, 2130-2141.

[33]M. Tsotsalas, A. Umemura, F. Kim, Y. Sakata, J. Reboul, S. Kitagawa, S. Furukawa, *Journal of Materials Chemistry* **2012**, *22*, 10159-10165.

[34] N. Yanai, S. Granick, *Angewandte Chemie* **2012**, *124*, 5736-5739.

[35] N. Yanai, M. Sindoro, J. Yan, S. Granick, *Journal of the American Chemical Society* **2012**, *135*, 34-37.

[36] Y. Yang, F. Wang, Q. Yang, Y. Hu, H. Yan, Y.-Z. Chen, H. Liu, G. Zhang, J. Lu, H.-L. Jiang, *ACS applied materials & interfaces* **2014**, *6*, 18163-18171.

[37] O. Shekhah, R. Swaidan, Y. Belmabkhout, M. du Plessis, T. Jacobs, L. J. Barbour, I. Pinnau, M. Eddaoudi, *Chemical Communications* **2014**, *50*, 2089-2092.

[38] Y. Pan, Y. Liu, G. Zeng, L. Zhao, Z. Lai, *Chemical Communications* **2011**, *47*, 2071-2073.

[39] H. Bux, A. Feldhoff, J. Cravillon, M. Wiebcke, Y.-S. Li, J. Caro, *Chemistry of Materials* **2011**, *23*, 2262-2269.

[40] C. Tseng, Y. Lu, M. El‐Aasser, J. Vanderhoff, *Journal of Polymer Science Part A: Polymer Chemistry* **1986**, *24*, 2995-3007.

[41] E. Bourgeat-Lami, J. Lang, *Journal of Colloid and Interface Science* **1998**, *197*, 293-308.

[42] S. Furukawa, J. Reboul, S. Diring, K. Sumida, S. Kitagawa, *Chemical Society Reviews* **2014**, *43*, 5700-5734.

4 MOFSOME VIA TRANSIENT PICKERING EMULSION TEMPLATE

This chapter is reprinted with permission from the paper published in *Advanced Materials Interfaces* (DOI: 10.1002/admi.201600294) by *He Zhu, Qi Zhang, and Shiping Zhu.*

The idea was generated through discussion with the supervisor and the team members. He Zhu performed experiments, provided breakthroughs, and prepared the first draft, which was then revised by Dr. Qi Zhang and Dr. Shiping Zhu.

4.1 Paper body

Colloidosomes, are usually prepared from the self-assembly of colloidal particles at an oil-water interface in emulsions. They are three dimensional hollow spheres consisting of close-packed colloidal particles as shell. Various particles have been prepared into colloidosomes, such as polymer particles,[1-6] iron oxide,[7,8] silicon dioxide,[9-12] quantum dots,[13,14] noble metal,[15,16] and mixture of these particles.[17-19] The hollow structure and the semi-permeability, resulted from the interstices between colloidal particles, have made colloidosomes promising in such applications as catalysis,[4,20] encapsulation,[21,22] and delivery vehicles.[10,23] The recent development of collodosomes fabricated from highly

functional particles has further broadened the potential applications of these materials in sensors, photothermal therapy, and microreactor.[15,16]

Metal-organic frameworks (MOF) are crystalline materials self-assembled from metal ions and organic bridging ligands. They represent an emerging class of highly functional particular materials having high porosity, large surface area, tunable pore structure, high thermal stability, and mild synthetic conditions.[24,25] MOFs have been intensively studied for various applications, such as catalysis,[26,27] gas adsorption and storage,[28,29] chemical separation,[30-33] sensors,[34,35] solar cell,[36,37] pollutant treatment,[38,39] and so on. The design and synthesis of new MOFs have progressed very rapidly over the years. Various MOF particles are synthesized and demonstrated to possess desired properties for targeted applications. However, most of the demonstrated properties are based on single particles, which must be fabricated into various ordered shapes and morphologies for real commercial exploitations. Unfortunately, it is challenging to process and manipulate MOF particles, as a building block, for various desired forms and architectures.

MOF-based membranes are well studied and they can be prepared by different methods.[40-44] However, it is still difficult to fabricate MOF particles into more complex structures, because of the very limited spatial control over the particles.[45] So far, there are only several approaches developed for preparation of MOF superstructures, including electric field induced MOF alignment,[46] Langmuir-Blodgett technique,[47,48] direct solvent evaporation method,[49] electrophoretic deposition,[50,51] and emulsion[52] and dispersion polymerization template.[53]

MOFsomes fabricated from MOF particles represent an emerging type of colloidosomes. This type of superstructures can significantly expand the range of potential applications for MOF materials. The assembly of single MOF particles in MOFsomes introduces the periodical pores besides the regular interstices, as well as the intrinsic functionalities that the single MOF particle possesses. To the best of our knowledge, there was only a single report in the literature on the preparation of MOFsomes, which is through a bottom-up strategy.[54] However, the development of top-down methods is of great importance, especially when it comes to harsh conditions are required when preparing MOF particles, where bottom-up methods are not applicable. Inspired by the work on gold colloidosomes,[15] herein, we introduce an alternative facile top-down approach for fabrication of multi-wall MOFsomes from UiO-66 (University of Oslo-66), a well-known type of MOF materials which have been investigated for various potential applications.[55-59] Moreover, a second type of particles, including MIL-96 (Material Institute de Lavoisier-96), silicon dioxide, and titanium dioxide, are incorporated as additional building blocks into the MOFsomes, achieving various types of multicomponent and multifunctional colloidosomes.

Colloidal UiO-66 particles were synthesized according to a reported protocol with minor modification.[60] Scanning electron microscopy (SEM) revealed the cubic structure of UiO-66 particles (Figure S4-1). The particles showed a zeta potential of -30.34 ± 0.06 mV, indicating a good colloidal stability.

In order to prepare MOFsome, 8 mg UiO-66 particles were first dispersed in 0.4 mL water under ultrasonication. Then 4 mL 1-butanol was added slowly to the suspension,

followed by a homogenizing procedure at a speed of 3,000 rpm for 15 seconds. UiO-66 particles absorbed spontaneously at the water/oil interface, driven by the minimization of the total interfacial free energy.[61,62] It yielded a UiO-66 stabilized water-in-oil Pickering emulsion. However, due to the partial solubility of water in 1-butanol (~19.7%), water gradually diffused out into 1-butanol phase through the interface, leading to the shrinkage of the water droplet. The formed UiO-66 particle layer was thus compressed due to their tendency of residing at the water/oil interface, resulting in a closely packed UiO-66 layer. Once the first layer particles could not be compressed anymore, a second layer was formed on the first layer as the diffusion of water continued, followed by third layer, forth layer, etc., until the depletion of all MOF particles in the water droplet (**Figure 4-1**). The formed MOFsome particles precipitated out and collected by decanting the water/1-butanol mixture. The system formed a water-in-oil Pickering emulsion at the start, but it finally became homogeneous. This method is thus named as the transient Pickering emulsion.

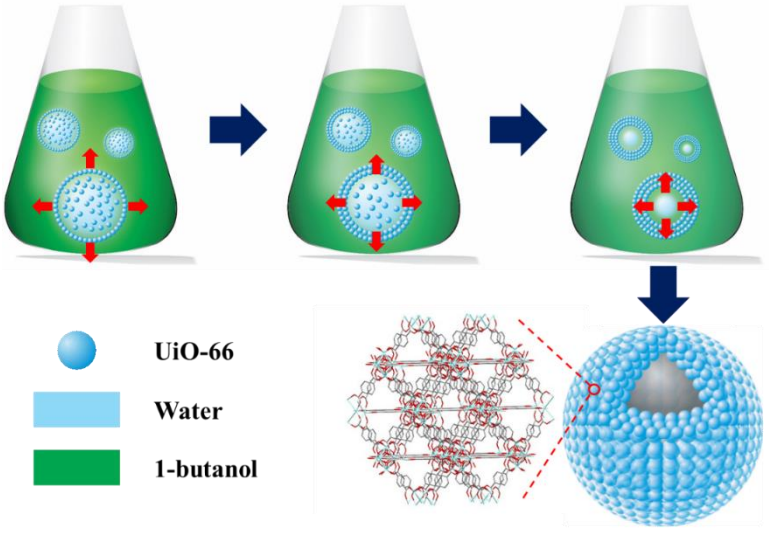

Figure 4-1. Fabrication of MOFsome via transient Pickering emulsion template.

The formed MOFsomes were characterized by X-ray diffraction (XRD), which showed the same pattern as the simulated and as-synthesized MOF particles (Figure S4-2), indicating the retention of UiO-66 particles. The morphology was revealed by SEM. A spherical MOFsome structure was clearly observed (**Figure 4-2**A & 4-2B). The resulted MOFsome had a broad size distribution (Figure 4-2A), attributed to limitations of the conventional emulsion method. The size ranged from several micrometers to tens of micrometers. Figure 4-2B shows a perfect spherical MOFsome structure with a diameter of ~15 μm. The high-magnification SEM imaging revealed that the MOFsome surface consisted of closely packed cubic UiO-66 particles (Figure 4-2C). Most MOFsomes had intact spherical structures with only a few exhibiting chipped structures (Figure 4-2D). The broken structures confirmed the characteristic features of internally hollow multilayer-shell MOFsomes.

In order to control the size of MOFsomes, a mixing solvent method was applied based on the second law of thermodynamics (See Experimental Section). A methanol-water mixture was used to disperse UiO-66 particles before applying the shear force. Three methanol-water compositions (methanol : water = 5 : 95, 10 : 90, 15 : 85, in weight) were investigated. Similar to the results of the pure water system, the MOFsomes had an intact perfect spherical structure with a few partially broken (Figure 4-2E, 4-2F, & 4-2G). The hollow feature was confirmed by SEM images of the broken MOFsomes, as well as by the scanning transmission electron microscopy (STEM) line scan of the intact spherical MOFsomes (Figure S4-3). A diameter histogram of 100 randomly selected MOFsomes demonstrated that the portion of large MOFsomes decreased as the methanol ratio

increased (Figure S4-4), attributed to the decreased surface tension of the methanol-water mixture (from 62.77 to 56.18 to 51.17 mN/m at 25 ºC).[63] The estimated average diameter data were depicted in Figure 4-2H & Figure S4-5D. The calculated average mean diameter showed anticipated trend, however, due to the conventional emulsion nature of the system, the size of the MOFsomes distributed broadly, leading to a large standard error, making the conclusion less evident. Future work will be focusing on figuring out a method to narrow the distribution in order to get a clearer evidence. Furthermore, we also demonstrated control of the shell thickness by varying the UiO-66 particle concentration. As shown in Figure 4-2 and Figure S4-5, when the UiO-66 amount increased from 1% to 2%, the corresponding shell thickness increased from about 1-3 μm to 4-8 μm, since more UiO-66 particles were assembled at the interfaces.

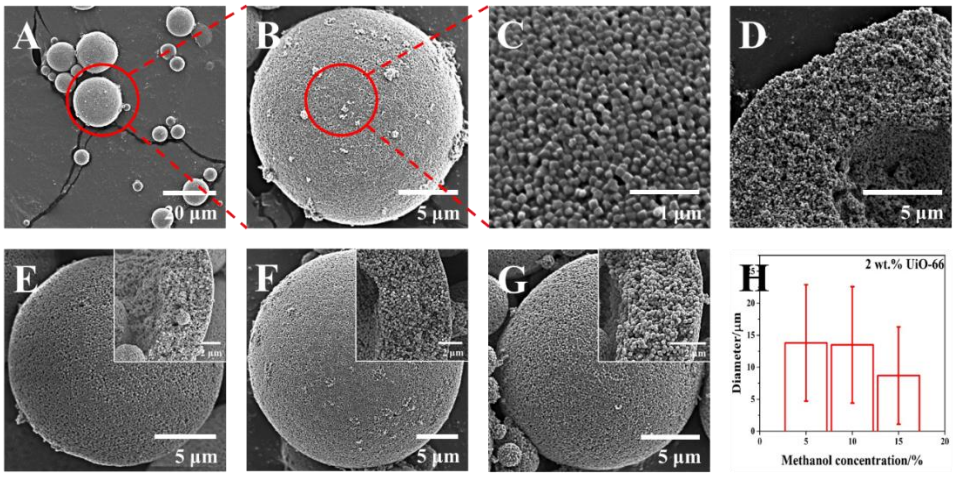

Figure 4-2. SEM images of MOFsomes formed with 2% UiO-66 in A, B, C, D) water, E) 5% methanol/water, F) 10% methanol/water, G) 15% methanol/water, H) estimated average diameter based on 100 randomly selected MOFsome prepared from 2% UiO-66 and different methanol concentration.

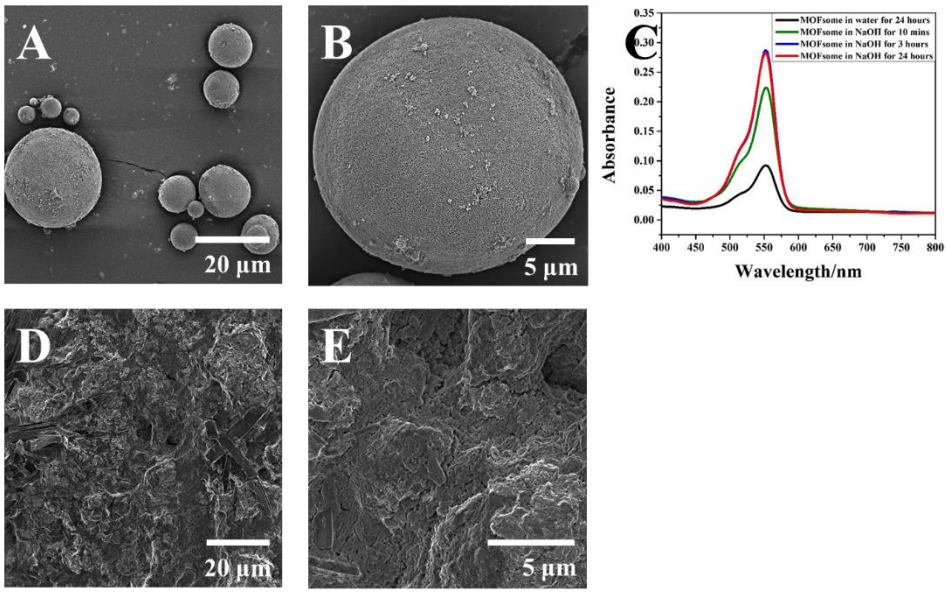

Figure 4-3. SEM images of A, B) MOFsomes washed with water and re-dispersed in water after 7 days, D, E) MOFsomes washed with water and re-dispersed in 1 N NaOH after 1 day. C) UV adsorption of dye release for MOFsomes dispersed in water and NaOH.

The stability of the prepared MOFsomes was tested by washing the samples twice with water and by soaking them in water for 7 days. SEM images showed no obvious disassembly of the spherical structure, which confirmed robustness of the obtained MOFsomes (**Figure 4-3**A & 4-3B). The dye encapsulation and stimuli-responsive release of the MOFsomes were then conducted to demonstrate a potential possibility of using this type of materials. Rhodamine B (RB) was dissolved in water prior to preparation of the MOFsomes. The obtained dye-encapsulated MOFsomes were washed with water and then re-dispersed either in water or in 1 N sodium hydroxide. The MOFsomes soaked in water showed little RB release after 24 hours, which was probably due to the release of adsorbed RB molecules on the surface layers of

MOFsomes, while MOFsomes soaked with sodium hydroxide released significant amount of encapsulated dye within the first 10 minutes. After 3 hours, almost all of the encapsulated dye was released, since its spectrum was the same as that of the MOFsomes soaked for 24 hours (Figure 4-3C). This burst release was due to disassembly of the MOFsome structure (Figure 4-3D & 4-3E), since UiO-66 is known to be sensitive to base and it decomposes under alkaline condition.[64]

Interestingly, we also found that the UiO-66 based MOFsomes could be used as a general platform to build multicomponent and multifunctional colloidosomes. Introducing a second type of particles having distinct physical and chemical properties could further expand potentials of the colloidosomes. Three different particle types, including MIL-96, titanium dioxide, and silicon dioxide, were incorporated into the MOFsomes prepared in this work (**Figure 4-4**). Figure 4-4A, B, & C shows the hybrid colloidosomes consisted of UiO-66 and MIL-96. The smaller cubes were UiO-66 particles while the bigger darker polyhedral particles were MIL-96 crystals. The MIL-96 particles were well separated from each other by the UiO-66 particles. Figure 4-4D, E, & F shows the UiO-66/TiO_2 hybrid colloidosomes. The tiny particles were TiO_2, which were less than 100 nm, while the bigger cubes were UiO-66 particles. Figure 4-4G, H, & I shows the hybrid colloidosomes containing UiO-66 and SiO_2. These two particles shared the same size but differed from each other in shape. The spherical particles were SiO_2 while UiO-66 were cubic.

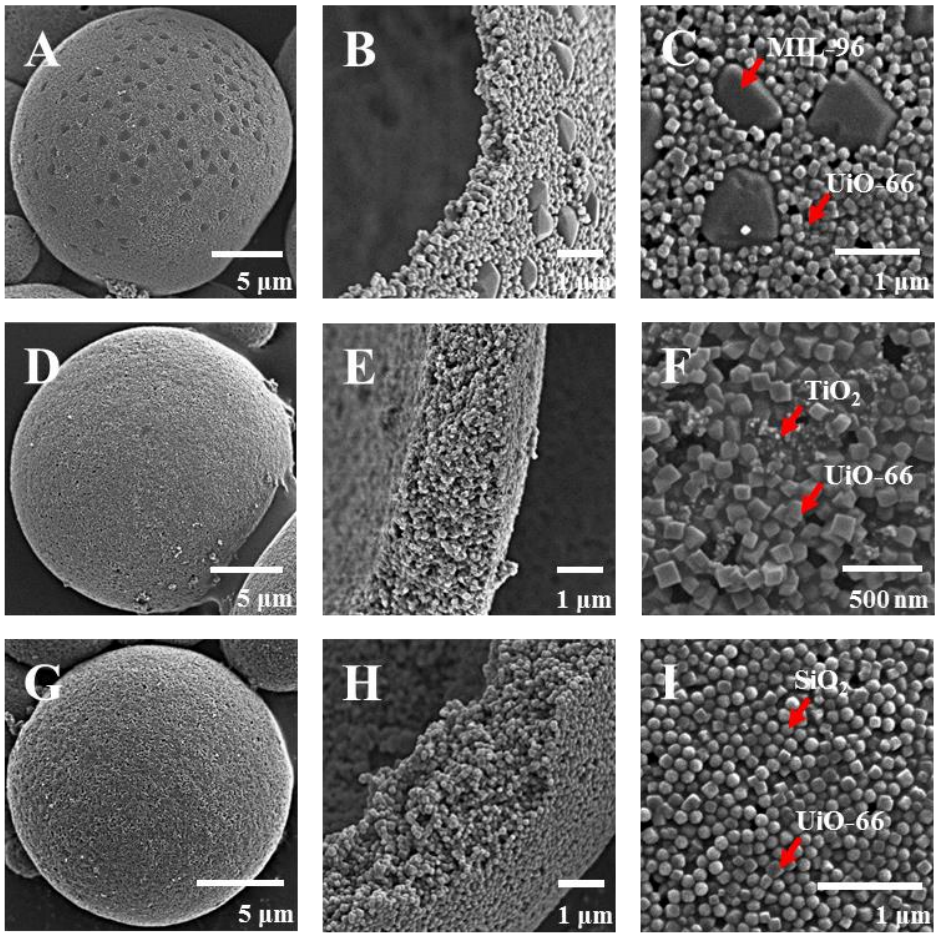

Figure 4-4. SEM images of multicomponent and multifunctinoal colloidosomes with 10% methanol, 1.5% UiO-66, and A, B, C) 0.5% MIL-96, D, E, F) 0.5% titanium dioxide, G, H, I) 0.05% silicon dioxide.

Similar to the single-component UiO-66 MOFsomes, the multicomponent colloidosomes remained the intact spherical structure. The incorporation of the second type of particles did not affect the formation of colloidosomes. SEM images of the surfaces and chipped edges showed that the second particles were randomly distributed within the shell. All the observed colloidosomes contained multiple components. To our best knowledge, there have been very few reports in the literature about combining two or more types of

particles in colloidosomes, while the combinations could be of great importance.[17-19] Therefore, this one-pot method paves the way for fabrication of multicomponent and multifunctional colloidosomes.

In summary, for the first time, we introduced a top-town transient Pickering emulsion templating method for the preparation of MOFsomes. The prepared MOFsomes have spherical structure with a multilayered shell. The size of the MOFsome seems to be controlled by varying surface tension between the two phases through mixing different types of solvents but needs further confirmation. The shell thickness can be regulated by changing MOF concentration. Finally, this type of MOFsomes can be used as a general platform for the preparation of multicomponet and multifunctional colloidosomes.

4.2 Experimental Section

Materials. Zirconium chloride (≥99.5%), terephthalic acid (98%), acetic acid (≥99.7%), aluminum nitrate nonahydrate (≥98%), trimesic acid (95%), Rhodamine B (≥95%), silicon dioxide (0.15 μm), and titanium dioxide (mixture of rutile and anatase, <150 nm) were purchased from Sigma-Aldrich and used without further purification. Other solvents were commercially available and used as received. The water was purified with a Barnstead Nanopure Diamond system first before any usage.

MOF synthesis. UiO-66 particles was prepared according to the reported protocol with minor modification.[60] Briefly, 915 mg of zirconium chloride and 645 mg of benzen-1,4-dicarboxylic acid were dissolved in the mixture of 225 mL dimethylformamide (DMF) and

6.7 mL acetic acid. The solution was then kept at 120 ^{o}C using an oil bath for 20 hours. The products were collected by centrifuge and washed with methanol 3 times.

MIL-96 particles was prepared according to the reported protocol with minor modification.[65] Briefly, 0.375 g of aluminum nitrate nonahydrate and 0.21 g of trimesic acid were dissolved in 14.43 mL and 10 mL mixture of water and DMF, respectively. Then 0.57 mL of acetic acid was added to the metal ion solution. The two solutions were mixed together and transferred to an oven under 130 ^{o}C for 24 hours. The products were collected by centrifuge and washed with methanol for 3 times.

MOFsome preparation. In a typical recipe, 8 mg UiO-66 was dispersed in 0.4 mL water or 0.4 mL methanol/water mixture (~2% particle content). 4 mL 1-butanol was slowly added to the suspension afterwards. Then the mixture was homogenized under 3,000 rpm for about 15 seconds and put still for 24 hours before any further tests.

Dye encapsulation and release. The recipe was the same as the normal MOFsome preparation (methanol : water = 10 : 90), except that 0.1 mg mL^{-1} Rhodamine B aqueous solution was used instead of water. It should be noted that not all dye molecules were encapsulated due to the fast exchange between water and 1-butanol. The prepared dye-encapsulated MOFsomes were washed with water twice, and re-dispersed either in 2 mL water or in 2 mL 1 N NaOH in order to test the dye release behavior.

Multicomponent colloidosome preparation. Similar to the procedure of the above MOFsome preparation, 1.5% UiO-66 and a second type of particle (0.5% MIL-96, 0.5% TiO_2, 0.05% SiO_2) were dispersed in methanol/water mixture (10% methanol). 4 mL 1-

butanol was slowly added to the suspension afterwards. Then the mixture was homogenized under 3,000 rpm for about 15 seconds and put still for 24 hours before any further tests.

Characterization. JEOL JSM 7000 Scanning Electron Microscopy (SEM) and JEOL 2010F field emission Transmission Electron Microscope (TEM) were used to characterize the UiO-66 particles, MOFsomes, and multicomponent colloidosomes. X-ray diffraction (XRD) was carried out on the Cu SMART6000 rotating anode diffractometer. Zeta potential of the UiO-66 particles was obtained on Brookhaven Instruments PALS Zeta Potential Analyzer. UV adsorption of the dye containing water was determined by DU 800 UV/Vis Spectrophotometer.

Mixing Solvent Method. Based on the second law of thermodynamics, the change of free energy before and after the emulsion forms can be expressed as:

$$\Delta G^{form} = \Delta A \gamma_{12} - T\Delta S^{conf},$$

where ΔG^{form} is the change of free energy, ΔA is the change of surface area, γ_{12} is the surface tension, T is temperature, and ΔS^{conf} is the configurational entropy.[66] Under most circumstances, the first term is far more significant than the second, thus

$$\Delta G^{form} = \Delta A \gamma_{12}.$$

Therefore, at a given energy in the emulsion preparation, a decreased surface tension between two phases is compensated by an increase in the surface area through the formation of smaller droplets.

4.3 Acknowledgements

We sincerely thank the Natural Sciences and Engineering Research Council (NSERC) of Canada and the Canada Research Chair (CRC) program of the Federal Government for supporting this research work.

4.4 References

[1] A. Dinsmore, M. F. Hsu, M. Nikolaides, M. Marquez, A. Bausch, D. Weitz, *Science* **2002**, *298*, 1006-1009.

[2] L. M. Croll, H. D. Stöver, *Langmuir* **2003**, *19*, 5918-5922.

[3] P. F. Noble, O. J. Cayre, R. G. Alargova, O. D. Velev, V. N. Paunov, *Journal of the American Chemical Society* **2004**, *126*, 8092-8093.

[4] Z. Wang, M. van Oers, F. P. Rutjes, J. van Hest, *Angewandte Chemie International Edition* **2012**, *51*, 10746-10750.

[5] K. L. Thompson, P. Chambon, R. Verber, S. P. Armes, *Journal of the American Chemical Society* **2012**, *134*, 12450-12453.

[6] O. D. Velev, K. Furusawa, K. Nagayama, *Langmuir* **1996**, *12*, 2374-2384.

[7] H. Duan, D. Wang, N. S. Sobal, M. Giersig, D. G. Kurth, H. Möhwald, *Nano letters* **2005**, *5*, 949-952.

[8] B. Samanta, D. Patra, C. Subramani, Y. Ofir, G. Yesilbag, A. Sanyal, V. M. Rotello, *Small* **2009**, *5*, 685-688.

[9] D. Lee, D. A. Weitz, *Small* **2009**, *5*, 1932-1935.

[10] S. Li, B. A. Moosa, J. G. Croissant, N. M. Khashab, *Angewandte Chemie* **2015**, *127*, 6908-6912.

[11] H. Wang, X. Zhu, L. Tsarkova, A. Pich, M. Möller, *Acs Nano* **2011**, *5*, 3937-3942.

[12] I. Akartuna, E. Tervoort, A. R. Studart, L. J. Gauckler, *Langmuir* **2009**, *25*, 12419-12424.

[13] Y. Lin, H. Skaff, T. Emrick, A. Dinsmore, T. Russell, *Science* **2003**, *299*, 226-229.

[14] H. Skaff, Y. Lin, R. Tangirala, K. Breitenkamp, A. Böker, T. P. Russell, T. Emrick, *Advanced Materials* **2005**, *17*, 2082-2086.

[15] D. Liu, F. Zhou, C. Li, T. Zhang, H. Zhang, W. Cai, Y. Li, *Angewandte Chemie International Edition* **2015**, *54*, 9596-9600.

[16] G. C. Phan‐Quang, H. K. Lee, I. Y. Phang, X. Y. Ling, *Angewandte Chemie* **2015**, *127*, 9827-9831.

[17] X.-W. Xu, X.-M. Zhang, C. Liu, Y.-L. Yang, J.-W. Liu, H.-P. Cong, C.-H. Dong, X.-F. Ren, S.-H. Yu, *Journal of the American Chemical Society* **2013**, *135*, 12928-12931.

[18] T. Bollhorst, S. Shahabi, K. Wörz, C. Petters, R. Dringen, M. Maas, K. Rezwan, *Angewandte Chemie* **2015**, *127*, 120-125.

[19] D. Lee, D. A. Weitz, *Advanced Materials* **2008**, *20*, 3498-3503.

[20] C. Zhang, C. Hu, Y. Zhao, M. Möller, K. Yan, X. Zhu, *Langmuir* **2013**, *29*, 15457-15462.

[21] P. H. Keen, N. K. Slater, A. F. Routh, *Langmuir* **2012**, *28*, 16007-16014.

[22] P. H. Keen, N. K. Slater, A. F. Routh, *Langmuir* **2014**, *30*, 1939-1948.

[23] O. J. Cayre, J. Hitchcock, M. S. Manga, S. Fincham, A. Simoes, R. A. Williams, S. Biggs, *Soft Matter* **2012**, *8*, 4717-4724.

[24] U. Mueller, M. Schubert, F. Teich, H. Puetter, K. Schierle-Arndt, J. Pastre, *Journal of Materials Chemistry* **2006**, *16*, 626-636.

[25] S. T. Meek, J. A. Greathouse, M. D. Allendorf, *Advanced Materials* **2011**, *23*, 249-267.

[26] Y. Liu, S.-Y. Moon, J. T. Hupp, O. K. Farha, *ACS nano* **2015**, *9*, 12358- 12364.

[27] J. E. Mondloch, M. J. Katz, W. C. Isley III, P. Ghosh, P. Liao, W. Bury, G. W. Wagner, M. G. Hall, J. B. DeCoste, G. W. Peterson, *Nature materials* **2015**, *14*, 512-516.

[28] A. R. Millward, O. M. Yaghi, *Journal of the American Chemical Society* **2005**, *127*, 17998-17999.

[29]J. A. Mason, J. Oktawiec, M. K. Taylor, M. R. Hudson, J. Rodriguez, J. E. Bachman, M. I. Gonzalez, A. Cervellino, A. Guagliardi, C. M. Brown, P. L. Llewellyn, N. Masciocchi, J. R. Long, *Nature* **2015**, *527*, 357-361.

[30] S. Sorribas, P. Gorgojo, C. Téllez, J. Coronas, A. G. Livingston, *Journal of the American Chemical Society* **2013**, *135*, 15201-15208.

[31] D. Liu, X. Ma, H. Xi, Y. Lin, *Journal of Membrane Science* **2014**, *451*, 85-93.

[32] Y. Peng, Y. Li, Y. Ban, H. Jin, W. Jiao, X. Liu, W. Yang, *Science* **2014**, *346*, 1356-1359.

[33] A. Ahmed, N. Hodgson, M. Barrow, R. Clowes, C. M. Robertson, A. Steiner, P. McKeown, D. Bradshaw, P. Myers, H. Zhang, *J Mater Chem A* **2014**, *2*, 9085-9090.

[34] J. Liu, F. Sun, F. Zhang, Z. Wang, R. Zhang, C. Wang, S. Qiu, *Journal of Materials Chemistry* **2011**, *21*, 3775-3778.

[35] M. Tu, S. Wannapaiboon, K. Khaletskaya, R. A. Fischer, *Advanced Functional Materials* **2015**, *25*, 4470-4479.

[36] D. Y. Lee, I. Lim, C. Y. Shin, S. A. Patil, W. Lee, N. K. Shrestha, J. K. Lee, S.-H. Han, *Journal of Materials Chemistry A* **2015**, *3*, 22669- 22676.

[37] T. H. Chang, C. W. Kung, H. W. Chen, T. Y. Huang, S. Y. Kao, H. C. Lu, M. H. Lee, K. M. Boopathi, C. W. Chu, K. C. Ho, *Advanced Materials* **2015**, *27*, 7229-7235.

[38] A. J. Howarth, M. J. Katz, T. C. Wang, A. E. Platero-Prats, K. W. Chapman, J. T. Hupp, O. K. Farha, *Journal of the American Chemical Society* **2015**, *137*, 7488-7494.

[39] D. Wisser, F. M. Wisser, S. Raschke, N. Klein, M. Leistner, J. Grothe, E. Brunner, S. Kaskel, *Angewandte Chemie International Edition* **2015**, *54*, 12588-12591.

[40] S. Hermes, F. Schröder, R. Chelmowski, C. Wöll, R. A. Fischer, *Journal of the American Chemical Society* **2005**, *127*, 13744-13745.

[41] O. Shekhah, H. Wang, S. Kowarik, F. Schreiber, M. Paulus, M. Tolan, C. Sternemann, F. Evers, D. Zacher, R. A. Fischer, *Journal of the American Chemical Society* **2007**, *129*, 15118-15119.

[42] T. Yang, Y. Xiao, T.-S. Chung, *Energy & Environmental Science* **2011**, *4*, 4171-4180.

[43] T. Rodenas, M. van Dalen, E. García‐Pérez, P. Serra‐Crespo, B. Zornoza, F. Kapteijn, J. Gascon, *Advanced Functional Materials* **2014**, *24*, 249-256.

[44] H. Zhu, S. Zhu, *The Canadian Journal of Chemical Engineering* **2015**, *93*, 63-67.

[45] S. Furukawa, J. Reboul, S. Diring, K. Sumida, S. Kitagawa, *Chemical Society Reviews* **2014**, *43*, 5700-5734.

[46] N. Yanai, M. Sindoro, J. Yan, S. Granick, *Journal of the American Chemical Society* **2012**, *135*, 34-37.

[47]M. Tsotsalas, A. Umemura, F. Kim, Y. Sakata, J. Reboul, S. Kitagawa, S. Furukawa, *Journal of Materials Chemistry* **2012**, *22*, 10159-10165.

[48] C. Cui, Y. Liu, H. Xu, S. Li, W. Zhang, P. Cui, F. Huo, *Small* **2014**, *10*, 3672-3676.

[49] N. Yanai, S. Granick, *Angewandte Chemie* **2012**, *124*, 5736-5739.

[50] I. Hod, W. Bury, D. M. Karlin, P. Deria, C. W. Kung, M. J. Katz, M. So, B. Klahr, D. Jin, Y. W. Chung, *Advanced Materials* **2014**, *26*, 6295-6300.

[51] H. Zhu, H. Liu, I. Zhitomirsky, S. Zhu, *Materials Letters* **2015**, *142*, 19-22.

[52] J. Huo, M. Marcello, A. Garai, D. Bradshaw, *Advanced Materials* **2013**, *25*, 2717-2722.

[53] H. Zhu, Q. Zhang, S. Zhu, *Dalton Transactions* **2015**, *44*, 16752-16757.

[54] M. Pang, A. J. Cairns, Y. Liu, Y. Belmabkhout, H. C. Zeng, M. Eddaoudi, *Journal of the American Chemical Society* **2013**, *135*, 10234-10237.

[55] S. Chavan, J. G. Vitillo, D. Gianolio, O. Zavorotynska, B. Civalleri, S. Jakobsen, M. H. Nilsen, L. Valenzano, C. Lamberti, K. P. Lillerud, *Physical Chemistry Chemical Physics* **2012**, *14*, 1614-1626.

[56] H. Wu, Y. S. Chua, V. Krungleviciute, M. Tyagi, P. Chen, T. Yildirim, W. Zhou, *Journal of the American Chemical Society* **2013**, *135*, 10525-10532.

[57] M. J. Katz, J. E. Mondloch, R. K. Totten, J. K. Park, S. T. Nguyen, O. K. Farha, J. T. Hupp, *Angewandte Chemie International Edition* **2014**, *53*, 497-501.

[58] M. S. Denny, S. M. Cohen, *Angewandte Chemie International Edition* **2015**, *54*, 9029-9032.

[59] M. J. Katz, R. C. Klet, S.-Y. Moon, J. E. Mondloch, J. T. Hupp, O. K. Farha, *ACS Catalysis* **2015**, *5*, 4637-4642.

[60] G. Lu, C. Cui, W. Zhang, Y. Liu, F. Huo, *Chem Asian J* **2013**, *8*, 69-72.

[61] Z. Niu, J. He, T. P. Russell, Q. Wang, *Angewandte Chemie International Edition* **2010**, *49*, 10052-10066.

[62] Z. Mao, H. Xu, D. Wang, *Advanced Functional Materials* **2010**, *20*, 1053-1074.

[63] G. Vazquez, E. Alvarez, J. M. Navaza, *Journal of chemical and engineering data* **1995**, *40*, 611-614.

[64]M. Kandiah, M. H. Nilsen, S. Usseglio, S. Jakobsen, U. Olsbye, M. Tilset, C. Larabi, E. A. Quadrelli, F. Bonino, K. P. Lillerud, *Chemistry of Materials* **2010**, *22*, 6632-6640.

[65]M. Sindoro, A.-Y. Jee, S. Granick, *Chemical Communications* **2013**, *49*, 9576-9578.

[66] T. F. Tadros, "*Emulsion formation and stability*", John Wiley & Sons, 2013.

4.5 Supporting information

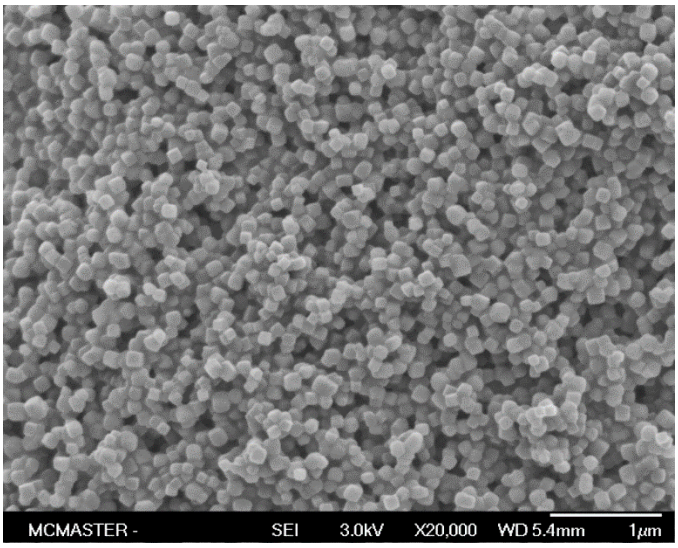

Figure S4-1. SEM images of the as synthesized UiO-66 particles.

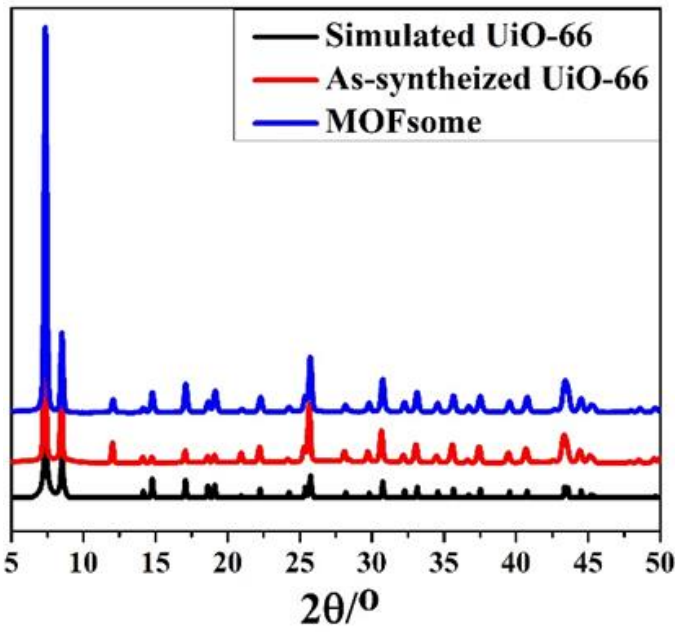

Figure S4-2. XRD pattern of simulated MOF, as synthesized MOF particle, and the fabricated MOFsome

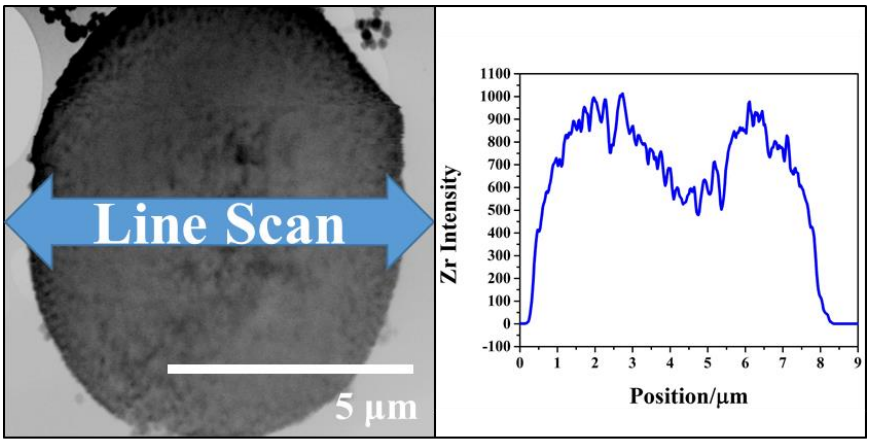

Figure S4-3. STEM image of the MOFsome prepared with 10% methanol and 2% UiO-66, and its hollow nature revealed by STEM line scan.

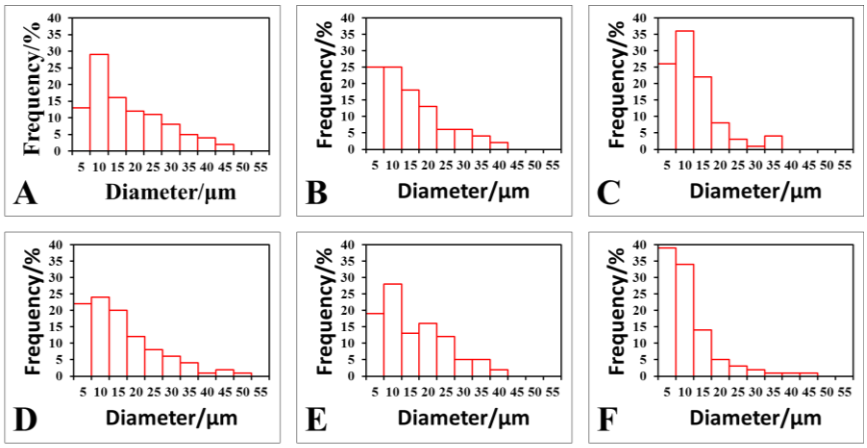

Figure S4-4. Statistical analysis of diameter based on 100 randomly selected MOFsomes. A) 1% UiO-66 and 5% methanol, B) 1% UiO-66 and 10% methanol, C) 1% UiO-66 and 15% methanol, D) 2% UiO-66 and 5% methanol, E) 2% UiO-66 and 10% methanol, F) 2% UiO-66 and 15% methanol.

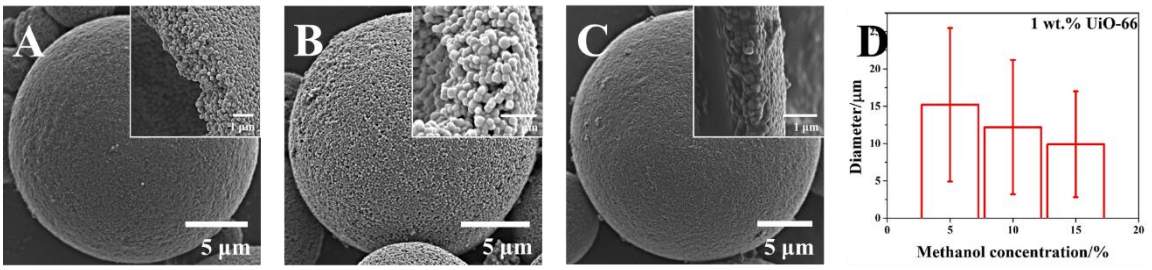

Figure S4-5. SEM images of MOFsomes formed with 1% UiO-66 in A) 5% methanol/water, B) 10% methanol/water, C)15% methanol/water, D) estimated average diameter based on 100 randomly selected

5 ASSEMBLY OF METAL–ORGANIC FRAMEWORK INTO 3D HIERARCHICAL POROUS MONOLITHS USING A PICKERING HIGH INTERNAL PHASE EMULSION TEMPLATE

This chapter is reprinted with permission from the paper published in *Chemistry-A European Journal* (DOI: 10.1002/chem.201600313) by *He Zhu, Qi Zhang, and Shiping Zhu.*

The idea was generated through discussion with the supervisor and the team members. He Zhu performed experiments, provided breakthroughs, and prepared the first draft, which was then revised by Dr. Qi Zhang and Dr. Shiping Zhu.

5.1 Abstract

3D Hierarchical porous metal–organic framework (MOF) monoliths are prepared by using Pickering high internal phase emulsion (HIPE) template. Pickering HIPEs were stabilized solely by UiO-66 MOF particles with internal phase up to 90 % of the volume. The effects of internal phase type and volume, as well as MOF particle concentration on the stability of resulting Pickering HIPEs were investigated. Furthermore, by adding small

amount of polyvinyl alcohol (PVA) as binder or polymerization in the continuous aqueous phase, followed by freeze-drying, two types of MOF-based 3D hierarchical porous monoliths with ultralow density (as low as 12 mg cm^{-3}) were successfully prepared. This Pickering HIPE template approach provides a facile and practical way for assembling of MOFs into complex structures.

5.2 Introduction

Metal-organic frameworks (MOFs) are a class of attractive porous crystalline materials, prepared from self-assembly of metal ions and organic bridging ligands.[1,2] They have received considerable attentions due to their large surface area, designable pore structure and functionality, high thermal stability, huge porosity, and so on.[1,2] These unique properties have made them promising in diverse applications, including gas storage[3,4] and separation,[5,6] chemical sensing,[7-9] catalysis,[10,11] waste water treatment,[12,13] proton conductors,[14,15] and drug delivery.[16,17] In addition to the enthusiasms in synthesizing new MOFs,[18,19] post-modification of existing MOFs,[20,21] and preparation of MOF membranes,[22,23] the study on fabrication of MOFs into complex structures has become an emerging hot topic recently.[24] However, the preparation of MOF materials in an ordered manner is still challenging, probably due to limited spatial control over MOF crystals.

Bottom-up strategy has been applied for the preparation of different MOF architectures. Pre-modified templates, such as alumina beads,[25] mesoporous silica spheres,[26] alumina aerogels,[27] and polystyrene spheres,[28,29] were commonly used to facilitate the growth of MOF particles into complex structures (mostly MOF spheres). Liquid-liquid[29-31] and

liquid-air[32,33] interface templates were also able to prepare MOF hollow spheres. Compared with bottom-up methods, top-down methods have a clear advantage in allowing pre-synthesis and characterization of well-defined MOF particles. However, it is challenging to position MOF particles after synthesis. Patterning pre-synthesized MOF particles into a desired form often requires more control over the system than synthesizing MOF particles from a patterned template. Nevertheless, the development of top-down methods is of great importance. In addition to the advantage of pre-synthesis and characterization, some MOF particles could only be synthesized under harsh conditions, where bottom-up methods are not applicable.

A comprehensive review of literatures reveals much fewer reports on top-down methods than bottom-up methods. Zero-dimensional (0D) MOF spheres are usually obtained through emulsion polymerization[34] and dispersion polymerization.[35] One-dimensional (1D) MOF chains have been achieved by applying AC electric field to induce dipolar attractions, leading to the alignment and linkage of MOF particles.[36] Two-dimensional (2D) MOF thin films can be prepared through Langmuir-Blodgett technique,[37,38] evaporation of salt solution,[39] and electrophoretic deposition.[6,40] So far, three-dimensional (3D) assemblies of MOF particles have been rarely reported.

High internal phase emulsions (HIPEs) are emulsions that contain more than 74% internal phase of the emulsion volume.[41] The ultralow ratio of the continuous phase makes HIPEs highly viscous and, thus they are also called emulsion gels. The unique properties of HIPEs offer them a high potential in such applications as food, cosmetics, pharmaceutical, and many other areas.[42] Conventional HIPEs are stabilized by large

amount surfactants (typically 20%), such as sodium dodecyl sulfate (SDS),[43] cetyltrimethylammonium bromide (CTAB),[44] and Span 80.[45] Recently, particle stabilized HIPEs, i.e. Pickering HIPEs, have drawn great attentions. Titania,[46] silica,[47,48] microgel,[49] cellulose nanocrystals (CNC),[50] lignin,[51] and carbonaceous microsphere particles[52] have been used as Pickering surfactants to stabilize HIPEs. Compared with conventional HIPEs, Pickering HIPEs provide several advantages. Firstly, the irreversible absorption of particles at the interface leads to more stable emulsion.[47,53,54] Secondly, the particles at interface can functionalize the cell walls of porous materials once HIPEs are polymerized. The latter provides a great opportunity for development of novel materials.[46,49]

The use of Pickering HIPEs as template for preparation of macroporous materials represents a promising practical way for sophisticated manipulation of particles. The objective of this work is to assemble MOF particles into a well-defined 3D structure through Pickering HIPEs. It is hypothesized that 3D hierarchical porous material is achievable if MOF particles could stabilize HIPEs. Herein, we report, for the first time, the preparation of MOF-stabilized oil-in-water Pickering HIPEs (Figure 5-1). We investigated the effect of internal phase volume and MOF particle concentration on the stability of resulting Pickering HIPEs. Pickering HIPEs were then employed to prepare MOF-based 3D hierarchical porous monoliths with ultralow density, through addition of small amount of polyvinyl alcohol (PVA) as binder, or through polymerization of the continuous aqueous phase, followed by freeze-drying, To the best of our knowledge, there is no report to date

on Pickering HIPEs solely stabilized by MOF particles, or the preparation of MOF-based 3D hierarchical porous monoliths through a Pickering HIPE template.

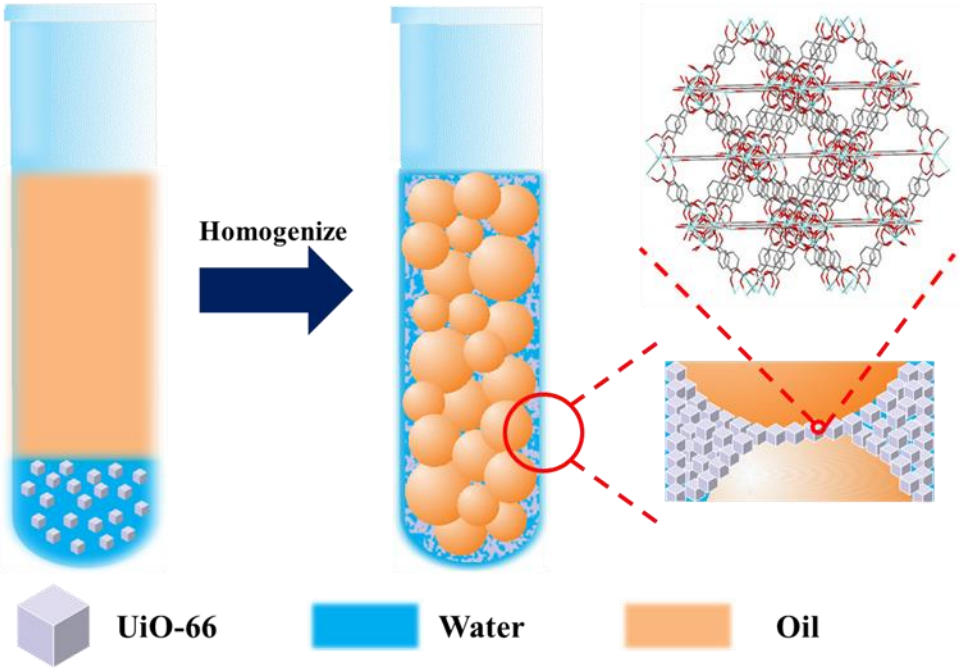

Figure 5-1. Schematic preparation of Pickering HIPEs stabilized by MOF particles.

5.3 Results and Discussion

In order to prepare HIPEs, we first synthesized MOF particles as Pickering surfactant. UiO-66 (University of Oslo-66) was chosen as model system, due to its high stability towards solvents and chemicals, as well as its high potential in various applications.[55-59] It was prepared through a hydrothermal method by using acetic acid as modulator.[60] Scanning electron microscopy (SEM) images (Supporting Information Figure S5-1) revealed that the resultant paritcles were cubic in shape and monodispersed in size. X-ray diffraction (XRD) confirmed the crystalline structure of UiO-66 particles (Supporting

Information Figure S5-2). The extra 2θ peak at 12^{o} was associated with solvent binding in UiO-66 particles, which has been studied in detail in the literature.[61] The particles showed a zeta potential of -30.34 ± 0.6 mV at room temperature in water, indicating a relative hydrophilicity, which would preferentially stabilize oil-in-water (o/w) emulsions.

MOF particle stabilized HIPEs were prepared by applying high shear forces to the mixture of cyclohexane and 5 wt.% of UiO-66 aqueous dispersion (80% oil phase volume). After homogenized at 10,000 rpm for 1 minute, a highly viscous toothpaste-like gel emulsion was obtained, suggesting the formation of HIPE. Pickering emulsions with an internal phase varying from 70 to 92 vol.%, were then prepared by using the same procedure and keeping the MOF concentration constant at 5 wt.%. The results were shown in Figure 5-2A (taken after 24 hours). For the Pickering emuslion having 70 vol.% dispersed phase fraction, the emulsion was quite stable without any obvious phase separation after 24 h, although its internal phase did not reach 74 vol.%. With the internal phase between 75 and 90 vol.%, the HIPE was typically highly viscosity and remarkably stable. These results clearly demonstrated the ability of MOF particles in stablizing HIPEs. As far as we know, this work represents the first Pickering HIPE system stabilized solely by MOF particles. These emulsions were still stable after 2 months, with no phase separation observed. However, further addition of oil to 92 vol.% led to a highly viscous emulsion surrounded by oil, similar to HIPEs stablized by silica.[47]

The obtained MOF stablized HIPEs were then examined by confocal microscopy. Aqueous phase was stained with FITC (25 mg L^{-1}) before taking confocal microscopy images. Interestingly, we found that UiO-66 particles absorbed FITC, which made the

particles visible under the confocal microscopy. As shown in Figure 5-2B, most dark oil droplets were spherical and had sizes varying from tens to hundreds of micrometers. The fluorescent UiO-66 particles could be clearly seen at the interface, as well as in the continous phase. The particles absorbed at the interface provided sufficient barrier against coalescence of the oil droplets. The excess MOF particles in the continuous phase were closely packed together, which resulted in a dramatic increase in viscosity and thus inhibited creaming and phase inversion. There was some similarity to the previously reported microgel-stabilized HIPEs,[49] since both MOF and microgel particles could absorb water, although microgel was much softer than MOF.

We then carried out a systematic investigation on the effect of MOF particle concentration on the stability of the resulted Pickering HIPEs (Figure 5-2C; Supporting Information Figure S5-3). Figure 5-2C showed the appearance of HIPEs having an internal cyclohexane phase of 80 vol.% stabilized by different amounts of UiO-66 particles. It was found that 1 wt.% particle loading was sufficient to yield a stable Pickering HIPE. It is in strong contrast to the conventional HIPEs, which usually require 5-50% surfactant, typically 20%, to stabilize the system.[62,63] However, some amount of cyclohexane was expelled out after 24 hours from the Pickering HIPEs stabilized by 1 wt.% UiO-66, while the others stayed the same as freshly prepared. In addition, we found that UiO-66 particles were also able to prepare Pickering HIPEs with different types of internal oil phases. Emulsions based commonly used solvents, such as cyclohexane, hexane, dodecane, and toluene, were stabilized by 5 wt.% UiO-66 particles with an internal phase of 80 vol.%,

suggesting the versatility of this system in the preparation of different Pickering HIPEs (Figure 5-2D; Supporting Information Figure S5-4).

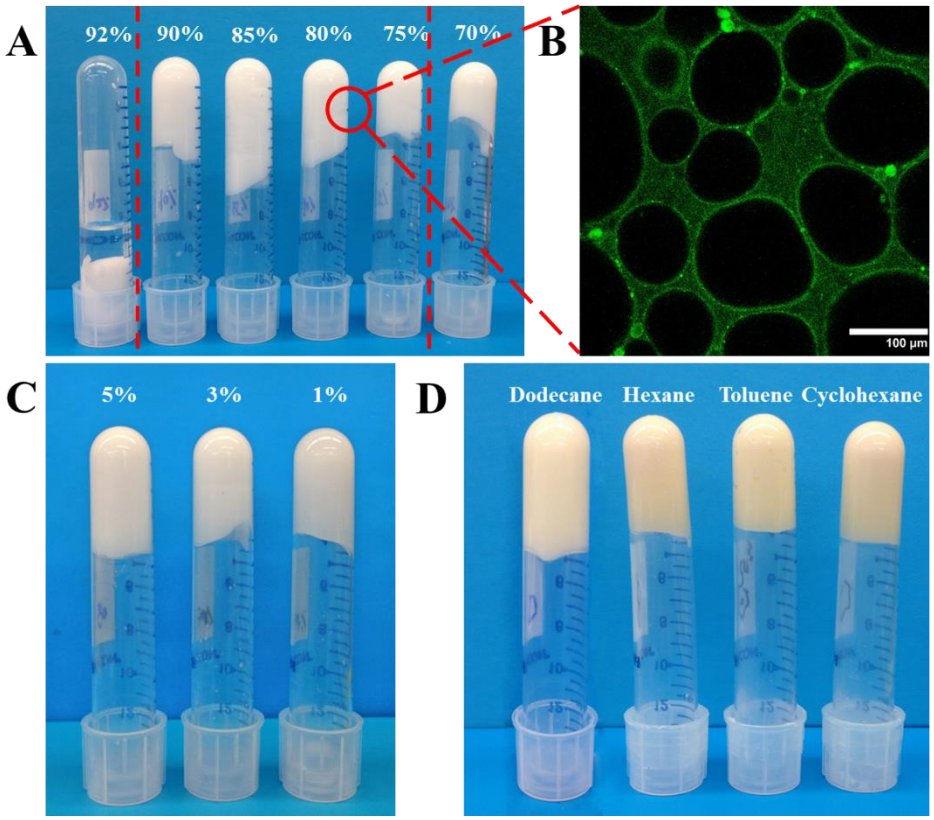

Figure 5-2. A) Optical images of MOF stabilized Pickering emulsions with different internal cyclohexane phase volume from 70% to 90%, where the continuous aqueous phase of all the mixtures consists of 5 wt.% of UiO-66 particles. (The volume of aqueous phase was halved in the case of 90% and 92% internal phase.) B) Confocal image (scale bar: 100 µm) of HIPE with 80 vol.% of cyclohexane oil phase, stabilized by 5 wt.% of UiO-66 particles. Water phase was stained with FITC prior to the test. The emulsion was excited by laser with wavelength of 488 nm. C) Pickering HIPEs stabilized by different amounts of UiO-66 particles, from 1 to 5 wt.%, with an 80 vol.% internal cyclohexane phase. D) Pickering HIPEs with an 80 vol.% internal oil phase prepared with different solvents, where the continuous aqueous phase of all mixtures contain 5 wt.% of UiO-66 particles with respect to water (stained with FITC).

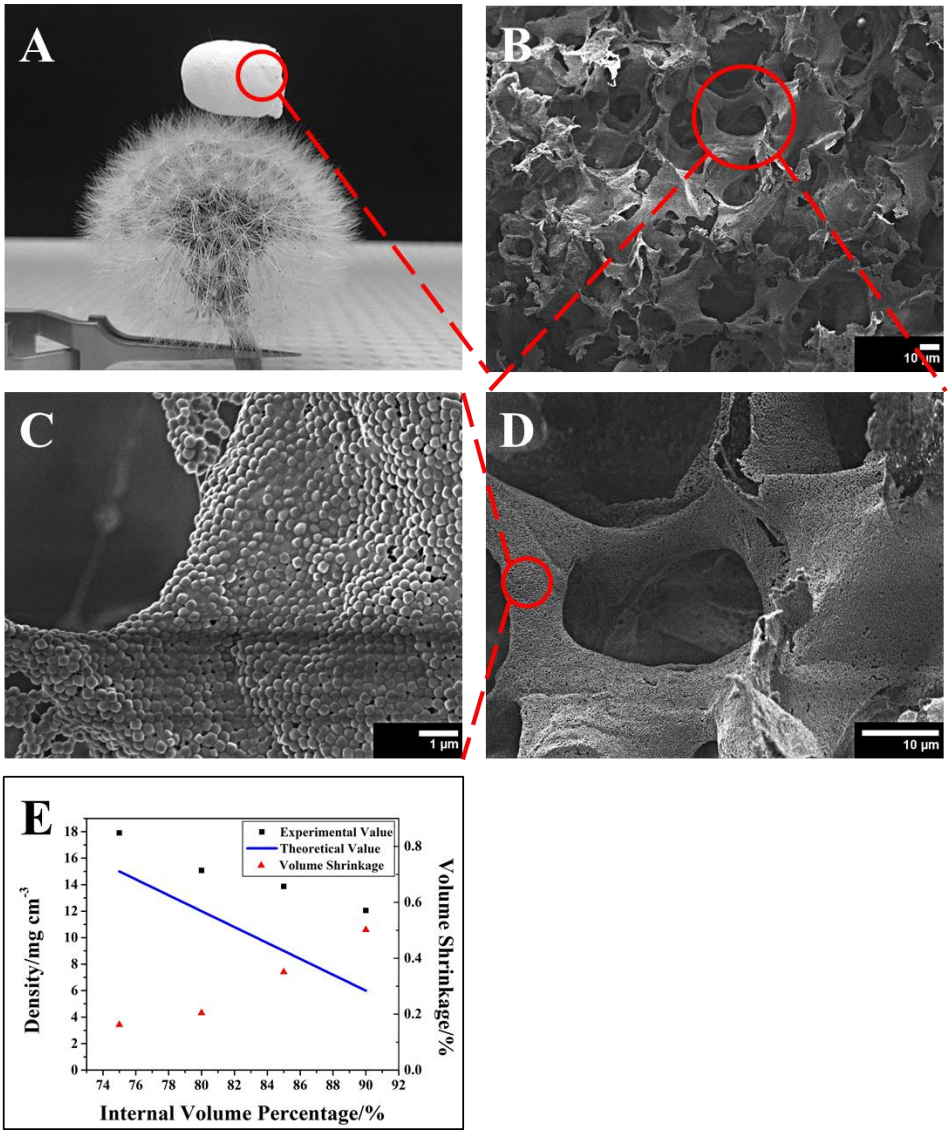

Figure 5-3. A) Optical image of MOF/PVA porous monolith on a dandelion flower (density=15 mg cm^{-3}). B, C, D) SEM images of the MOF/PVA porous monolith. The monolith was prepared from Pickering HIPE with 80 vol.% of cyclohexane internal phase stabilized by 5 wt.% of UiO-66 particles with the help of 1 wt.% PVA in aqueous phase. E) The theoretical, calculated density, and the volume shrinkage percentage of the MOF/PVA porous monolith.

Since the MOF particles were assembled within the aqueous phase of Pickering HIPEs, how to use this template to prepare useful hierarchical MOF materials was of our major

interest in this work. Direct evaporation of solvent without performing any polymerization has been reported for preparation of ordered structures in the cases of microgel and CNC stabilized Pickering HIPEs.[49,50] However, in our case, simply freeze-drying of the MOF-stabilized Pickering HIPEs would lead to collapsing of the ordered structures (Supporting Information Figure S5-5), probably due to weak interactions between the MOF particles. Therefore, we added 1 wt.% polyvinyl alcohol (PVA) (with respect to water) as an adhesive to the aqueous phase before applying high shear forces to the oil/water mixture. As a good emulsifier, PVA helped to stabilize the Pickering HIPEs, but more importantly, it also acted as an adhesive to bind MOF particles together so that the porous structure could survive upon removal of the solvent. The resultant Pickering HIPEs were then freeze-dried for 18 hours, and a free-standing UiO-66/PVA porous monolith was successfully achieved, as shown in Figure 5-3A. The monolith showed an open-cell foam structure with pore sizes ranging from tens to hundreds of micrometers (Figure 5-3B & 5-3D), which is comparable with the oil droplet diameters of the precursor emulsions. The foam wall was constituted of UiO-66 particles that were closely packed together and bonded by PVA (Figure 5-3C).

The UiO-66 particles within this porous monolith remained its crystallinity, as confirmed by XRD (Supporting Information Figure S5-2). The density of the prepared porous monolith could be controlled by fine-tuning internal oil phase volume. The measured and theoretical densities were shown in Figure 5-3E. The measured densities were slightly higher than the theoretical ones, indicating there was some volume shrinkage during the freeze-drying process. As the internal phase increased, the density of the monolith decreased, but the volume shrinkage increased from about 16% to 50% due to

more internal phase was removed (Figure 5-3E). Ultralight porous monoliths could be obtained with a density as low as 12 mg cm^{-3}, making it possible to sit on a dandelion flower (Figure 5-3A). This template of Pickering HIPEs paves the way of fabricating MOF particles into 3D hierarchical porous materials with ultralow density.

On the other hand, adding monomers to the continuous phase in preparation poly(Pickering HIPEs) is also a common practice to prepare porous materials.[46,47,52] Herein, we added acrylamide (10 wt.% with respect to water) as monomer, bisacrylamide (5 wt.% with respect to the monomer) as crosslinker, and 2,2'-azobis(2-methylpropionamidine) dihydrochloride (V50) (5 wt.% with respect to the monomer) as initiator to the UiO-66 aqueous dispersion. We then prepared the HIPE with 80 vol.% toluene internal phase. Polymerization was carried out by heating the resulted Pickering HIPE at 60 ^{o}C for 24 hours. After evaporation of the solvent for overnight, it was freeze-dried for 18 hours in order to remove the residual water within the polymer matrix, and finally a white porous monolith was obtained.

The monolith was also very light with an estimated density of around 50 mg cm^{-3}, and able to sit on a dandelion flower (Figure 5-4A). XRD result confirmed the retaining of UiO-66 crystallinity (Supporting Information Figure S5-2). SEM images revealed a closed cell structure of the poly(Pickering HIPE) (Figure 5-4B). The size of the cells ranged from tens to hundreds of micrometers, and the cell wall was decorated with UiO-66 particles (Figure 5-4C & 5-4D). The reason of forming closed-cell structure here rather than open-cell structure in the case of MOF/PVA monolith could be attributed to the wall thickness being formed.[64] Acrylamide was 10 wt.% with respect to water in the aqueous phase,

which was much more than 1 wt.% of PVA in the MOF/PVA monolith. Upon removal of the solvent, the latter had thinner wall and thus tended to form an open-cell structure, while the former was thicker for a closed cell structure.

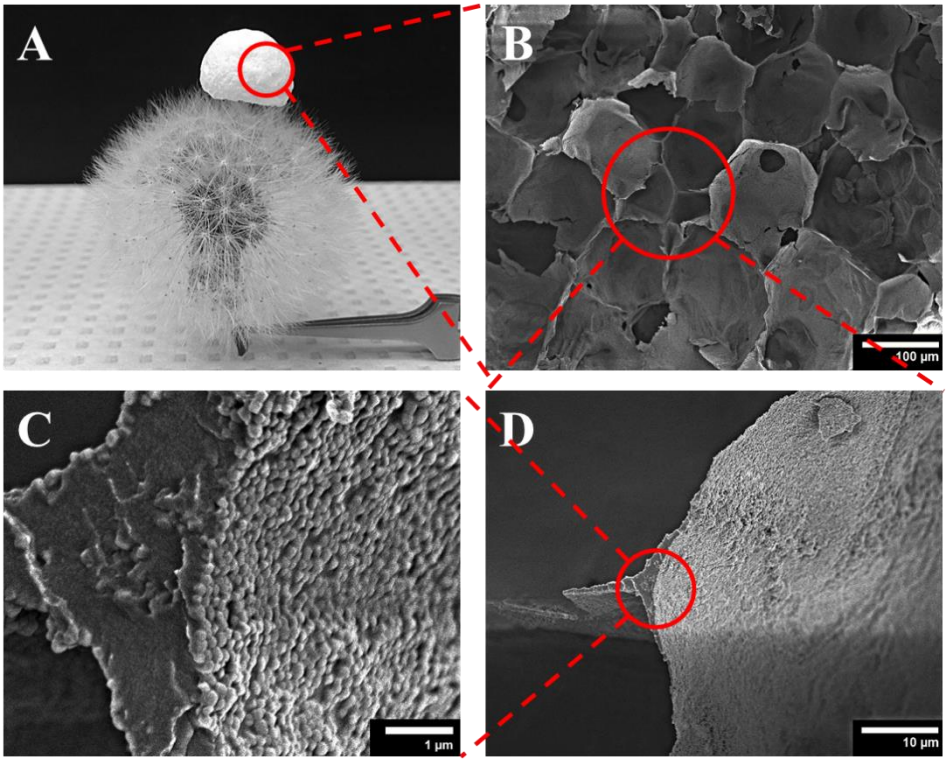

Figure 5-4. A) Optical and B, C, D) SEM images of poly(Pickering HIPE) with different magnification.

A final point worth to be pointed out is that an independent paper appeared very recently also demonstrated the concept of MOF-containing HIPEs.[65] However, the present work systematically studied the effects of internal phase type and volume, as well as MOF particle concentration, on stability of the resulted Pickering HIPEs. Pickering HIPE with its internal phase up to 90 % solely stabilized by UiO-66 MOF particles were achieved. In

addition, the MOF particles used in this work (UiO-66) has better stability against hydrolysis.

To conclude, we have successfully developed a useful but easy way for the preparation of 3D hierarchical porous MOF monoliths through Pickering HIPE template. Pickering HIPEs were stabilized solely by UiO-66 particles with the internal phase up to 90 vol.%. The effects of the internal phase type and volume, as well as the MOF particle concentration on the stability of Pickering HIPEs were investigated. Furthermore, by adding small amount of polyvinyl alcohol (PVA) as binder or polymerization in the continuous aqueous phase, followed by freeze-drying, two types of MOF-based 3D hierarchical porous monoliths with an ultralow density (as low as 12 mg cm^{-3}) were successfully achieved. This Pickering HIPEs template approach provides a practical way to construct MOF particles into complex structures.

5.4 Acknowledgements

We sincerely thank the Natural Sciences and Engineering Research Council (NSERC) of Canada and the Canada Research Chair (CRC) program of the Federal Government for supporting this research work.

5.5 References

[1] U. Mueller, M. Schubert, F. Teich, H. Puetter, K. Schierle-Arndt, J. Pastre, *Journal of Materials Chemistry* **2006**, *16*, 626-636.

[2] S. T. Meek, J. A. Greathouse, M. D. Allendorf, *Advanced Materials* **2011**, *23*, 249-267.

[3] A. R. Millward, O. M. Yaghi, *Journal of the American Chemical Society* **2005**, *127*, 17998-17999.

[4] J. Pang, F. Jiang, M. Wu, C. Liu, K. Su, W. Lu, D. Yuan, M. Hong, *Nature communications* **2015**, *6*.

[5] H. T. Kwon, H.-K. Jeong, *Journal of the American Chemical Society* **2013**, *135*, 10763-10768.

[6] H. Zhu, H. Liu, I. Zhitomirsky, S. Zhu, *Materials Letters* **2015**, *142*, 19-22.

[7] J. Liu, F. Sun, F. Zhang, Z. Wang, R. Zhang, C. Wang, S. Qiu, *Journal of Materials Chemistry* **2011**, *21*, 3775-3778.

[8] M. Tu, S. Wannapaiboon, K. Khaletskaya, R. A. Fischer, *Advanced Functional Materials* **2015**, 25, 4470-4479.

[9] S. Wannapaiboon, M. Tu, K. Sumida, K. Khaletskaya, S. Furukawa, S. Kitagawa, R. A. Fischer, *Journal of Materials Chemistry A* **2015**, 3, 23385-23394.

[10] J. E. Mondloch, M. J. Katz, W. C. Isley III, P. Ghosh, P. Liao, W. Bury, G. W. Wagner, M. G. Hall, J. B. DeCoste, G. W. Peterson, *Nature materials* **2015**, 14, 512-516.

[11] E. López‐Maya, C. Montoro, L. M. Rodríguez‐Albelo, S. D. Aznar Cervantes, A. A. Lozano‐Pérez, J. L. Cenís, E. Barea, J. A. Navarro, *Angewandte Chemie International Edition* **2015**, 127, 6894-6898.

[12] F. Ke, L.-G. Qiu, Y.-P. Yuan, F.-M. Peng, X. Jiang, A.-J. Xie, Y.-H. Shen, J.-F. Zhu, *Journal of hazardous materials* **2011**, *196*, 36-43.

[13] S.-H. Huo, X.-P. Yan, *Journal of Materials Chemistry* **2012**, *22*, 7449-7455.

[14] G. K. Shimizu, J. M. Taylor, S. Kim, *Science* **2013**, *341*, 354-355.

[15] J. M. Taylor, K. W. Dawson, G. K. Shimizu, *Journal of the American Chemical Society* **2013**, *135*, 1193-1196.

[16] P. Horcajada, T. Chalati, C. Serre, B. Gillet, C. Sebrie, T. Baati, J. F. Eubank, D. Heurtaux, P. Clayette, C. Kreuz, *Nature materials* **2010**, *9*, 172-178.

[17] L. Cooper, T. Hidalgo, M. Gorman, T. Lozano-Fernández, R. Simón-Vázquez, C. Olivier, N. Guillou, C. Serre, C. Martineau, F. Taulelle, *Chemical Communications* **2015**, *51*, 5848-5851.

[18] S. Khatua, S. Goswami, S. Biswas, K. Tomar, H. S. Jena, S. Konar, *Chemistry of Materials* **2015**, 27, 5349-5360.

[19] D. Sun, F. Liu, Y. Xu, L. Zhao, L. Zhang, W. Guo, R. Wang, *Journal of Materials Chemistry A* **2015**, 3, 21545-21552.

[20] Z. Wang, S. M. Cohen, *Journal of the American Chemical Society* **2007**, *129*, 12368-12369.

[21] H. Liu, H. Zhu, S. Zhu, *Macromolecular Materials and Engineering* **2015**, *300*, 191-197.

[22] H. Zhu, S. Zhu, *The Canadian Journal of Chemical Engineering* **2015**, *93*, 63-67.

[23] Z. Zhong, J. Yao, R. Chen, Z. Low, M. He, J. Z. Liu, H. Wang, *Journal of Materials Chemistry A* **2015**, *3*, 15715-15722.

[24] S. Furukawa, J. Reboul, S. Diring, K. Sumida, S. Kitagawa, *Chemical Society Reviews* **2014**, *43*, 5700-5734.

[25] S. Aguado, J. Canivet, D. Farrusseng, *Chemical Communications* **2010**, *46*, 7999-8001.

[26] S. Sorribas, B. Zornoza, C. Téllez, J. Coronas, *Chemical Communications* **2012**, *48*, 9388-9390.

[27] J. Reboul, S. Furukawa, N. Horike, M. Tsotsalas, K. Hirai, H. Uehara, M. Kondo, N. Louvain, O. Sakata, S. Kitagawa, *Nature materials* **2012**, *11*, 717-723.

[28] H. J. Lee, W. Cho, M. Oh, *Chemical Communications* **2012**, *48*, 221-223.

[29] M. Pang, A. J. Cairns, Y. Liu, Y. Belmabkhout, H. C. Zeng, M. Eddaoudi, *Journal of the American Chemical Society* **2013**, *135*, 10234-10237.

[30] R. Ameloot, F. Vermoortele, W. Vanhove, M. B. Roeffaers, B. F. Sels, D. E. De Vos, *Nature chemistry* **2011**, *3*, 382-387.

[31] Y. Yang, F. Wang, Q. Yang, Y. Hu, H. Yan, Y.-Z. Chen, H. Liu, G. Zhang, J. Lu, H.-L. Jiang, *ACS applied materials & interfaces* **2014**, *6*, 18163-18171.

[32] A. Carné-Sánchez, I. Imaz, M. Cano-Sarabia, D. Maspoch, *Nature chemistry* **2013**, *5*, 203-211.

[33] Z. Wang, D. Ananias, A. Carné‐Sánchez, C. D. Brites, I. Imaz, D. Maspoch, J. Rocha, L. D. Carlos, *Advanced Functional Materials* **2015**, *25*, 2824-2830.

[34] J. Huo, M. Marcello, A. Garai, D. Bradshaw, *Advanced Materials* **2013**, *25*, 2717-2722.

[35] H. Zhu, Q. Zhang, S. Zhu, *Dalton Transactions* **2015**, 44, 16752-16757.

[36] N. Yanai, M. Sindoro, J. Yan, S. Granick, *Journal of the American Chemical Society* **2012**, *135*, 34-37.

[37]M. Tsotsalas, A. Umemura, F. Kim, Y. Sakata, J. Reboul, S. Kitagawa, S. Furukawa, *Journal of Materials Chemistry* **2012**, *22*, 10159-10165.

[38] C. Cui, Y. Liu, H. Xu, S. Li, W. Zhang, P. Cui, F. Huo, *Small* **2014**, *10*, 3672-3676.

[39] N. Yanai, S. Granick, *Angewandte Chemie* **2012**, *124*, 5736-5739.

[40] I. Hod, W. Bury, D. M. Karlin, P. Deria, C. W. Kung, M. J. Katz, M. So, B. Klahr, D. Jin, Y. W. Chung, *Advanced Materials* **2014**, *26*, 6295-6300.

[41] N. R. Cameron, *Polymer* **2005**, *46*, 1439-1449.

[42] V. G. Babak, M.-J. Stébé, *Journal of dispersion science and technology* **2002**, *23*, 1-22.

[43] H. Zhang, A. Cooper, *Chemistry of materials* **2002**, *14*, 4017-4020.

[44] S. Zhang, J. Chen, V. T. Perchyonok, *Polymer* **2009**, *50*, 1723-1731.

[45] A. Barbetta, N. R. Cameron, *Macromolecules* **2004**, *37*, 3188-3201.

[46] A. Menner, V. Ikem, M. Salgueiro, M. S. Shaffer, A. Bismarck, *Chemical Communications* **2007**, 4274-4276.

[47] V. O. Ikem, A. Menner, A. Bismarck, *Angewandte Chemie International Edition* **2008**, *47*, 8277-8279.

[48] V. O. Ikem, A. Menner, T. S. Horozov, A. Bismarck, *Advanced Materials* **2010**, *22*, 3588-3592.

[49] Z. Li, T. Ming, J. Wang, T. Ngai, *Angewandte Chemie International Edition* **2009**, *48*, 8490-8493.

[50] I. Capron, B. Cathala, *Biomacromolecules* **2013**, *14*, 291-296.

[51] Y. Yang, Z. Wei, C. Wang, Z. Tong, *Chemical Communications* **2013**, *49*, 7144-7146.

[52] S. Yu, H. Tan, J. Wang, X. Liu, K. Zhou, *ACS applied materials & interfaces* **2015**, *7*, 6745-6753.

[53] B. P. Binks, *Current opinion in colloid & interface science* **2002**, *7*, 21-41.

[54] R. Aveyard, B. P. Binks, J. H. Clint, *Advances in Colloid and Interface Science* **2003**, *100*, 503-546.

[55] S. Chavan, J. G. Vitillo, D. Gianolio, O. Zavorotynska, B. Civalleri, S. Jakobsen, M. H. Nilsen, L. Valenzano, C. Lamberti, K. P. Lillerud, *Physical Chemistry Chemical Physics* **2012**, *14*, 1614-1626.

[56] H. Wu, Y. S. Chua, V. Krungleviciute, M. Tyagi, P. Chen, T. Yildirim, W. Zhou, *Journal of the American Chemical Society* **2013**, *135*, 10525-10532.

[57] M. J. Katz, J. E. Mondloch, R. K. Totten, J. K. Park, S. T. Nguyen, O. K. Farha, J. T. Hupp, *Angewandte Chemie International Edition* **2014**, *53*, 497-501.

[58] M. S. Denny, S. M. Cohen, *Angewandte Chemie International Edition* **2015**, 54, 9029-9032.

[59] M. J. Katz, R. C. Klet, S.-Y. Moon, J. E. Mondloch, J. T. Hupp, O. K. Farha, *ACS Catalysis* **2015**, 5, 4637-4642.

[60] G. Lu, C. Cui, W. Zhang, Y. Liu, F. Huo, *Chem Asian J* **2013**, *8*, 69-72.

[61] L. Valenzano, B. Civalleri, S. Chavan, S. Bordiga, M. H. Nilsen, S. Jakobsen, K. P. Lillerud, C. Lamberti, *Chemistry of Materials* **2011**, *23*, 1700-1718.

[62] J. M. Williams, *Langmuir* **1991**, *7*, 1370-1377.

[63] N. Cameron, D. Sherrington, "High internal phase emulsions (HIPEs)—structure, properties and use in polymer preparation", in *Biopolymers liquid crystalline polymers phase emulsion*, Springer, 1996, p. 163-214.

[64] A. Menner, A. Bismarck, "New evidence for the mechanism of the pore formation in polymerising high internal phase emulsions or why polyHIPEs have an interconnected pore network structure", in *Macromolecular symposia*, Wiley Online Library, 2006, p. 242/19-24.

[65] Work that is closely related was independently submitted on the same day to Sci. Rep.: B. Zhang, J. Zhang, C. Liu, L. Peng, X. Sang, B. Han, X. Ma, T. Luo, X. Tan, G. Yang, *Scientific Reports* **2016**, *6*, 21401.

5.6 Supporting Information

Experimental

Materials

Zirconium chloride (≥99.5%), terephthalic acid (98%), acetic acid (≥99.7%), polyvinyl alcohol (average Mw 13-23 kD, 98% hydrolyzed) (PVA), bisacrylamide (97%), and 2,2'-azobis(2-methylpropionamidine) dihydrochloride (97%) (V50) were purchased from Sigma-Aldrich and used without further purification. Acrylamide (Sigma-Aldrich, 97%) was purified by recrystallization. Other solvents were commercially available and used as received. The water was purified with a Barnstead Nanopure Diamond system first before any usage.

MOF synthesis

UiO-66 was synthesized according to the reported method with minor modification.[1] Briefly, 915 mg of zirconium chloride and 645 mg of terephthalic acid were dissolved in 225 mL dimethylformamide (DMF) containing 6.7 mL acetic acid. The solution was then kept at 120℃ for 24 hours. After cooling to room temperature, the products were collected by centrifugation and washed with methanol for 3 times.

HIPE Preparation

UiO-66 stabilized Pickering HIPEs were prepared by applying high shear forces to the mixture of oil and aqueous dispersion of UiO-66 particles. Typically, 50 mg of UiO-66

was dispersed in 1 mL of water under sonication. 4 mL of cyclohexane (80% internal phase) was added into the aqueous dispersion under 10,000 rpm for about 1 minute.

Preparation of porous MOF monolith

UiO-66/PVA porous monolith was prepared by freeze-drying of the aforementioned Pickering HIPEs except for that 1 wt.% PVA aqueous solution was used instead of pure water to disperse UiO-66 particles (cyclohexane as internal phase). After preparation of the UiO-66/PVA HIPE, it was placed in freezer for overnight, in order to fully freeze the HIPE, and then it was freeze-dried for 18 hours.

Poly(Pickering HIPE) was prepared by conducting polymerization at 60 ^{o}C for 24 hours of the aforementioned Pickering HIPEs of 80 vol.% internal oil phase (toluene) except for that the aqueous phase contains 10 wt.% acrylamide (with respect to water) as monomer, bisacrylamide (5 wt.% with respect to the monomer) as crosslinker, and V50 (5 wt.% with respect to the monomer) as initiator. The obtained poly(Pickering HIPE) was placed in fumefood overnight, in order to remove toluene before it was transferred to the freezer. The frozen poly(Pickering HIPE) was then freeze-dried for 18 hours to remove the residual water trapped in the polymer matrix.

Characterization

JEOL JSM 7000 Scanning Electron Microscopy (SEM) and Zeiss LSM 510 Meta Confocal Microscope (CLSM) were used to characterize the UiO-66 particles, the Pickering HIPEs and the UiO-66/PVA porous monolith. Water phase was stained with fluorescein isothiocyanate (FITC) before the CLSM test. IKA T18 digital Ultra-Turrax was

used to provide the high shear force. X-ray diffraction (XRD) was carried out on the Cu SMART6000 rotating anode diffractometer. Zeta potential of the UiO-66 particles was obtained under ambient temperature with water as solvent on Brookhaven Instruments PALS Zeta Potential Analyzer.

[1] G. Lu, C. Cui, W. Zhang, Y. Liu, F. Huo, *Chemistry–An Asian Journal* **2013**, *8*, 69-72.

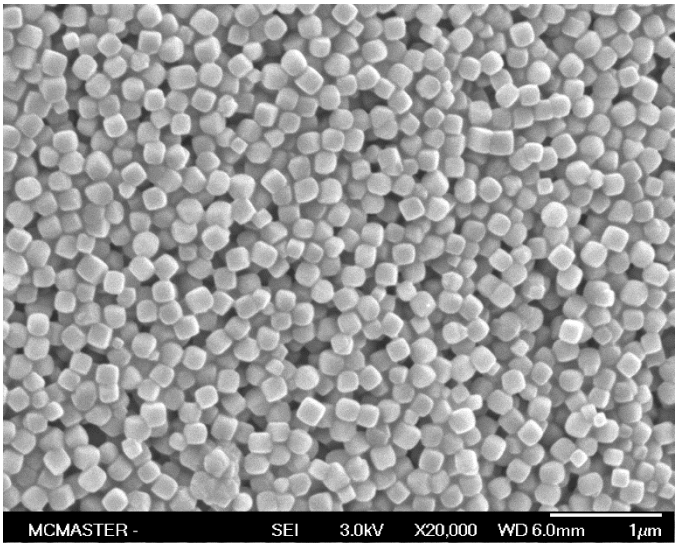

Figure S5-1. SEM images of UiO-66 particles.

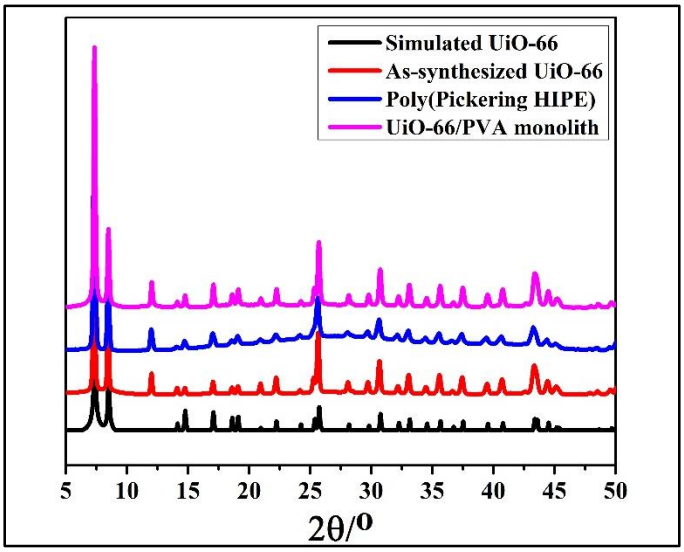

Figure S5-2. XRD pattern of simulated and as-synthesized UiO-66 powder, poly(Pickering HIPE) and MOF/PVA porous monolith.

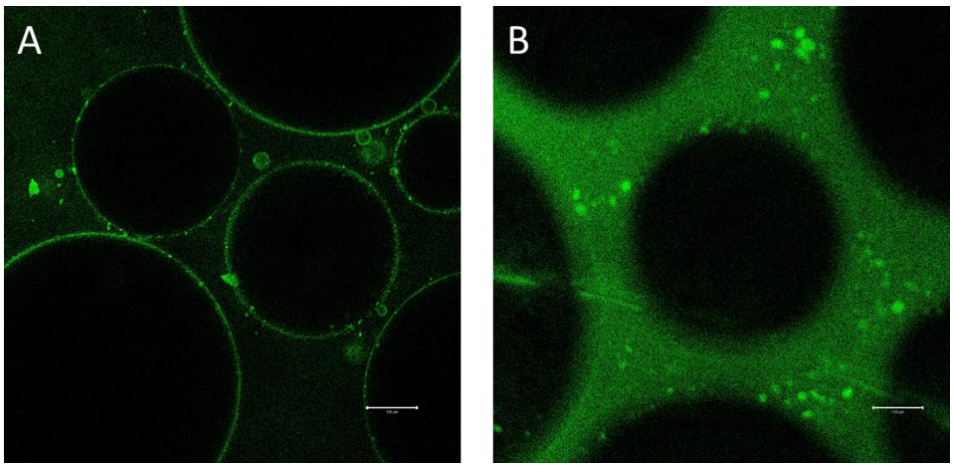

Figure S5-3. Confocal images of Pickering HIPEs stabilized by different amounts of UiO-66 particles, A) 1 wt.%, B) 3 wt.%, with 80 vol.% internal cyclohexane phase Water phase was stained with FITC. The emulsion was excited by laser with wavelength of 488 nm. Scale bar: 100 μm.

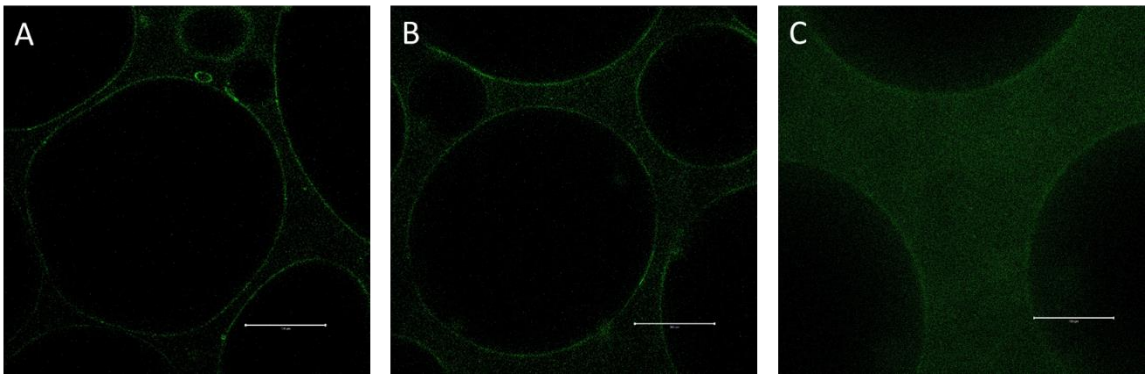

Figure S5-4. Confocal images of the emulsion with 80% of internal oil phase: A) toluene, B) hexane, C) dodecane. Water phase was stained with FITC. The emulsion was excited by laser with wavelength of 488 nm. Scale bar: 100 μm.

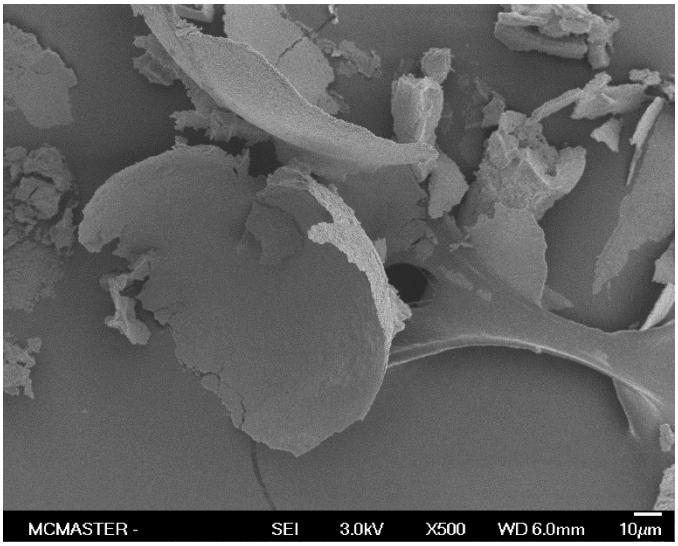

Figure S5-5. SEM image of the collapsed MOF structure after freeze-drying. This was prepared from Pickering HIPE with 80 vol.% of cyclohexane internal phase stabilized by 5 wt.% of UiO-66 particles without the help of 1 wt.% PVA in aqueous phase.

6 FLEXIBLE AND POROUS NANOCELLULOSE AEROGELS WITH HIGH LOADINGS OF METAL-ORGANIC FRAMEWORK PARTICLES FOR SEPARATIONS APPLICATIONS

This chapter is reprinted with permission from the paper published in *Advanced Materials* (DOI: 10.1002/adma.201601351) by *He Zhu, Xuan Yang, Emily D. Cranston, and Shiping Zhu.*

The idea was generated through discussion with the supervisor and the team members. Xuan Yang prepared CNCs, aerogels, and did DLS tests. Xuan Yang and He Zhu conducted SEM. He Zhu prepared MOFs and conducted PXRD, UV-Vis adsorption, TGA, and ICP-OES. He Zhu processed the data and prepared the first draft, which was then revised by Xuan Yang, Dr. Emily D. Cranston and Dr. Shiping Zhu.

6.1 Paper body

This work overcomes the longstanding challenge of processing metal-organic framework (MOF) powders into a convenient and tailorable form by entrapping them within a cellulose nanocrystal (CNC) aerogel. MOFs are a new class of porous materials,

assembled from metal ions or ion clusters bridged by organic ligands. Since the pioneering work on MOF-5 reported by Yaghi and co-workers,[1] MOFs have received great attention due to their large surface area and porosity, high thermal stability, and tunable pore structure. MOFs have shown great potential in various applications including gas separation[2,3] and storage,[4,5] chemical sensing,[6,7] catalysis,[8,9] and so on. Designing and preparing new MOFs,[10-12] post-modification of existing MOFs,[13,14] and fabrication of MOFs into different structures[15-17] are currently of great interest. However, due to the crystalline nature of MOFs, they are most commonly found in powder form and their processability and handling remain a significant challenge.[18] Integrating MOFs onto or within various substrates to produce a shapeable, cost-efficient, and chemically inert product is one way to expand the potential applications of these functional materials.

The deposition and growth of MOF particles on substrates has become a highly researched area but is severely constrained by the physical and chemical requirements of the substrate and gives materials with limited functionality.[19,20] Usually surface modifications are needed in order to increase the compatibility between MOFs and substrates, and while different methods to grow MOFs exist, including solvothermal,[21,22] secondary,[23,24] layer by layer growth,[25,26] and electrochemical deposition,[27,28] the substrates have to be stable during the process or restricted synthetic conditions must be employed.[29,30] Incorporation of MOF particles onto polymer or fiber substrates (of both synthetic[31-35] and natural origin[36-42]), by blending, deposition or *in situ* growth, has been demonstrated. However, while these approaches overcome some of the disadvantages of preparing MOF-only materials or planar MOF films, most examples reported to date are

either limited by low MOF loadings or reduced flexibility.[32,43-45] One alternative approach used to avoid processing or depositing MOFs is to produce metal organic framework gels (MOGs) which are high surface area MOF-like materials but they generally lack the ordered crystal lattice and desired physical properties of MOFs.[46,47]

Nanocellulose shows great promise for use as a supporting substrate[48-50] or templating material[51-53], especially in the form of cellulose aerogels and foams, because of its high strength, light weight, low cost, non-toxicity and its ability to be processed easily in water.[54,55] Cellulose nanocrystals (CNCs), cellulose nanofibrils (CNFs), and bacterial cellulose are the most common types of nanocellulose which are now being produced with consistency in industrial-scale quantities yet few commercial products exist.[56] Interestingly, CNCs and CNFs have been found to help unstable colloidal nanoparticles like carbon nanotubes (CNT), boron nitride, manganese dioxide or molybdenum disulfide suspend better in water.[49,57,58] Moreover, the co-suspended nanoparticles can be processed to give hybrid nanocomposites with uniform distribution of components.[49] Only one literature example exists combining MOFs and nanocellulose; it is an elegant study of growing MOFs (up to 44 wt.% loading) *in situ* on CNFs and preparing a densely-packed film supported by filter paper for gas separations.[59] Due to the combination of amorphous and crystalline cellulose regions in CNFs, they are known to pack well, forming good barrier films with low oxygen permeability, and when the MOFs were incorporated only gas molecules smaller than the MOF pores could penetrate the film.[59] In contrast, we use highly crystalline rigid rod-shaped CNC nanoparticles. When cross-linked together, the

nanoparticles form highly porous self-supported 3D materials, which have tailorable absorbent and mechanical performance.[60,61]

Herein, we report a facile and novel method to combine functional MOFs and structural CNCs into a flexible and porous aerogel with hierarchical structure without the use of chemical modifiers. The hybrid materials are prepared through a straightforward sol-gel process, followed by freeze-drying.[49] Three different MOF-containing aerogels are demonstrated with up to 50 wt.% of uniformly distributed MOFs. This new strategy is based on orthogonally functionalized celluloses, which are prepared via simple water-based chemistry through multistep processes to impart cross-linking ability. The celluloses individually form colloidally stable suspensions (or solutions) but assemble into covalently cross-linked clusters with entrapped MOFs, when mixed together. The combination of MOFs, cross-linked clusters and freeze drying, gives hybrid aerogels with hierarchical pores that remain intact in liquid under compression. MOFs retain their crystallinity, porosity and accessibility in the aerogel format making them ideal absorbents for water purification and other separations applications.

Hybrid MOF aerogels were prepared by mixing MOF particles with cross-linkable CNCs to form a stable colloidal suspension in water, and then added to an aqueous solution of cross-linkable carboxymethyl cellulose (CMC). More specifically, cross-linkable celluloses were based on aldehyde modified CNCs (CHO-CNCs) and hydrazide modified CMC ($NHNH_2$-CMC) which form hydrazone cross-links when in contact. The mixture thus contained cross-linked clusters composed of MOFs trapped in CNCs cross-linked to CMC, however these clusters remained colloidally stable. The MOF-cellulose interaction

is primarily due to physical entanglement and van der Waals interactions between MOF particles and cellulose.[57] The suspension of clusters was frozen and freeze-dried to prepare the hybrid aerogels shown schematically in **Figure 6-1**A. Three MOF types with different sizes and functionalities were synthesized and successfully incorporated into the cellulose aerogels, including zeolitic imidazolate framework-8 (ZIF-8),[62] University of Oslo-66 (UiO-66),[63] and Material Institute de Lavoisier-100(Fe) (MIL-100(Fe)).[64] The resultant hybrid aerogels were uniform, flexible, and could easily be handled without any loss of structural integrity (Figure 6-1B and Supporting Information Video S6-1). Powder X-ray diffraction (PXRD) of the aerogels showed that the MOF crystallinity was retained during the processing (Supporting Information Figure S6-1).

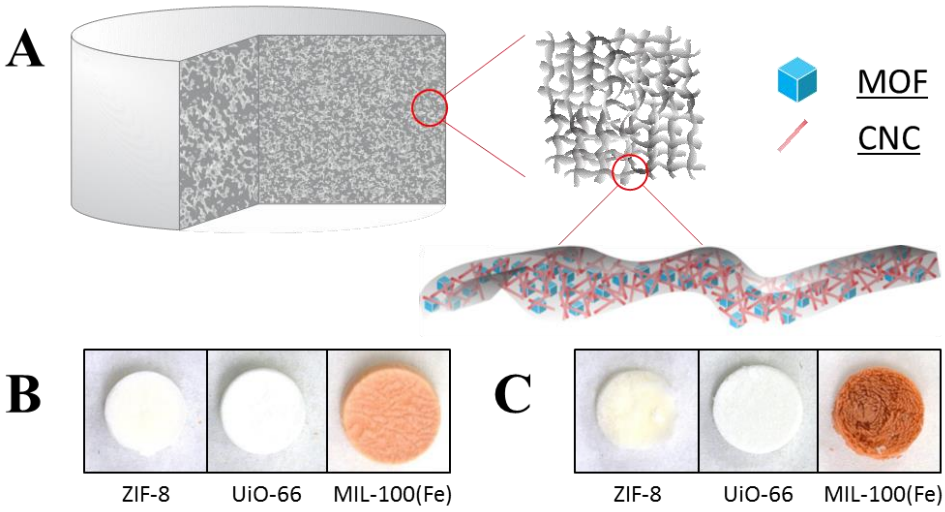

Figure 6-1. (A) Schematic of MOF-cellulose hybrid aerogel. Photographs of (B) CNC-CMC based hybrid aerogels (CNC:CMC:MOF=1:1:1 by weight), and (C) all-CNC based hybrid aerogels (CNC:CNC:MOF=1:1:1 by weight); aerogels are about 7 mm in diameter and 5 mm in height.

Similarly, hybrid aerogels were prepared without CMC such that the substrate was entirely composed of orthogonally functionalized CNC nanoparticles (i.e., CHO-CNCs and $NHNH_2$-CNCs).[61] However, when high loadings of MOFs were used the hybrid aerogels exhibited a more loosely connected structure and fell apart easily (Figure 6-1C). As the MOF particles and CNCs are both rigid crystalline structures we believe that the ability to form CNC-CNC cross-links is sterically hindered in this system and thus the flexible $NHNH_2$-CMC is needed to gives aerogels with robust mechanical behavior.

The loading of MOF particles within the cellulose aerogels can be controlled by tuning the ratio of the three components in the initial suspensions. UiO-66-containing aerogels were chosen as an example to investigate the effect of MOF loading on the aerogel morphology and performance. We achieved loadings as high as 50 wt.%, above which the clusters were no longer stable in suspension and visibly sedimented; as such, these mixtures could not be processed by the sol-gel method which requires uniform dispersions prior to the ice crystal templating (freezing) step. Aerogels with 20, 33.3, and 50 wt.% UiO-66 added were prepared and characterized by thermogravimetric analysis (TGA) and scanning electron microscopy (SEM). The UiO-66 loadings determined by TGA were consistent with the nominal values indicating that all MOFs added to the suspension were incorporated into the aerogel (Supporting Information Table S6-1 and Figure S6-2). The hybrid aerogels had ultralow densities, increasing slightly with MOF loading from 18.4 ± 0.2 mg/cm^3 for 20 wt.% to 22 ± 1 mg/cm^3 and 32.8 ± 0.4 mg/cm^3 for 33.3 and 50 wt.% MOFs, respectively. This implies that we have significant control over the MOF loading and density and that the aerogels are extremely porous with a large accessible surface area.

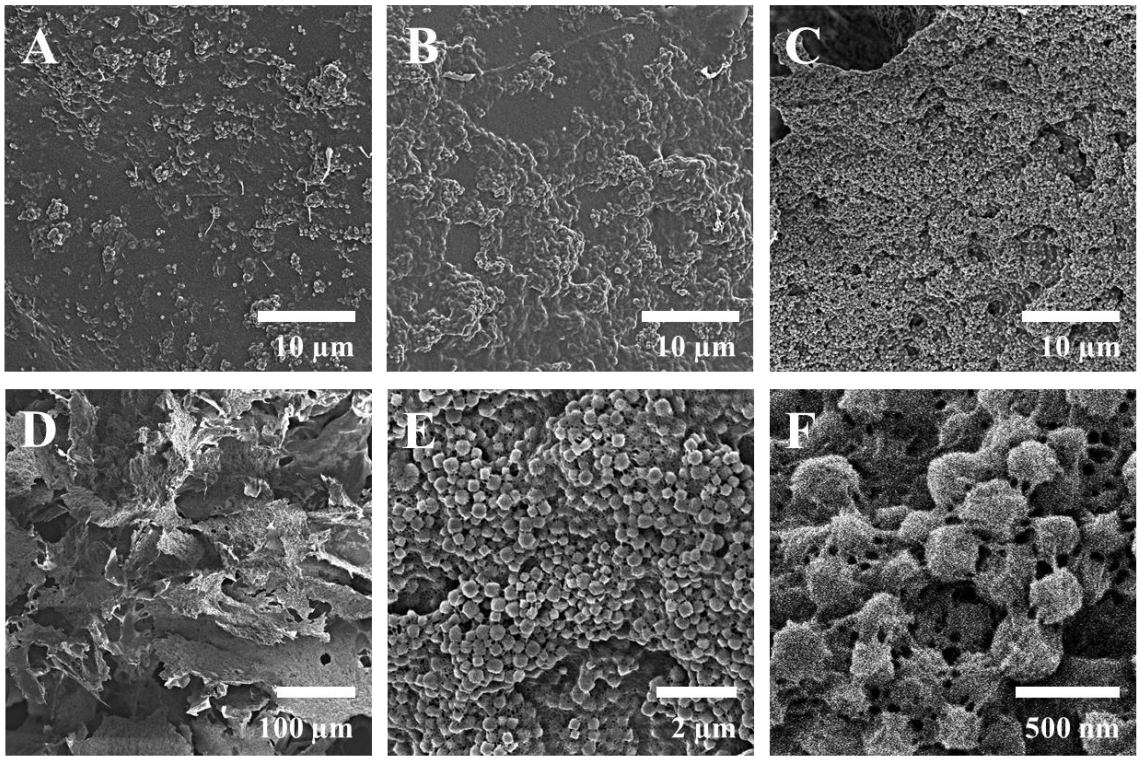

Figure 6-2. SEM images of UiO-66-containing cellulose aerogels. (A) Aerogel with 20 wt.% UiO-66, (B) aerogel with 33.3 wt.% UiO-66, (C, D, E, F) aerogels with 50 wt.% UiO-66 at different magnifications.

The morphology of these hybrid aerogels was studied by SEM to investigate the hierarchical structure (**Figure 6-2**). In general, all aerogels exhibit a similar internal pore structure, consisting of micro pores from the well-defined MOF pores (not visible by SEM), meso pores between the cross-linked CNCs and CMC which make up the "walls" of the structure, and macro pores templated from the ice crystals that grow when the suspension of clusters is frozen. Additionally, MOF particles are well dispersed within the "walls" and no MOF agglomerates are observed. We believe this uniformity stems from the ability for CNCs to aid in the suspension of MOF particles and the regularity in the cross-linked clusters, highlighting the intricacies of our processing method. The versatility of the

approach is also confirmed through the preparation of aerogels with ZIF-8 and MIL-100(Fe) which exhibit similar morphology (Supporting Information Figure S6-3).

At low MOF loadings, macroscopic regions without any MOFs are observed in the mesoporous "walls" of the aerogels (Figure 6-2A and 6-2B); however, at high MOF loadings, the "walls" are predominantly MOF particles (Figures 6-2E and 6-2F). Importantly, the MOFs appear entrapped within the cellulose matrix and are not merely attached to the surface (Figure 6-2F). This structure is predicted to minimize MOF loss and leaching during use, as tested below. The high MOF loading achieved and the porous structure of the aerogel indicate that we have produced a novel hybrid material, which retains the favourable properties of both MOFs and CNCs. We expect that the morphology of the aerogels has led to one of the highest surface-area accessible and lightweight MOF-containing materials reported to date. While MOF-only powders/films are known to have higher surface areas than hybrid materials, they are difficult to process into useful forms.

Although MOFs are intended for various applications, here we test the water purification abilities of our hybrid aerogels to demonstrate that the MOFs are still functional when entrapped in the cellulose matrix. This is a particularly promising application area for this type of material as CNC aerogels are recognized to function as absorbents and can take up more than 100 times their own mass in water, be compressed to remove the liquid and re-used.[61] Specifically we looked at using the UiO-66-containing aerogels to remove the hazardous compound potassium dichromate, which is the most toxic form of chromium, Cr(VI), which often ends up in water streams due to industrial pollution.[65,66] In the test, a small aerogel (~0.8 cm^3) was placed into 10 mL of an aqueous solution containing 10

mg/L potassium dichromate. The Cr(VI) contaminated water was initially light yellow but became colorless after the hybrid aerogel adsorbed the contaminants, while conversely the color of the hybrid aerogel itself changed from white to light yellow (**Figure 6-3**A). This color change due to water purification was even more striking in the case of MIL-100(Fe)-containing aerogels which removed Rhodamine B (Supporting Information Figure S6-4).

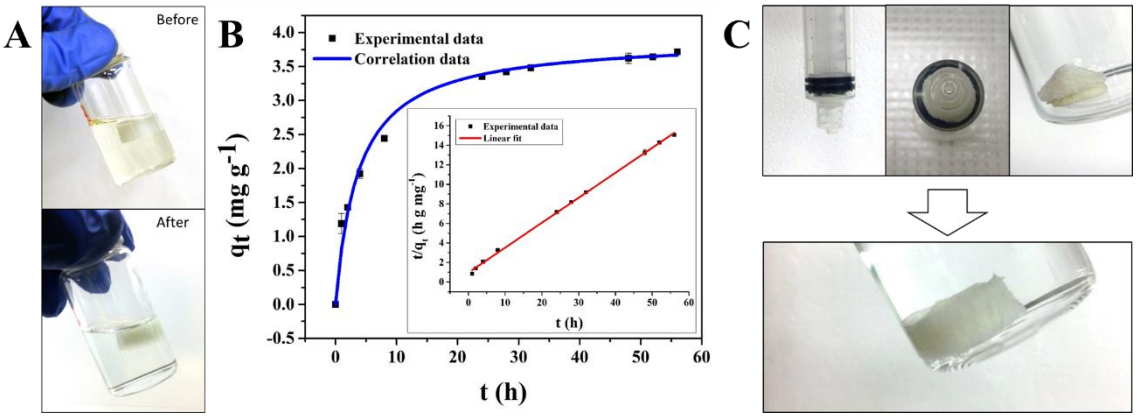

Figure 6-3. (A) Photographs of the contaminated aqueous solution before and after adsorbing Cr(VI) in the aerogel with 50 wt.% UiO-66 and (B) the time dependent adsorption (correlation curve was drawn using the kinetic parameters calculated from the pseudo-second-order model) and pseudo-second-order plots (inset). (C) Photographs showing that a wet hybrid aerogels (50 wt.% UiO-66) can be incorporated into a syringe and compressed fully by the piston (top left), also shown from the bottom view of the syringe (top middle). When removed from the syringe, the compressed aerogel in air maintains the shape of the container it was compressed in (top right) but recovers its original shape completely when place in solution again (bottom), this is also demonstrated in the Supporting Information Video S1.

The adsorptive capacities (q_t in mg/g) of the MOF particles within the aerogels at different times (t) were obtained to study the kinetic behavior (see Experimental Section for details). The time-dependence of the adsorption was well-fitted to a pseudo-second-order kinetic model with rate constant k_2 (Figure 6-3B and Supporting Information Figure

S6-5) which is the expected diffusion limited behavior of MOFs and implies that the cellulose support is not hindering the accessibility of the MOF pores. The values of the kinetic parameters are summarized in the Supporting Information Table S6-2. The aerogel containing 50 wt.% UiO-66 adsorbed 85% of the Cr(VI) after 24 hours, while aerogels with lower MOF loadings adsorbed 67% (33.3 wt.% UiO-66) and 51% (20 wt.% UiO-66) of the Cr(VI) due to the lower MOF content. Aerogels without MOFs (control sample) did not show any removal of Cr(VI) after 24 hours according to UV-Vis spectroscopy. No MOF particles were released from the aerogels into the water after 24 hours of soaking as tested by dynamic light scattering (DLS) and similarly, no breakdown of MOFs or leaching was detected by inductively coupled plasma optical emission spectrometry (ICP-OES) testing for trace Zr content (Supporting Information Table S6-3).

Table 6-1. Adsorption capacities of Cr(VI) for aerogel with UiO-66, UiO-66 portion of aerogel, and UiO-66 powder.

UiO-66 loading	Adsorption capacity q_t (mg g^{-1})[a]		
	Aerogel with MOF	MOF portion of aerogel[b]	MOF powder[c]
20 wt.%	3.60	18.02	15.50
33.3 wt.%	3.89	11.66	8.40
50 wt.%	3.35	6.70	6.96

[a] The adsorption was conducted over 24 hours without any agitation. [b] This capacity was calculated with the same data used for the aerogel with MOF, but only the UiO-66 mass was used instead of the total aerogel mass. [c] The amount of the UiO-66 powder used for characterizing adsorption capacity was the same as the amount of the UiO-66 powder trapped within the aerogel.

The adsorption capacity of pure UiO-66 powder was also tested to compare with the MOF-containing aerogels. When the same mass of MOF powder as was present in the aerogel was used, the powder was found to adsorb 85% of the Cr(VI) after 24 hours, which is the same as the corresponding hybrid aerogel. However, if the total mass of the aerogel is considered then the mass specific adsorption capacity is slightly lower for the aerogels. In all cases, equivalent or superior adsorption capacity (based on mass of MOFs) was observed for the aerogels (**Table 6-1**), indicating that all of the MOF particles within the aerogel are functional. We believe the aerogel's hierarchical porous structure contributes significantly to this good performance where the combination of easy accessibility through macropores, and capillary effect of mesopores, allow for fast water uptake and contact between the MOF micropores and the contaminants.

In addition to adsorbing large amounts of contaminants, the aerogels could be compressed to squeeze out the water, which always contained a lower concentration of contaminants than the bulk solution; for example, in one test, after 8 hours of soaking, the concentration of Cr(VI) within the aerogel (with 50 wt.% UiO-66) was 1.8 mg/L while the bulk solution had a concentration of 3.7 mg/L. This concentration difference contributed to the aerogel performance by consistently driving more contaminated water into the aerogel until saturation. Additionally, no leaching of MOF particles occurred during the compression process since no particle signal was detected by DLS. The compressed aerogels quickly recovered their shape when re-immersed in water (Figure 6-3C). Hybrid aerogels with ZIF-8 and MIL-100 were also tested for water treatment and showed a high capacity for the removal of other hazardous materials including benzotriazole and

Rhodamine B, for ZIF-8 and for MIL-100(Fe) aerogels, respectively (Supporting Information Figure S6-4 and Table S6-2).

In conclusion, we have demonstrated a facile way of combining two emerging materials – MOFs and CNCs – into one highly functional aerogel. The CNCs act as the structural component supporting the functional MOFs in a three dimensional flexible and lightweight networked material. The MOF loading can be tailored by changing the initial ratio of components, up to 50 wt.% MOF content can be easily achieved. Three different types of MOFs were embedded into the CNC-based aerogels, highlighting the versatility of the processing method and materials, and showing that the MOFs retain their crystallinity and function. Water treatment applications were demonstrated based on the good absorption properties of aerogels, however these materials may also be extended to be used as air filters, substrate-supported catalysis, and sensors, to name just a few examples.

6.2 Experimental

Materials. Whatman cotton ashless filter aid was purchased from GE Healthcare Canada, and sulfuric acid (95−98%) was purchased from VWR Canada. Dimethyl sulfoxide (DMSO, reagent grade) was purchased from Caledon Laboratory Chemicals (Georgetown, ON, Canada). Sodium carboxmethyl cellulose (CMC, Mw ~ 250000 g/mol, degree of substitution = 0.9), adipic acid dihydrazide (ADH, 98%), N-hydroxysuccinimide (NHS, 97%), N'-ethyl-N-(3-dimethylaminopropyl)-carbodiimide (EDC, commercial grade), zinc nitrate hexahydrate (98%), 2-methylimidazole (99%), zirconium chloride (≥99.5%), terephthalic acid (BDC, 98%), acetate acid (≥99.7%), iron (III) chloride hexahydrate

(≥98%), trimethyl 1,3,5-benzenetricarboxylate (95%), benzotriazole (99%), potassium dichromate (≥99%), and Rhodamine B (≥95%) were purchased from Sigma-Aldrich and used without further purification. All water used was purified Type I water with a resistivity of 18.2 MΩ· cm (Barnstead NANOpure DIamond system, Thermo Scientific, Asheville, NC).

MOFs. ZIF-8 (Zeolitic Imidazolate Framework-8), UiO-66 (University of Oslo-66), and MIL-100(Fe) (Material Institute de Lavoisier-100(Fe)) were prepared using the methods reported in the literatures [67-69]. Briefly, ZIF-8 was prepared by dropping zinc nitrate solution (1.17 g zinc nitrate hexahydrate in 8 g water) into 2-methylimidazole solution (22.7 g 2-methylimidazole in 80 g water) under stirring for 10 minutes and collected by ultracentrifugation and washed 3 times with water. UiO-66 was prepared by dissolving zirconium chloride (915 mg) and BDC (645 mg) in 225 mL DMF containing 6.7 mL acetic acid, which was kept under 120 ℃ for 24 hours and collected by centrifugation and washed with methanol (3 times) afterwards. MIL-100(Fe) was prepared by dispersing iron (III) chloride hexahydrate (0.162 g) and trimethyl 1,3,5-benzenetricarboxylate (0.138 g) in 5 mL water, which was then kept under 130 ℃ for 3 days. The product was centrifuged and washed with acetone (3 times).

Preparation of Carboxymethyl Cellulose-Hydrazide ($NHNH_2$-CMC), Hydrazide-Modified CNCs ($NHNH_2$-CNCs) and Aldehyde-Modified CNCs (CHO-CNCs). $NHNH_2$-CNCs and CHO-CNCs were synthesized using the method described in our previous work [60]. Briefly, hydrazide groups were introduced onto CMC (or CNC) by reacting ADH with CMC (or CNC) through the NHS/EDC coupling system; aldehyde groups were generated

by the oxidization of the CNC using $NaIO_4$. Solutions/suspensions were stored at 4 ℃ before further experiments.

Preparation of Hybrid Aerogels. MOF nanoparticles were suspended into 1 wt.% CHO-CNC suspensions, with 15 min of probe sonication. The resulting suspensions were mixed with an equal volume of 1 wt.% $NHNH_2$-CMC, or $NHNH_2$-CNCs, using a vortex mixer (Level 8, Analog Vortex Mixer, VWR) for 2 min. We note that MOFs needed to be premixed with colloidally stable CNCs first and then the CMC was added, if MOFs were added to CMC first, precipitation was observed. All suspensions were in ultrapure water without pH adjustment and the native pH of CHO-CNC suspensions and $NHNH_2$-CMC solutions was between 5 and 6. The final suspension of cross-linked clusters was transferred into a cylindrical glass vial (14.5 mm in diameter) and allowed to set for another 10 min before transfer into the freezer (-20 ℃). The final hybrid aerogels were obtained by freeze-drying the ice-gel.

Adsorption. Adsorption kinetics were studied by soaking the aerogels or MOF particles in 10 mL aqueous solution containing different contaminants (200 mg/L benzotriazole for ZIF-8, 10 mg/L potassium dichromate for UiO-66, and 0.01 mM Rhodamine B for MIL-100(Fe)) for a predetermined time. Then the solution was analyzed by UV-Vis to determine the concentration based on a calibration curve prepared from solutions with known contaminant concentrations. The adsorption capacity at time t was calculated using the following equation:

$$q_t = \frac{(C_0 - C_t)V}{m}$$

where V is the solution volume, m is the mass of the aerogel or the mass of MOF particles, C_0 is the initial concentration, C_t is the concentration at time t. The time-dependence of the adsorption was fitted with the pseudo-second-order kinetic model, which is:

$$\frac{t}{q_t} = \frac{1}{k_2 q_e^2} + \frac{1}{q_e} t$$

where q_t and q_e are the adsorption capacities at time t and equilibrium, respectively, and k_2 is the rate constant of the pseudo-second-order model.

Characterization. JEOL JSM 7000 Scanning Electron Microscopy (SEM) was used to characterize the MOF particles and aerogels with a 5 nm platinum coating. Powder X-ray diffraction (PXRD) was conducted on a Bruker D8 Advance X-Ray Diffractometer with a scan speed of 1 deg min, a step size of 0.05°, and a 2θ range of 2-50 °. The concentration of the contaminated water was determined by DU 800 UV/Vis Spectrophotometer. UiO-66 nanoparticle size distribution (Supporting Information Figure S6-6) was obtained by measuring 100 randomly selected nanoparticles using the software *Nano Measure*, giving an average size of 180 ± 30 nm from SEM analysis. The presence of MOFs in purified water test (leaching) were determined using a Malvern Zetasizer Nanoparticle Analyzer (dynamic light scattering apparatus) at 25 ℃. Thermogravimetric analysis (TGA) was performed on a TA Q5000 thermogravimetric analyzer with a ramp rate of 10 ℃ min^{-1} up to 700 ℃, and then held at that temperature for 10 min. Inductively coupled plasma optical emission spectrometry (ICP-OES) was conduceted on Varian ICP-OES Vista Pro.

6.3 Acknowledgements

The authors thank Professors R. Pelton and A. Guarné for access to equipment, and Dr. G. de Silveira for training. This work was carried out using instruments in the Biointerfaces Institute and the Canadian Centre for Electron Microscopy. We sincerely thank the Natural Sciences and Engineering Research Council (NSERC) of Canada and the Canada Research Chair (CRC) program of the Federal Government for supporting this research.

6.4 References

[1] H. Li, M. Eddaoudi, M. O'Keeffe, O. M. Yaghi, *Nature* **1999**, *402*, 276-279.

[2] H. T. Kwon, H.-K. Jeong, *Journal of the American Chemical Society* **2013**, *135*, 10763-10768.

[3] H. Zhu, H. Liu, I. Zhitomirsky, S. Zhu, *Materials Letters* **2015**, *142*, 19-22.

[4] A. R. Millward, O. M. Yaghi, *Journal of the American Chemical Society* **2005**, *127*, 17998-17999.

[5] X. Wang, L. Xie, K.-W. Huang, Z. Lai, *Chemical Communications* **2015**, *51*, 7610-7613.

[6] G. Lu, J. T. Hupp, *Journal of the American Chemical Society* **2010**, *132*, 7832-7833.

[7] J. Liu, F. Sun, F. Zhang, Z. Wang, R. Zhang, C. Wang, S. Qiu, *Journal of Materials Chemistry* **2011**, *21*, 3775-3778.

[8] M. J. Katz, S.-Y. Moon, J. E. Mondloch, M. H. Beyzavi, C. J. Stephenson, J. T. Hupp, O. K. Farha, *Chemical Science* **2015**, *6*, 2286-2291.

[9] J. E. Mondloch, M. J. Katz, W. C. Isley III, P. Ghosh, P. Liao, W. Bury, G. W. Wagner, M. G. Hall, J. B. DeCoste, G. W. Peterson, *Nature materials* **2015**, 14, 512-516.

[10] L. Cooper, T. Hidalgo, M. Gorman, T. Lozano-Fernández, R. Simón-Vázquez, C. Olivier, N. Guillou, C. Serre, C. Martineau, F. Taulelle, *Chemical Communications* **2015**, *51*, 5848-5851.

[11] E.-L. Zhou, P. Huang, C. Qin, K.-Z. Shao, Z.-M. Su, *Journal of Materials Chemistry A* **2015**, *3*, 7224-7228.

[12] A. K. Crane, B. O. Patrick, M. J. MacLachlan, *Dalton Transactions* **2013**, *42*, 8026-8033.

[13] M. Kim, J. F. Cahill, Y. Su, K. A. Prather, S. M. Cohen, *Chemical Science* **2012**, *3*, 126-130.

[14] H. Liu, H. Zhu, S. Zhu, *Macromolecular Materials and Engineering* **2015**, *300*, 191-197.

[15] N. Yanai, M. Sindoro, J. Yan, S. Granick, *Journal of the American Chemical Society* **2012**, *135*, 34-37.

[16] M. Pang, A. J. Cairns, Y. Liu, Y. Belmabkhout, H. C. Zeng, M. Eddaoudi, *Journal of the American Chemical Society* **2013**, *135*, 10234-10237.

[17] H. Zhu, Q. Zhang, S. Zhu, *Dalton Transactions* **2015**, 44, 16752-16757.

[18] S. Furukawa, J. Reboul, S. Diring, K. Sumida, S. Kitagawa, *Chemical Society Reviews* **2014**, *43*, 5700-5734.

[19] A. Bétard, R. A. Fischer, *Chemical reviews* **2011**, *112*, 1055-1083.

[20] S. Qiu, M. Xue, G. Zhu, *Chemical Society Reviews* **2014**, *43*, 6116-6140.

[21] S. Hermes, M. K. Schröter, R. Schmid, L. Khodeir, M. Muhler, A. Tissler, R. W. Fischer, R. A. Fischer, *Angewandte Chemie International Edition* **2005**, *44*, 6237-6241.

[22] H. Zhu, S. Zhu, *The Canadian Journal of Chemical Engineering* **2015**, *93*, 63-67.

[23] K. Tao, L. Cao, Y. Lin, C. Kong, L. Chen, *Journal of Materials Chemistry A* **2013**, *1*, 13046-13049.

[24] D. Liu, X. Ma, H. Xi, Y. Lin, *Journal of Membrane Science* **2014**, *451*, 85-93.

[25] O. Shekhah, H. Wang, S. Kowarik, F. Schreiber, M. Paulus, M. Tolan, C. Sternemann, F. Evers, D. Zacher, R. A. Fischer, *Journal of the American Chemical Society* **2007**, *129*, 15118-15119.

[26] O. Shekhah, R. Swaidan, Y. Belmabkhout, M. du Plessis, T. Jacobs, L. J. Barbour, I. Pinnau, M. Eddaoudi, *Chemical Communications* **2014**, *50*, 2089-2092.

[27] M. Li, M. Dincă, *Chemical Science* **2014**, *5*, 107-111.

[28] I. Stassen, M. Styles, T. Van Assche, N. Campagnol, J. Fransaer, J. Denayer, J.-C. Tan, P. Falcaro, D. De Vos, R. Ameloot, *Chemistry of Materials* **2015**, *27*, 1801-1807.

[29] N. Stock, S. Biswas, *Chemical reviews* **2011**, *112*, 933-969.

[30] M. S. Denny, S. M. Cohen, *Angewandte Chemie International Edition* **2015**, *54*, 9029-9032.

[31] H. Yehia, T. Pisklak, J. Ferraris, K. Balkus, I. Musselman, "Methane facilitated transport using copper (II) biphenyl dicarboxylate-triethylenediamine/poly (3-acetoxyethylthiophene) mixed matrix membranes", in *ABSTRACTS OF PAPERS OF THE AMERICAN CHEMICAL SOCIETY*, AMER CHEMICAL SOC 1155 16TH ST, NW, WASHINGTON, DC 20036 USA, 2004, p. 227/U351-U351.

[32] T. Rodenas, M. van Dalen, E. García‐Pérez, P. Serra‐Crespo, B. Zornoza, F. Kapteijn, J. Gascon, *Advanced Functional Materials* **2014**, *24*, 249-256.

[33]M. G. Schwab, I. Senkovska, M. Rose, M. Koch, J. Pahnke, G. Jonschker, S. Kaskel, *Advanced Engineering Materials* **2008**, *10*, 1151-1155.

[34] M. Rose, B. Boehringer, M. Jolly, R. Fischer, S. Kaskel, *Advanced Engineering Materials* **2011**, *13*, 356-360.

[35] Y.-n. Wu, F. Li, H. Liu, W. Zhu, M. Teng, Y. Jiang, W. Li, D. Xu, D. He, P. Hannam, *Journal of Materials Chemistry* **2012**, *22*, 16971-16978.

[36] D. Wisser, F. M. Wisser, S. Raschke, N. Klein, M. Leistner, J. Grothe, E. Brunner, S. Kaskel, *Angewandte Chemie International Edition* **2015**, *54*, 12588-12591.

[37] P. Küsgens, S. Siegle, S. Kaskel, *Advanced Engineering Materials* **2009**, *11*, 93-95.

[38] A. R. Abbasi, K. Akhbari, A. Morsali, *Ultrasonics sonochemistry* **2012**, *19*, 846-852.

[39] M. da Silva Pinto, C. A. Sierra-Avila, J. P. Hinestroza, *Cellulose* **2012**, *19*, 1771-1779.

[40] E. López‐Maya, C. Montoro, L. M. Rodríguez‐Albelo, S. D. Aznar Cervantes, A. A. Lozano‐Pérez, J. L. Cenís, E. Barea, J. A. Navarro, *Angewandte Chemie International Edition* **2015**, 127, 6894-6898.

[41] H. S. Rodríguez, J. P. Hinestroza, C. Ochoa‐Puentes, C. A. Sierra, C. Y. Soto, *Journal of Applied Polymer Science* **2014**, *131*.

[42] M. A. Bunge, K. N. Ruckart, S. Leavesley, G. W. Peterson, N. Nguyen, K. N. West, T. G. Glover, *Industrial & Engineering Chemistry Research* **2015**, *54*, 3821-3827.

[43] K. Díaz, M. López-González, L. F. del Castillo, E. Riande, *Journal of Membrane Science* **2011**, *383*, 206-213.

[44] T. Rodenas, I. Luz, G. Prieto, B. Seoane, H. Miro, A. Corma, F. Kapteijn, F. X. L. i Xamena, J. Gascon, *Nature materials* **2015**, *14*, 48-55.

[45] S. Hwang, W. S. Chi, S. J. Lee, S. H. Im, J. H. Kim, J. Kim, *Journal of Membrane Science* **2015**, *480*, 11-19.

[46] M. R. Lohe, M. Rose, S. Kaskel, *Chemical Communications* **2009**, 6056-6058.

[47] L. Li, S. Xiang, S. Cao, J. Zhang, G. Ouyang, L. Chen, C.-Y. Su, *Nature communications* **2013**, *4*, 1774.

[48] M. Hamedi, E. Karabulut, A. Marais, A. Herland, G. Nyström, L. Wågberg, *Angewandte Chemie International Edition* **2013**, *52*, 12038-12042.

[49] X. Yang, K. Shi, I. Zhitomirsky, E. D. Cranston, *Advanced Materials* **2015**, *27*, 6104-6109.

[50] M. Kaushik, A. Moores, *Green Chemistry* **2016**, 18, 622-637.

[51] K. E. Shopsowitz, H. Qi, W. Y. Hamad, M. J. MacLachlan, *Nature* **2010**, *468*, 422-425.

[52] K. E. Shopsowitz, W. Y. Hamad, M. J. MacLachlan, *Angewandte Chemie International Edition* **2011**, *50*, 10991-10995.

[53] M. Giese, L. K. Blusch, M. K. Khan, W. Y. Hamad, M. J. MacLachlan, *Angewandte Chemie International Edition* **2014**, *53*, 8880-8884.

[54] R. J. Moon, A. Martini, J. Nairn, J. Simonsen, J. Youngblood, *Chemical Society Reviews* **2011**, *40*, 3941-3994.

[55] M. Roman, *Industrial Biotechnology* **2015**, *11*, 25-33.

[56] D. Klemm, F. Kramer, S. Moritz, T. Lindström, M. Ankerfors, D. Gray, A. Dorris, *Angewandte Chemie International Edition* **2011**, *50*, 5438-5466.

[57] M. M. Hamedi, A. Hajian, A. B. Fall, K. Håkansson, M. Salajkova, F. Lundell, L. Wågberg, L. A. Berglund, *ACS nano* **2014**, *8*, 2467-2476.

[58] Y. Li, H. Zhu, F. Shen, J. Wan, S. Lacey, Z. Fang, H. Dai, L. Hu, *Nano Energy* **2015**, *13*, 346-354.

[59] M. Matsumoto, T. Kitaoka, *Advanced Materials* **2016**, 28, 1765-1769.

[60] X. Yang, E. Bakaic, T. Hoare, E. D. Cranston, *Biomacromolecules* **2013**, *14*, 4447-4455.

[61] X. Yang, E. D. Cranston, *Chemistry of Materials* **2014**, *26*, 6016-6025.

[62] K. S. Park, Z. Ni, A. P. Côté, J. Y. Choi, R. Huang, F. J. Uribe-Romo, H. K. Chae, M. O'Keeffe, O. M. Yaghi, *Proceedings of the National Academy of Sciences* **2006**, *103*, 10186-10191.

[63] J. H. Cavka, S. Jakobsen, U. Olsbye, N. Guillou, C. Lamberti, S. Bordiga, K. P. Lillerud, *Journal of the American Chemical Society* **2008**, *130*, 13850-13851.

[64] P. Horcajada, S. Surblé, C. Serre, D.-Y. Hong, Y.-K. Seo, J.-S. Chang, J.-M. Greneche, I. Margiolaki, G. Férey, *Chemical Communications* **2007**, 2820-2822.

[65] R. Ramos, A. Martinez, R. Coronado, *Water Science and Technology* **1994**, *30*, 191-197.

[66] H. Daraei, A. Mittal, J. Mittal, H. Kamali, *Desalination and Water Treatment* **2014**, *52*, 1307-1315.

[67] Y. Pan, Y. Liu, G. Zeng, L. Zhao, Z. Lai, *Chemical Communications* **2011**, *47*, 2071-2073.

[68] R. Canioni, C. Roch-Marchal, F. Sécheresse, P. Horcajada, C. Serre, M. Hardi-Dan, G. Férey, J.-M. Greneche, F. Lefebvre, J.-S. Chang, *Journal of Materials Chemistry* **2011**, *21*, 1226-1233.

[69] G. Lu, C. Cui, W. Zhang, Y. Liu, F. Huo, *Chem Asian J* **2013**, *8*, 69-72.

6.5 Supporting Information

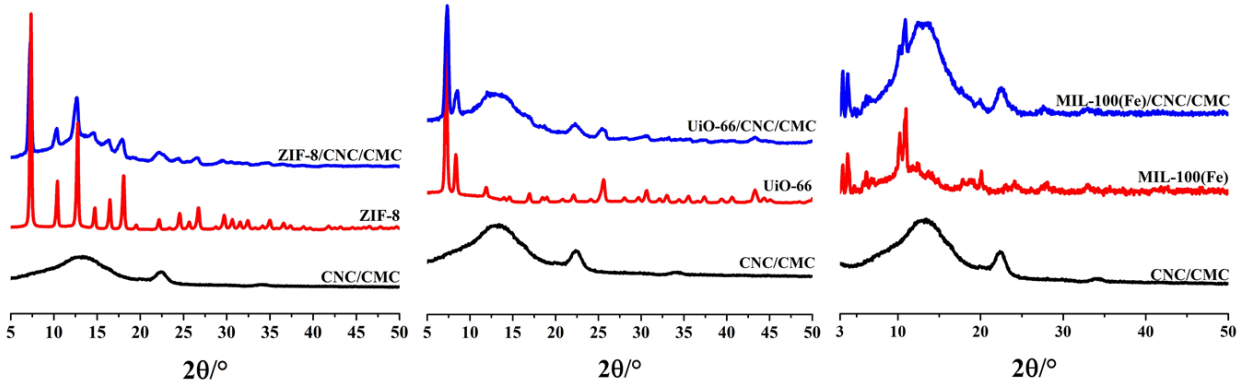

Figure S6-1. PXRD spectra of a CNC-CMC aerogel, pristine MOFs, and MOF-containing CNC-CMC aerogels.

Table S6-1. Nominal and measured weight percentage of UiO-66 within aerogels as determined by TGA.

	UiO-66-containing CNC-CMC aerogels[a]		
Nominal mass	20%	33.3%	50%
Ash content	10.46%	15.27%	22.05%
Measured mass	20.86%	33.41%	51.10%

[a] Ash content of plain CNC-CMC aerogel and UiO-66 powders are 2.465% and 40.79% after TGA testing.

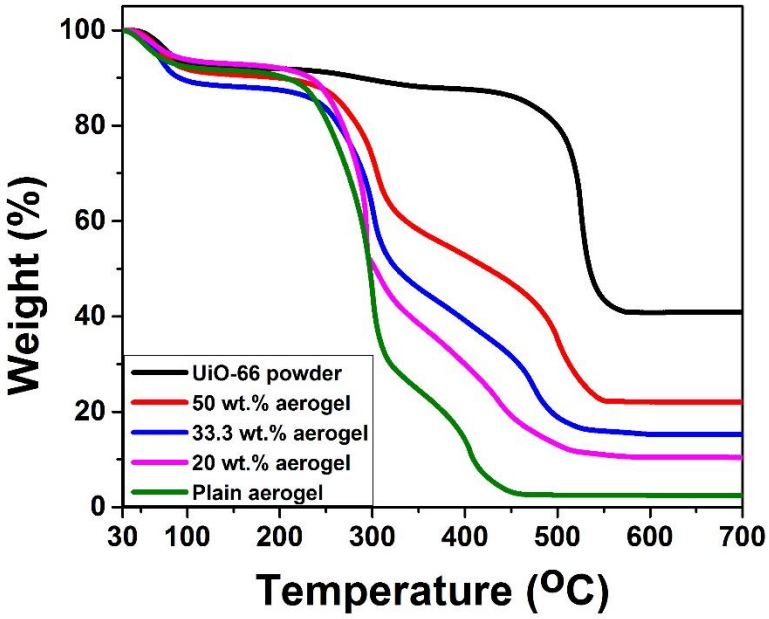

Figure S6-2. TGA curves for UiO-66 powder, CNC-CMC aerogel without MOF, and UiO-66 containing aerogel with different MOF loadings.

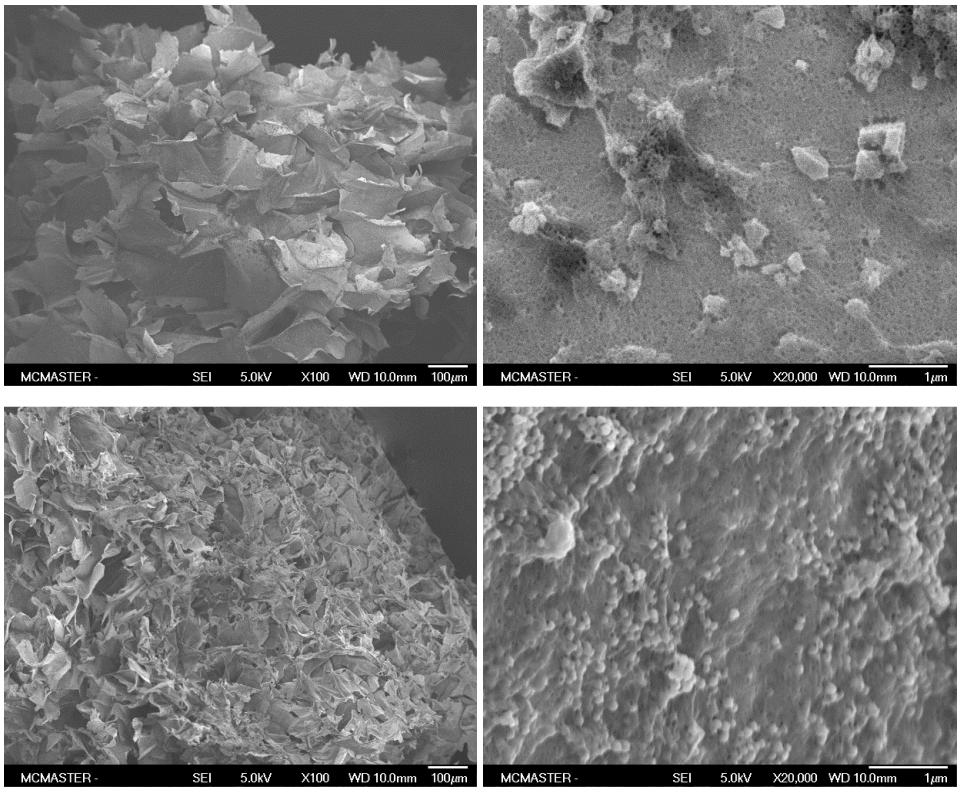

Figure S6-3. SEM images of ZIF-8 and MIL-100(Fe)-containing aerogels. Upper two images are aerogels with 33.3 wt.% MIL-100(Fe) at different magnifications. Lower two images are aerogels with 40 wt.% ZIF-8 at different magnifications.

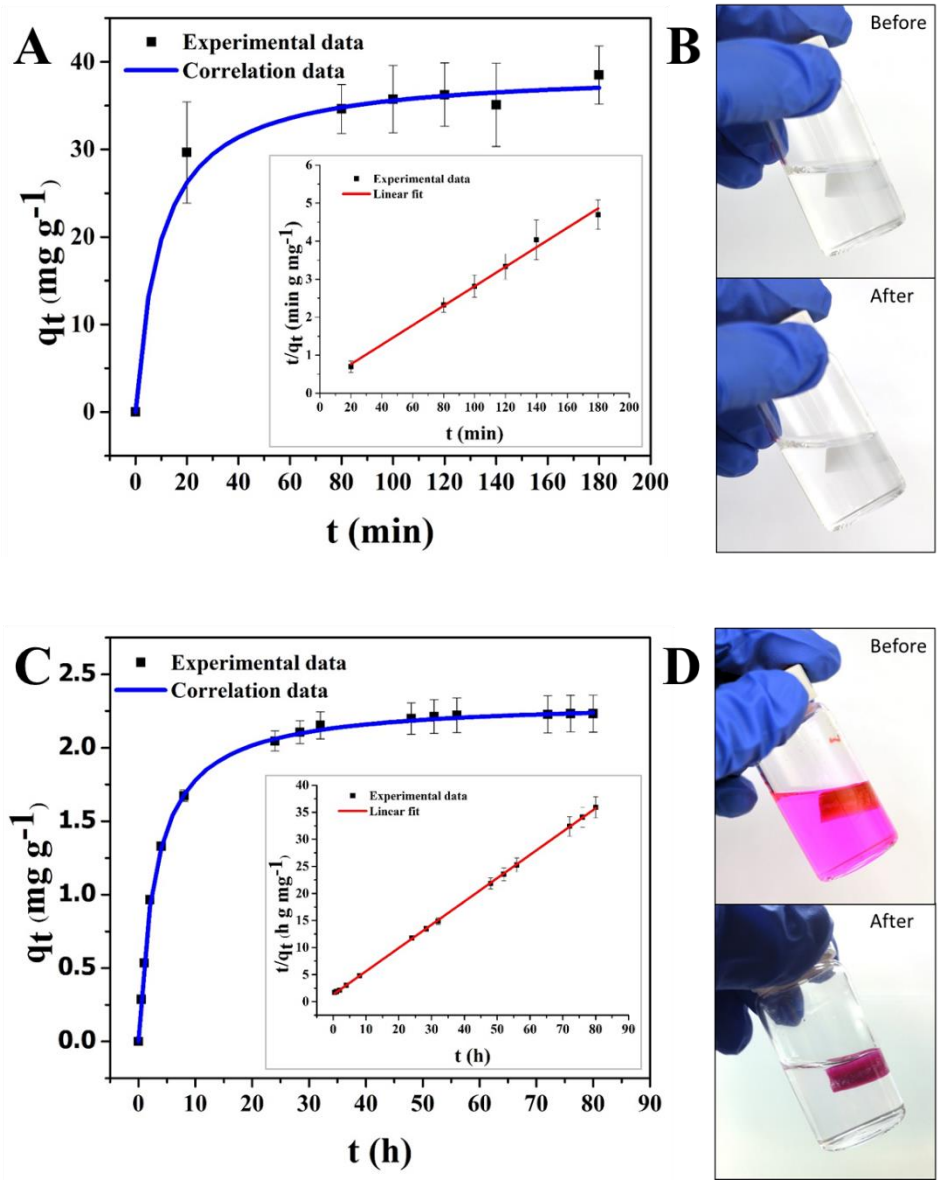

Figure S6-4. Time dependent adsorption (correlation curve was drawn using the kinetic parameters calculated from the pseudo-second-order model), pseudo-second-order plots (inset) and photographs of the contaminated aqueous solution before and after adsorption of (A, B) benzotriazole on ZIF-8 (40 wt.%) aerogel, (C, D) Rhodamine B on MIL-100(Fe) (33.3 wt.%) aerogel.

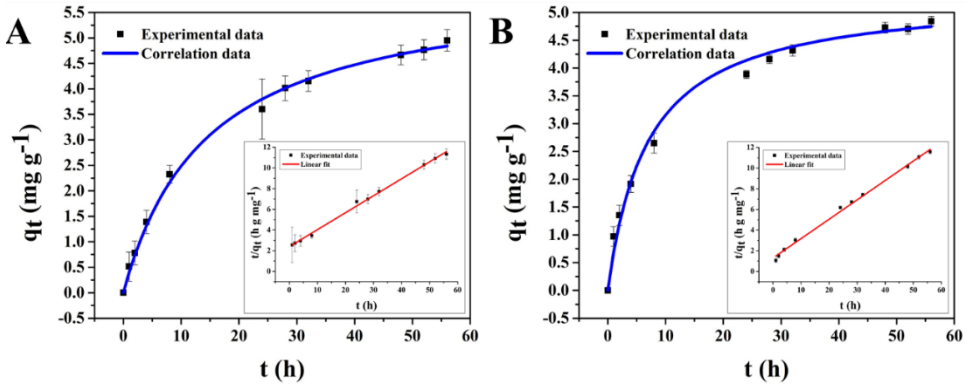

Figure S6-5. Time dependent adsorption (correlation curve was drawn using the kinetic parameters calculated from the pseudo-second-order model) and pseudo-second-order plots (inset) of the contaminated aqueous solution before and after absorption of Cr(VI) on (A) 20 wt.%, (B) 33.3 wt% loaded UiO-66 aerogel.

Table S6-2. Kinetic parameters for the adsorption of contaminants (Cr(VI) for UiO-66, benzotriazole for ZIF-8, Rodamine B for MIL-100(Fe)) on MOF loaded aerogels.

		Kinetic parameters		
	MOF loading	$q_{(e)cal}$ (mg g^{-1})	k_2 (g mg^{-1} h^{-1})	R^2
UiO-66	20 wt.%	6.1	0.01	0.9971
	33.3 wt.%	5.33	0.03	0.9963
	50 wt.%	3.91	0.07	0.9990
ZIF-8	40 wt.%	39.06	0.16	0.9927
MIL-100(Fe)	33.3 wt.%	2.32	0.14	0.9999

Table S6-3. Zr concentration detected by ICP-OES on pure water and water after treatment with 50 wt.% loaded UiO-66 aerogel.

	Pure water	Pure water after hydrogel compression[a]	Cr(VI) water after hydrogel adsorption[b]
Zr concentration (ppm)	0.077	0.076	0.076

[a] Water was obtained after compression of the 50 wt.% loaded UiO-66 aerogel showed in Supporting Information Video S1. [b] Cr(VI) water was obtained after soaking with 50 wt.% loaded UiO-66 aerogel for 24 hours.

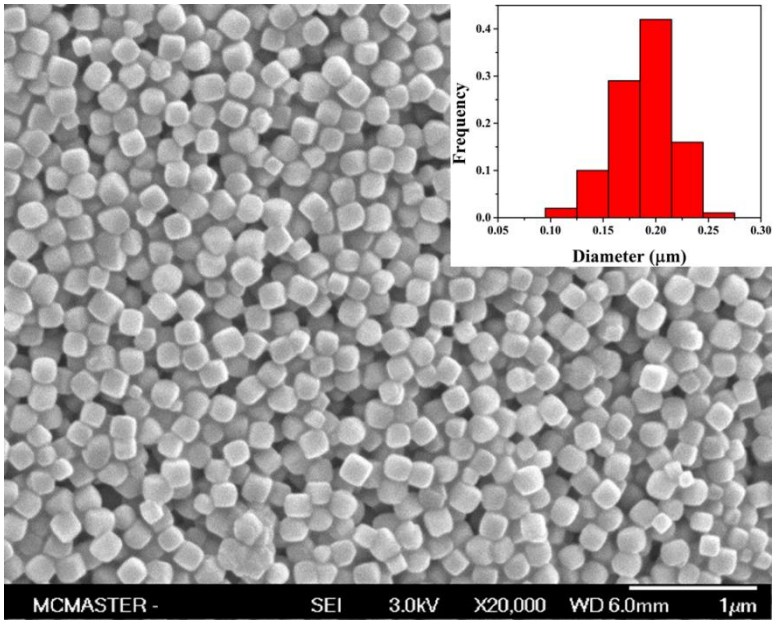

Figure S6-6. SEM image of UiO-66 particles and their size distribution determined digitally by measuring 100 randomly selected particles with the software Nano Measure (inset histogram). The average particles size is 180 ± 30 nm.

7 ALGINATE HYDROGEL: A SHAPEABLE AND VERSATILE PLATFORM FOR IN-SITU PREPARATION OF MOF-POLYMER COMPOSITES

This chapter is reprinted with permission from the paper published in *ACS Applied Materials & Interfaces* (DOI: 10.1021/acsami.6b04505) by *He Zhu, Qi Zhang, and Shiping Zhu.*

The idea was generated through discussion with the supervisor and the team members. He Zhu performed experiments, provided breakthroughs, and prepared the first draft, which was then revised by Dr. Qi Zhang and Dr. Shiping Zhu.

7.1 Abstract

This work reports a novel *in-situ* growth approach to incorporate metal-organic framework (MOF) materials into alginate substrate, which overcomes the challenges of processing MOF particles into specially shaped structures for real industrial applications. The MOF-alginate composites are prepared through the post-treatment of metal ion cross-linked alginate hydrogel with MOF ligand solution. MOF particles are well distributed and embedded in, as well as on the surface of the composites. The macroscopic shape of the

composite can be designed by controlling the shape of the corresponding hydrogel, thus MOF-alginate beads, fibers, and membranes are obtained. In addition, four different MOF-alginate composites, including HKUST-1-, ZIF-8-, MIL-100(Fe)-, and ZIF-67-alginate, were successfully prepared using different metal ion cross-linked alginate hydrogels. The formation mechanism is revealed and the composite is demonstrated to be an effective absorbent for water purification.

7.2 Introduction

Metal-organic frameworks (MOFs) are an emerging class of porous crystalline materials, prepared from self-assembly of metal ions and organic bridging ligands. Their highly ordered periodic porous structures give superior surface areas up to 7,000 m^2/g,[1,2] which is not attainable by traditional porous materials. In addition, high thermal stability, tunable pore property, and various chemical reactive sites have attracted great attention from many different areas, including gas storage,[3,4] gas separation,[5,6] chemical sensor,[7,8] catalysis,[9,10] proton conductor,[11,12] battery,[13,14] and drug delivery.[15,16]

Numerous types of MOFs have been designed, synthesized, modified, and studied in their particle forms.[17-20] It has been well demonstrated that MOF particles possess excellent properties. However, in real commercial applications, particle forms limit their potential and specially ordered shapes and morphologies are often required. Thus, increasing efforts have been focused on processing MOF particles into spheres,[21,22] chains,[23] membranes,[24-27] and structures with higher dimension.[28] Significant efforts have been made to deposit MOFs onto chemically stable and cost efficient shapeable

substrates, such as synthetic polymers[29,30] and ceramics.[6,31,32] However, this deposition approach is severely constrained by physical and chemical requirements of the substrates. Surface modification is usually needed prior to the deposition in order to increase their compatibility.[33,34]

Integration of MOF particles into polymer substrate through blending has then been demonstrated as an alternative to prepare robust and flexible MOF-polymer composites.[35-41] Incorporation of MOF particles into two-dimensional membranes, i.e. mixed-matrix membranes (MMMs), has been widely studied. Various polymer substrates have been reported for preparation of MMMs, such as polyimide,[36,39] polybenzimidazole,[42,43] polysulfone,[44,45] poly(ionic liquid),[46] and poly(vinylidene fluoride),[47,48] mainly for gas separation applications. Meanwhile, incorporation of MOF particles into three-dimensional polymer substrates has also been reported, either prepared via electrospun of polymer/MOF solution,[40,41] or through high internal phase emulsion as template.[49]

However, MOF-polymer composites prepared from simple blending often suffer from particle aggregation and poor particle-polymer matrix interaction, which can harm the composite performance.[50] *In-situ* MOF growth, on the other hand, is a promising approach to overcome these drawbacks, however, it has been much less studied. Alginate, as one of the natural polymers, derived from brown seaweeds, is consisted of 1,4-linked β-D-mannuronic (M block) and α-L-guluronic acid residues (G block).[51,52] It is a well-known polymer that can form hydrogels though ionotropic gelation under mild conditions.[53] Different divalent and trivalent metal ions have been reported to be able to cross-link alginate and prepare hydrogels.[54-56] This type of metal ion cross-linked hydrogels provides

a great candidate as *in-situ* MOF growth template for preparation of MOF-polymer composite materials.

In this work, we report a robust and straightforward *in-situ* growth method for preparation of MOF-alginate composites. We demonstrate that the metal ion cross-linked alginate hydrogels can be converted into MOF-alginate composites through a post-treatment of the hydrogels in MOF ligand solutions. The obtained MOF-alginate composites retain the shape of the corresponding hydrogels, which enables us to control the shape of the composite in the macroscopic level. MOF particles are well distributed in the alginate structure, as well as decorated on the surface. These composite materials can be easily used as convenient absorbents for removal of dye from water. This simple method for composite preparation greatly facilitates processing MOF materials into various shapes and morphologies often desired in real applications. It can combine the advantages of MOF materials in application and polymers in processing and fabrication.

7.3 Experimental

Materials. Copper nitrate trihydrate (99-104%), iron (III) chloride hexahydrate (≥98%), trimesic acid (95%), zinc nitrate hexahydrate (98%), cobalt nitrate hexahydrate (≥98%), 2-methylimidazole (99%), sodium formate (≥99%), alginic acid sodium salt, and Rhodamine B (≥95%) were purchased from Sigma-Aldrich and used without further purification. All water used was purified Type I water with a resistivity of 18.2 MΩ • cm (Barnstead NANOpure DIamond system, Thermo Scientific, Asheville, NC).

Metal ion cross-linked hydrogels. All hydrogels were prepared with the same protocol. Here we use Cu^{2+} cross-linked hydrogel as an example. The bead-like hydrogel was prepared by adding 3 mL 10 mg/mL sodium alginate aqueous solution dropwisely into 15 mL 30 mg/mL copper nitrate trihydrate aqueous solution. The prepared hydrogel beads were left in the solution overnight and then washed with water (X2) and ethanol (X2) to remove the excess Cu^{2+}. The fiber-like hydrogel was prepared by continuously injecting the sodium alginate solution into the Cu^{2+} solution using syringe with a needle on top. The membrane-like hydrogel was obtained by drop casting the sodium alginate solution on a glass slide, which was then carefully immersed into the Cu^{2+} solution. The other hydrogels were prepared under the same condition, except for in different metal aqueous solutions. In addition, the Co^{2+} and Zn^{2+} cross-linked hydrogels were soaked in their metal ion solution for 2 days to assure sufficient metal ion exchange and washed with water (X2) and methanol (X2).

MOF-alginate composites. The prepared Cu^{2+} and Fe^{3+} hydrogels were transferred into 15 mL 30 mg/mL trimesic acid ethanol solution for MOF growth under 85 ^{o}C for 18 hours. The prepared Co^{2+} and Zn^{2+} hydrogels were transferred into 20 mL methanol solution containing 0.2592 g 2-methylimidazolate and 0.1072 g sodium formate for MOF growth under 85 ^{o}C for 24 hours. The obtained MOF-alginate composites were washed with ethanol (X2) and hot ethanol (X2), and then dried under 80 ^{o}C.

Dye absorption of MIL-100-alginate composite. The MIL-100-alginate composite prepared from 0.5 mL sodium alginate solution was placed in 10 mL 0.01 mM Rhodamine B aqueous solution for 5 days before UV-Vis characterization. The Fe^{3+} cross-linked

hydrogel prepared from 0.5 mL sodium alginate solution was also tested for dye absorption under the same condition for comparison.

Characterization. MOF-alginate composites with a 5 nm platinum coating were characterized on JEOL JSM 7000 Scanning Electron Microscopy (SEM), the energy-dispersive X-ray spectroscopy characterization (EDX) was also done with the same equipment. Powder X-ray diffraction (PXRD) was carried out on Cu SMART6000 rotating anode diffractometer. UV-Vis absorption of dye contaminated water was conducted on DU 800 UV/Vis Spectrophotometer. Thermogravimetric analysis (TGA) was performed on TA Q5000 thermogravimetric analyzer with a ramp rate of 10℃/min. Nitrogen isotherm was conducted on Quantachrome Autosorb-IQ2-MP at 77K.

7.4 Results and Discussion

MOF-alginate composites were obtained by a post-treatment of the corresponding metal ion cross-linked hydrogels with MOF ligand precursor solutions. Hong Kong University of Science and Technology-1(HKUST-1)-alginate was chosen as a model system to demonstrate the feasibility of this method. Specifically, 3 mL 10 mg/mL sodium alginate aqueous solution was dropwisely added into 15 mL 30 mg/mL copper nitrate trihydrate aqueous solution. Spherical hydrogel beads were formed instantaneously, and left in the Cu^{2+} solution overnight for complete cross-linking. The prepared hydrogel beads were then washed with water twice and rewashed with ethanol twice to remove the excess Cu^{2+}. The hydrogel beads were then added into 15 mL 30 mg/mL trimesic acid (TMA) ethanol solution and kept under 85 ^{o}C for 18 hours for the preparation of HKUST-1-alginate

composite, as shown in Figure 7-1A. The formed Cu^{2+} cross-linked hydrogel was transparent with a light blue colour (Figure 7-1B & 7-1C), while turned opaque with a sky blue colour after incubation in the TMA ethanol solution (Figure 7-1D). The formation of HKUST-1 crystals was confirmed by powder X-ray diffraction (PXRD) (Figure S7-1).

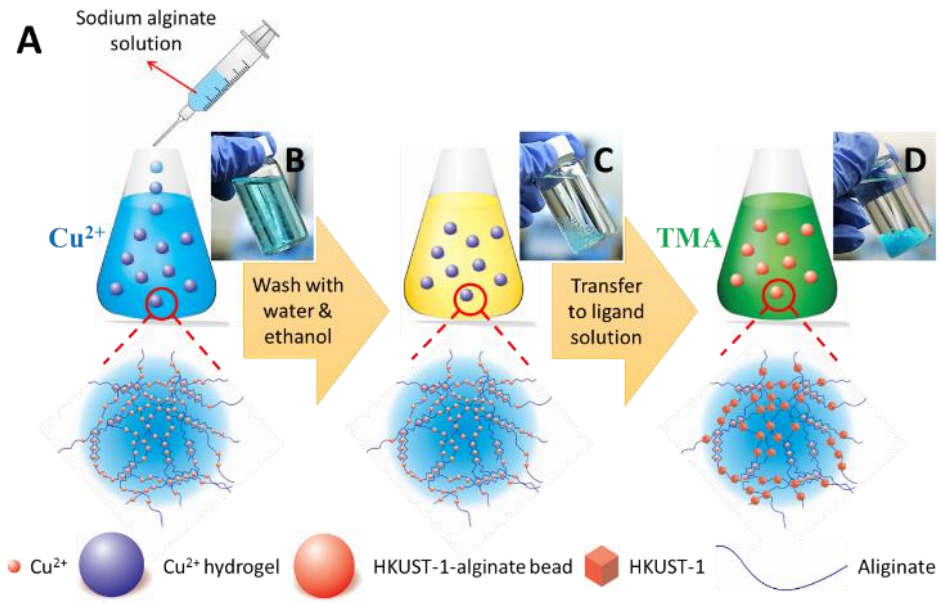

Figure 7-1. (A) Schematic of the preparation of MOF-alginate composite. Photographs of (B) alginate hydrogels cross-linked by Cu^{2+} right after the addition of sodium alginate aqueous solution into Cu^{2+} aqueous solution, (C) alginate hydrogels cross-linked by Cu^{2+} after washed with water and ethanol, and (D) HKUST-1-alginate hydrogels.

The ultrafast cross-linking between metal ion and alginate assisted in control over the macroscopic shape of the hydrogel. The shape was then inherited by the MOF-alginate composite after treated with the ligand solution (Supporting Information Figure S7-2). A spherical bead composite was achieved by adding the alginate aqueous solution dropwisely into the metal ion aqueous solution, as demonstrated above (Supporting Information Figure

S7-2A). A fiber-like composite was obtained by continuously injecting the alginate aqueous solution in syringe into metal ion aqueous solution (Supporting Information Figure S7-2B). A membrane shape composite was realized by drop casting the alginate aqueous solution on top of a glass slide, which was then carefully immersed into metal ion aqueous solution (Supporting Information Figure S7-2C). These macroscopic-shape-designable MOF-alginate composites have high potential in paving the way of processing MOF particles for real industrial applications.

The morphology was investigated by scanning electron microscopy (SEM) with the fiber-like Cu^{2+} cross-linked hydrogel and its corresponding HKUST-1-alginate composite. The fibers were obtained by directly drying the prepared samples under 80 ^{o}C. Wrinkles were seen on surface of the dried Cu^{2+} cross-linked hydrogel due to shrinkage upon drying (Figure 7-2E). A mesoporous structure was evident both on the surface and inside the dried hydrogel (Figure 7-2E & 7-2F). The HKUST-1-alginate composite showed a surface (Figure 7-2A & 7-2D) and internal (Figure 7-2B & 7-2C) porous structure similar to the hydrogel. The composite also contained a large amount of octahedral HKUST-1 particles well distributed and embedded in (Figure 7-2B & 7-2C), as well as on top of the surface (Figure 7-2D). HKUST-1 loading of the fiber-like composite was 23.8 ± 1.3 wt.% determined by thermogravimetric analysis (TGA) (Figure S7-3 & Table S7-1), suggesting about 58% copper inside the hydrogel converted into HKUST-1 particles. The theoretical maximum of HKUST-1 loading is 36.6 wt.% if all of Cu^{2+} converted into MOF particles.

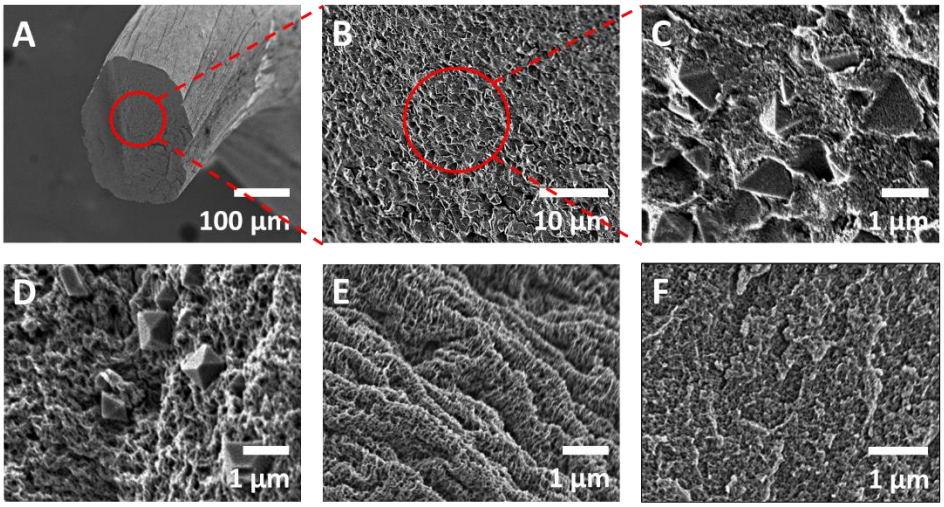

Figure 7-2. SEM images of the dried Cu^{2+} cross-linked hydrogel and the corresponding HKUST-1-alginate composite. (A, B, C) Cross-section of the HKUST-1-alginate composite with different magnification. (D) Surface of the HKUST-1-alginate composite. (E) Surface of the Cu^{2+} cross-linked hydrogel. (F) Cross-section of the Cu^{2+} cross-linked hydrogel.

We then hypothesized that various MOF-alginate composites can be prepared with this protocol under appropriate MOF synthetic conditions, because alginate is cross-linkable by different metal ions. Herein, we prepared four different MOF-alginate composites, including HKUST-1-alginate, zeolitic imidazolate framework-8(ZIF-8)-alginate, Material Institute de Lavoisier-100(Fe)(MIL-100(Fe))-alginate, and zeolitic imidazolate framework-67(ZIF-67)-alginate composite, based on corresponding Cu^{2+}, Zn^{2+}, Fe^{3+}, and Co^{2+} cross-linked hydrogels, respectively (Figure 7-3). The formation of different MOFs within the alginate matrix was confirmed by PXRD (Figure S7-1). All composites had similar morphologies. MOF particles could be seen on the surface, as well as inside the alginate matrix, as revealed by SEM characterization (Figure 7-3 & Figure S7-4-S7-6).

This proves the robustness and versatility of this method in preparation of different MOF based alginate composites, which could be potentially used in different applications.

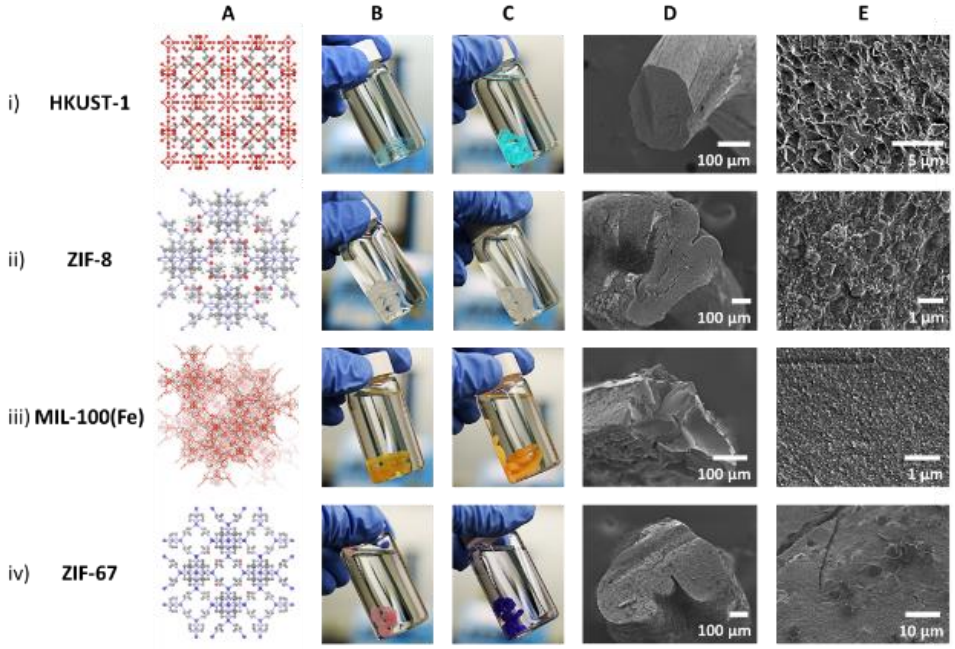

Figure 7-3. (i) HKUST-1-alginate composite. (ii) ZIF-8-alginate composite. (iii) MIL-100(Fe)-alginate composite. (iv) ZIF-67-alginate composite. (A) MOF structure. (B) Photographs of the fiber-like metal-ion cross-linked hydrogel. (C) Photographs of the corresponding MOF-alginate composite. (D, E) SEM images of the MOF-alginate composite. All fibers were prepared with 1 mL sodium alginate solution.

The mechanism involved in the formation of MOF-alginate composites was proposed based on the energy-dispersive X-ray spectroscopy characterization (EDX). EDX elemental maps of the cross-section of the HKUST-1- and ZIF-67-alginate composites showed distinct element distributions (Figure 7-4). Carbon, oxygen, and copper were uniformly distributed within the selected area. There were no sodium and nitrogen found in the case of HKUST-1-alginate composite (Figure 7-4A). However, in the case of ZIF-67-alginate composite, only carbon was uniform. Oxygen and sodium, nitrogen and cobalt

were consistent with each other, respectively. The distributions of oxygen and sodium were exclusive from those of nitrogen and cobalt (Figure 7-4B). This difference between copper- and cobalt-based MOF-alginate composite provided some insight into the formation mechanism.

Alginate is a copolymer composed of G blocks, GM alternative blocks, and M blocks, among which only G blocks are believed to participate the gel formation, which forms an "egg-box" structure (Figure 7-4F).[52] Hence, the ionic bindings between free GM and M blocks with metal ions provide good sources for MOF growth. However, the degree of affinity between divalent metal ion and alginate decreases as Pb > Cu > Cd> Ba > Sr > Ca > Co, Ni, Zn > Mn.[53,57] Therefore, all sodium ions were replaced by copper but were not by cobalt in preparation of the hydrogels. Thus, no sodium was found in the HKUST-1-alginate, while abundant in the ZIF-67-alginate. This indicated that cobalt cross-linked only with G blocks, but did not bind with GM and M blocks as copper did, due to its low degree of affinity. During the formation of HKUST-1 particles, the copper ions bound with GM and M blocks could easily react with TMA ligand and formed the MOF particles (Figure 7-4D). In the case of ZIF-67 as comparison, only the cross-linked cobalt could serve as metal source for the MOF growth, thus the cross-linking points were broken during the formation of ZIF-67 particles (Figure 7-4E). However, due to the insolubility of alginate in alcohol, the structure of ZIF-67-alginate was preserved.

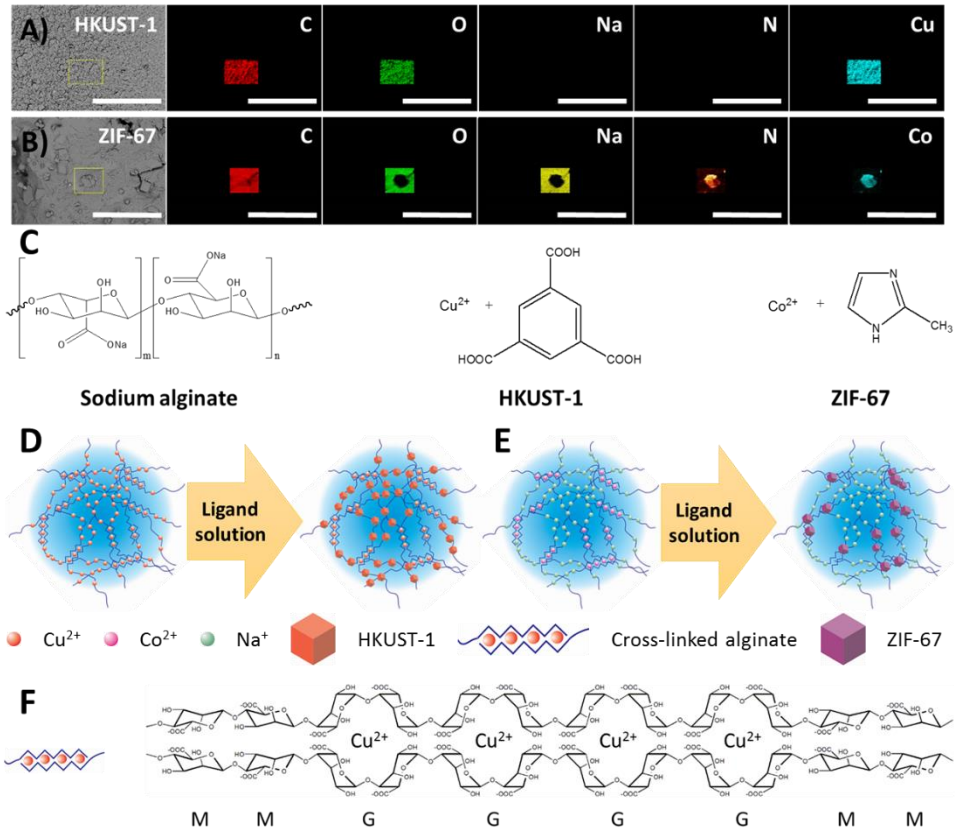

Figure 7-4. Cross-section back-scattered electron images of (A) HKUST-1- and (B) ZIF-67-alginate composites and their corresponding EDX elemental maps (Scale bar 60 μm). (C) Chemical composition of sodium alginate, HKUST-1, and ZIF-67. Schematic of the formation of (D) HKUST-1-alginate composite, (E) ZIF-67-alginate composite, and (F) "egg-box" model of metal ion cross-linked alginate.

In order to support this hypothesis, HKUST-1 and ZIF-67 based alginate composites were immersed in water, respectively. The former remained its structure, while the latter was completely disassembled within an hour, due to the breaking of cross-linking points. The ZIF-8-alginate composite was disassembled in water as well, because the degree of affinity of zinc towards alginate is the same as cobalt. However, MIL-100-alginate composite remained its structure in water. Their EDX analyses showed similar results:

MIL-100-alginate did not contain any sodium, while ZIF-8-alginate contained a lot (Figure S7-7). It should be noted that the EDX maps of ZIF-8-alginate showed a homogeneous distribution of all elements, which is different from those of ZIF-67-alginate, due to the smaller crystal size of ZIF-8. This experiment confirmed that the growth of ZIF-67 particles was only associated with the cross-linked cobalt ions. The cross-linking points were broken in order to support the ZIF-67 growth. In contrast, the copper ions loosely bound with GM and M blocks could serve as metal source for HKUST-1 growth, resulting in the formation of HKUST-1-alginate composite. This composite maintained its structure when immersed in aqueous solution, which was due to retention of the cross-linking points.

Interestingly, we also found that these two types of composites possessed totally different surface areas. HKUST-1- and MIL-100-alginate, which remained cross-linked, showed low surface area, while ZIF-8- and ZIF-67-alginate showed high surface areas (ZIF-8: 563 $m^2 g^{-1}$, ZIF-67: 317 $m^2 g^{-1}$) (Table S7-2 and Figure S7-8). Our hypothesis is that, due to the retention of cross-linking points, the growth of HKUST-1 and MIL-100 crystal was confined within limited spaces, leading to the interpenetration of alginate chains into MOF pores, and thus reducing the accessible surface area. This could impose some limitations to potential applications, which require high surface areas. In the case of ZIF-8 and ZIF-67, the crystals could squeeze in between alginate chains due to the loss of cross-linking points, resulting in less or none interpenetration of alginate chains.

Finally, the prepared MOF-alginate composite was employed as absorbent for the removal of dye from contaminated water, which can be handled easily due to the confinement of MOFs within the composite. The purpose was to demonstrate potential uses

of such composites. MIL-100(Fe)-alginate composite was prepared from 0.5 mL sodium alginate solution and it was immersed into 10 mL 0.01 mM Rhodamine B aqueous solution. After 5 days of soaking, the solution became colorless while the MIL-100(Fe)-alginate composite became crimson (Figure 7-5). On the contrast, the corresponding Fe^{3+} cross-linked hydrogel showed little absorption (Figure 7-5), suggesting that the dye adsorption behavior was solely associated with MIL-100(Fe).

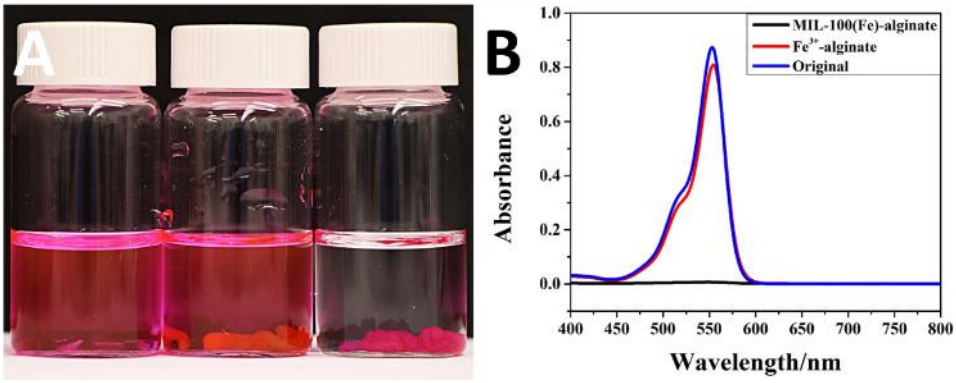

Figure 7-5. (A) Photographs of 0.01 mM Rhodamine B aqueous solution, 0.01 mM Rhodamine B aqueous solution after 5 days soaking with Fe^{3+} cross-linked hydrogel, and 0.01 mM Rhodamine B aqueous solution after 5 days soaking with MIL-100(Fe)-alginate composite (from left to right). (B) UV-Vis spectrums of the aforementioned aqueous solutions.

7.5 Conclusion

In conclusion, we have demonstrated a novel method to incorporate MOF particles into alginate substrates. The metal ion cross-linked alginate hydrogels provided excellent templates for *in-situ* MOF growth, and the shapes of hydrogels were readily inherited by their corresponding MOF-alginate composites. MOF particles were well distributed and embedded inside, as well as decorated on surfaces of the composites. Four different types

of MOF-alginate composites based on different metal ions were obtained, highlighting the robustness and versatility of this processing method. The mechanistic study revealed that the alginate hydrogels prepared with high affinity metal ions (Cu^{2+} for example) could be converted into MOF-alginate composites through coordination between ligand molecules and metal ions loosely bound with alginate GM and M blocks, while the G blocks remained cross-linked. However, a large amount of sodium ions bound with GM and M blocks remained in the alginate hydrogels prepared with low affinity metal ions (Co^{2+} for example). The cross-linked metal ions had to serve as metal source for the MOF growth, leading to disassembly of the obtained composites upon exposure to an aqueous solution because of loss of cross-linking points. Finally, it was demonstrated that the prepared composites were effective as an absorbent in treating dye contaminated water. This simple method greatly facilitates preparation of MOF materials into various shapes and morphologies, which really combines application property of MOF material with processability of polymers.

7.6 Acknowledgement

We sincerely thank the Natural Sciences and Engineering Research Council (NSERC) of Canada and the Canada Research Chair (CRC) program of the Federal Government for supporting this research work.

7.7 References

[1] O. K. Farha, I. Eryazici, N. C. Jeong, B. G. Hauser, C. E. Wilmer, A. A. Sarjeant, R. Q. Snurr, S. T. Nguyen, A. O. z. r. Yazaydın, J. T. Hupp, *Journal of the American Chemical Society* **2012**, *134*, 15016-15021.

[2] I. Senkovska, S. Kaskel, *Chemical Communications* **2014**, *50*, 7089-7098.

[3] A. R. Millward, O. M. Yaghi, *Journal of the American Chemical Society* **2005**, *127*, 17998-17999.

[4] D. Alezi, Y. Belmabkhout, M. Suyetin, P. M. Bhatt, Ł. J. Weseliński, V. Solovyeva, K. Adil, I. Spanopoulos, P. N. Trikalitis, A.-H. Emwas, *Journal of the American Chemical Society* **2015**, *137*, 13308-13318.

[5] Y. Peng, Y. Li, Y. Ban, H. Jin, W. Jiao, X. Liu, W. Yang, *Science* **2014**, *346*, 1356-1359.

[6] Y. Hu, J. Wei, Y. Liang, H. Zhang, X. Zhang, W. Shen, H. Wang, *Angewandte Chemie International Edition* **2015**, 55, 2048-2052.

[7] J. Liu, F. Sun, F. Zhang, Z. Wang, R. Zhang, C. Wang, S. Qiu, *Journal of Materials Chemistry* **2011**, *21*, 3775-3778.

[8] M. Tu, S. Wannapaiboon, K. Khaletskaya, R. A. Fischer, *Advanced Functional Materials* **2015**, *25*, 4470-4479.

[9] Y. Fu, D. Sun, Y. Chen, R. Huang, Z. Ding, X. Fu, Z. Li, *Angewandte Chemie* **2012**, *124*, 3420-3423.

[10] J. E. Mondloch, M. J. Katz, W. C. Isley III, P. Ghosh, P. Liao, W. Bury, G. W. Wagner, M. G. Hall, J. B. DeCoste, G. W. Peterson, *Nature materials* **2015**, *14*, 512-516.

[11] G. K. Shimizu, J. M. Taylor, S. Kim, *Science* **2013**, *341*, 354-355.

[12] J. M. Taylor, K. W. Dawson, G. K. Shimizu, *Journal of the American Chemical Society* **2013**, *135*, 1193-1196.

[13] P. Qi, Y. Han, J. Zhou, X. Fu, S. Li, J. Zhao, L. Wang, X. Fan, X. Feng, B. Wang, *Chemical Communications* **2015**, *51*, 12391-12394.

[14] Z. Wang, B. Wang, Y. Yang, Y. Cui, Z. Wang, B. Chen, G. Qian, *ACS applied materials & interfaces* **2015**, *7*, 20999-21004.

[15] P. Horcajada, T. Chalati, C. Serre, B. Gillet, C. Sebrie, T. Baati, J. F. Eubank, D. Heurtaux, P. Clayette, C. Kreuz, *Nature materials* **2010**, *9*, 172-178.

[16] C. Orellana-Tavra, E. F. Baxter, T. Tian, T. D. Bennett, N. K. Slater, A. K. Cheetham, D. Fairen-Jimenez, *Chemical Communications* **2015**, *51*, 13878-13881.

[17] B. Chen, C. Liang, J. Yang, D. S. Contreras, Y. L. Clancy, E. B. Lobkovsky, O. M. Yaghi, S. Dai, *Angewandte Chemie International Edition* **2006**, *45*, 1390-1393.

[18] B. Chen, L. Wang, F. Zapata, G. Qian, E. B. Lobkovsky, *Journal of the American Chemical Society* **2008**, *130*, 6718-6719.

[19] M. Kim, J. F. Cahill, Y. Su, K. A. Prather, S. M. Cohen, *Chemical Science* **2012**, *3*, 126-130.

[20] H. Liu, H. Zhu, S. Zhu, *Macromolecular Materials and Engineering* **2015**, *300*, 191-197.

[21] J. Huo, M. Marcello, A. Garai, D. Bradshaw, *Advanced Materials* **2013**, *25*, 2717-2722.

[22] H. Zhu, Q. Zhang, S. Zhu, *Dalton Transactions* **2015**, *44*, 16752-16757.

[23] N. Yanai, M. Sindoro, J. Yan, S. Granick, *Journal of the American Chemical Society* **2012**, *135*, 34-37.

[24] O. Shekhah, H. Wang, S. Kowarik, F. Schreiber, M. Paulus, M. Tolan, C. Sternemann, F. Evers, D. Zacher, R. A. Fischer, *Journal of the American Chemical Society* **2007**, *129*, 15118-15119.

[25]M. Tsotsalas, A. Umemura, F. Kim, Y. Sakata, J. Reboul, S. Kitagawa, S. Furukawa, *Journal of Materials Chemistry* **2012**, *22*, 10159-10165.

[26] H. Zhu, H. Liu, I. Zhitomirsky, S. Zhu, *Materials Letters* **2015**, *142*, 19-22.

[27] H. Zhu, S. Zhu, *The Canadian Journal of Chemical Engineering* **2015**, *93*, 63-67.

[28] J. Reboul, S. Furukawa, N. Horike, M. Tsotsalas, K. Hirai, H. Uehara, M. Kondo, N. Louvain, O. Sakata, S. Kitagawa, *Nature materials* **2012**, *11*, 717-723.

[29] Y. Mao, J. Li, W. Cao, Y. Ying, L. Sun, X. Peng, *ACS applied materials & interfaces* **2014**, *6*, 4473-4479.

[30] A. J. Brown, N. A. Brunelli, K. Eum, F. Rashidi, J. Johnson, W. J. Koros, C. W. Jones, S. Nair, *Science* **2014**, *345*, 72-75.

[31] G. Xu, J. Yao, K. Wang, L. He, P. A. Webley, C.-s. Chen, H. Wang, *Journal of Membrane Science* **2011**, *385*, 187-193.

[32] M. He, J. Yao, Z.-X. Low, D. Yu, Y. Feng, H. Wang, *RSC Advances* **2014**, *4*, 7634-7639.

[33] D. Bradshaw, A. Garai, J. Huo, *Chemical Society Reviews* **2012**, *41*, 2344-2381.

[34] S. Qiu, M. Xue, G. Zhu, *Chemical Society Reviews* **2014**, *43*, 6116-6140.

[35] S. Basu, A. Cano-Odena, I. F. Vankelecom, *Journal of Membrane Science* **2010**, *362*, 478-487.

[36] T. Rodenas, M. van Dalen, E. García‐Pérez, P. Serra‐Crespo, B. Zornoza, F. Kapteijn, J. Gascon, *Advanced Functional Materials* **2014**, *24*, 249-256.

[37] T. Rodenas, I. Luz, G. Prieto, B. Seoane, H. Miro, A. Corma, F. Kapteijn, F. X. L. i Xamena, J. Gascon, *Nature materials* **2015**, *14*, 48-55.

[38] S. Hwang, W. S. Chi, S. J. Lee, S. H. Im, J. H. Kim, J. Kim, *Journal of Membrane Science* **2015**, *480*, 11-19.

[39] A. Sabetghadam, B. Seoane, D. Keskin, N. Duim, T. Rodenas, S. Shahid, S. Sorribas, C. L. Guillouzer, G. Clet, C. Tellez, M. Daturi, J. Coronas, F. Kapteijn, J. Gascon, *Advanced Functional Materials* **2016**, 26, 3154-3163.

[40] M. Rose, B. Böhringer, M. Jolly, R. Fischer, S. Kaskel, *Advanced Engineering Materials* **2011**, *13*, 356-360.

[41] Y.-n. Wu, F. Li, H. Liu, W. Zhu, M. Teng, Y. Jiang, W. Li, D. Xu, D. He, P. Hannam, G. Li, *Journal of Materials Chemistry* **2012**, *22*, 16971-16978.

[42] T. Yang, Y. Xiao, T.-S. Chung, *Energy & Environmental Science* **2011**, *4*, 4171-4180.

[43] Z. Kang, Y. Peng, Z. Hu, Y. Qian, C. Chi, L. Y. Yeo, L. Tee, D. Zhao, *Journal of Materials Chemistry A* **2015**, *3*, 20801-20810.

[44] K. Díaz, M. López-González, L. F. del Castillo, E. Riande, *Journal of Membrane Science* **2011**, *383*, 206-213.

[45] N. C. Su, D. T. Sun, C. M. Beavers, D. K. Britt, W. L. Queen, J. J. Urban, *Energy & Environmental Science* **2016**, 9, 922-931.

[46] L. Hao, P. Li, T. Yang, T.-S. Chung, *Journal of Membrane Science* **2013**, *436*, 221-231.

[47] M. S. Denny, S. M. Cohen, *Angewandte Chemie International Edition* **2015**, *54*, 9029-9032.

[48] J. B. DeCoste, M. S. Denny Jr, G. W. Peterson, J. J. Mahle, S. M. Cohen, *Chemical Science* **2016**, 7, 2711-2716.

[49] S. Kovačič, M. Mazaj, M. Ješelnik, D. Pahovnik, E. Žagar, C. Slugovc, N. Z. Logar, *Macromolecular rapid communications* **2015**, *36*, 1605-1611.

[50] A. Knebel, S. Friebe, N. C. Bigall, M. Benzaqui, C. Serre, J. Caro, *ACS applied materials & interfaces* **2016**, 8, 7536-7544.

[51] A. Martinsen, G. Skjåk‐Bræk, O. Smidsrød, *Biotechnology and bioengineering* **1989**, *33*, 79-89.

[52] K. Y. Lee, D. J. Mooney, *Progress in polymer science* **2012**, *37*, 106-126.

[53] J.-Y. Leong, W.-H. Lam, K.-W. Ho, W.-P. Voo, M. F.-X. Lee, H.-P. Lim, S.-L. Lim, B.-T. Tey, D. Poncelet, E.-S. Chan, *Particuology* **2015**, 24, 44-60.

[54] J.-Y. Sun, X. Zhao, W. R. Illeperuma, O. Chaudhuri, K. H. Oh, D. J. Mooney, J. J. Vlassak, Z. Suo, *Nature* **2012**, *489*, 133-136.

[55] C. H. Yang, M. X. Wang, H. Haider, J. H. Yang, J.-Y. Sun, Y. M. Chen, J. Zhou, Z. Suo, *ACS applied materials & interfaces* **2013**, *5*, 10418-10422.

[56] G. Du, F. Wu, Y. Cong, L. Nie, S. Liu, G. Gao, J. Fu, *Chemical Communications* **2015**, *51*, 15534-15537.

[57] Ý. A. Mørch, I. Donati, B. L. Strand, G. Skjåk-Bræk, *Biomacromolecules* **2006**, *7*, 1471-1480.

7.8 Supporting information

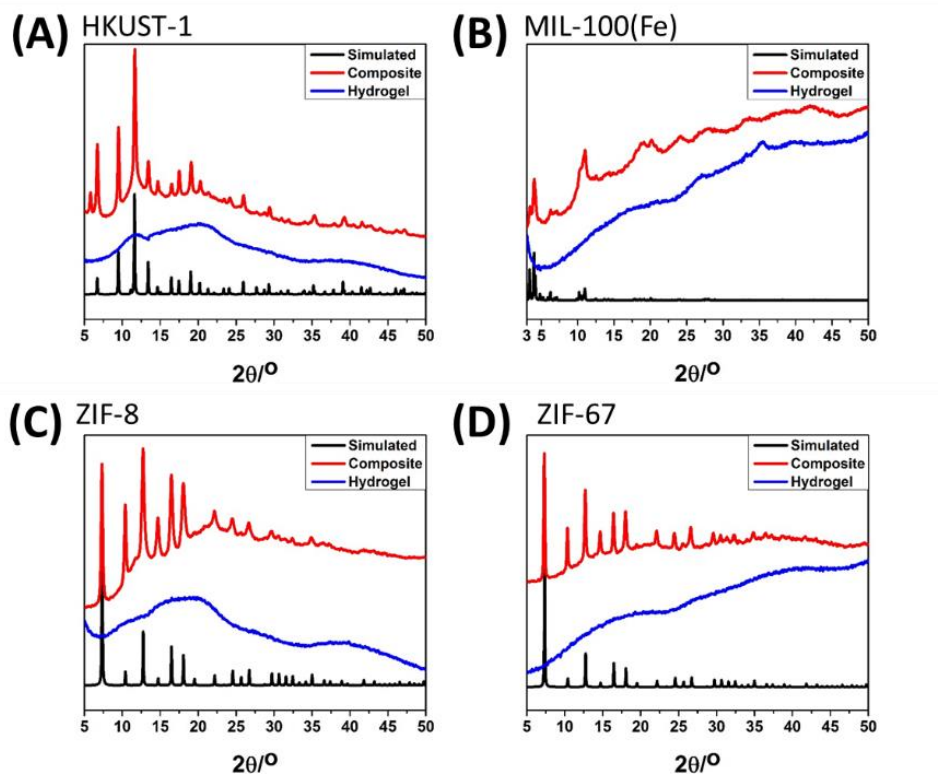

Figure S7-1. PXRD pattern of simulated MOF, metal cross-linked hydrogel, and MOF-alginate composite.

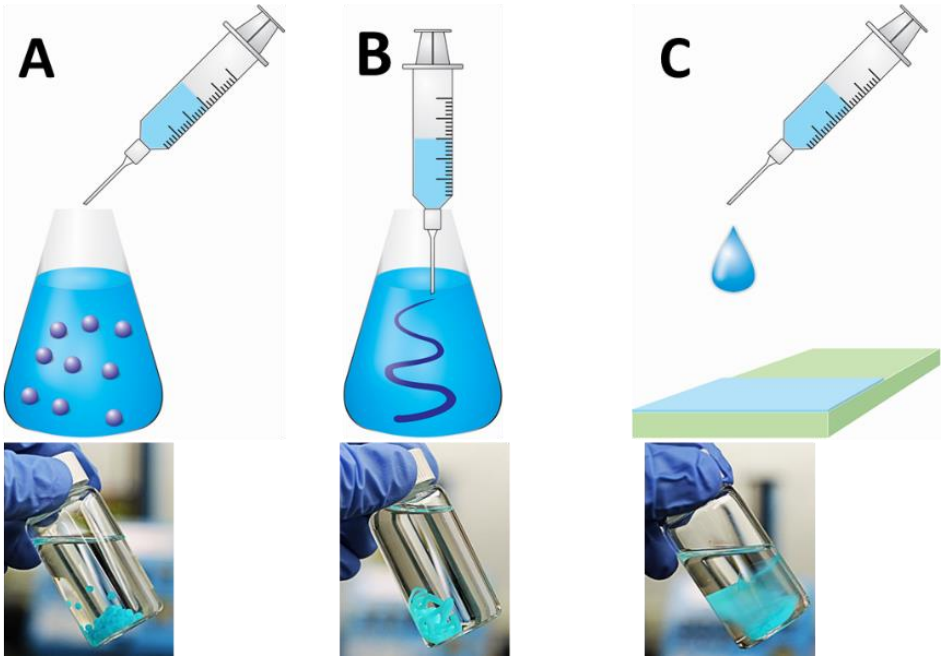

Figure S7-2. Schematics and photographs of the Cu^{2+} cross-linked hydrogel with different shapes and its corresponding HKUST-1-alginate composite. (A) Bead-like. (B) Fiber-like. (C) Membrane-like.

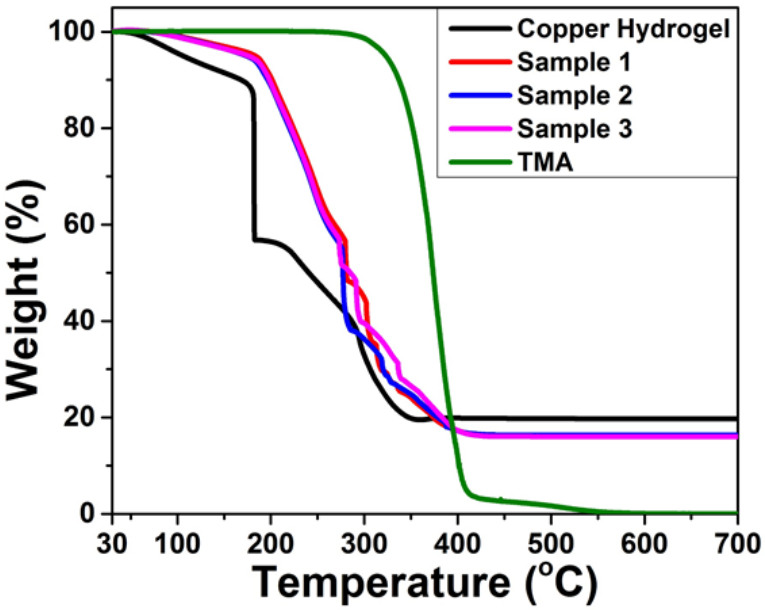

Figure S7-3. TGA traces of copper cross-linked hydrogel, HKUST-1-alginate composites, and trimesic acid (TMA).

Table S7-1. Measured weight percentage of HKUST-1 in the HKUST-1-alginate composites as determined by TGA.

	Ash content	HKUST-1 content a
Sample 1	15.99%	25.23%
Sample 2	16.33%	22.65%
Sample 3	16.20%	23.64%

Ash content of Cu^{2+} cross-linked alginate hydrogel and TMA powder are 19.32% and 0% after TGA testing. [a] The content of TMA within the composite after preparation was determined first, and then HKUST-1 content was estimated based on the TMA content and its molecular formula.

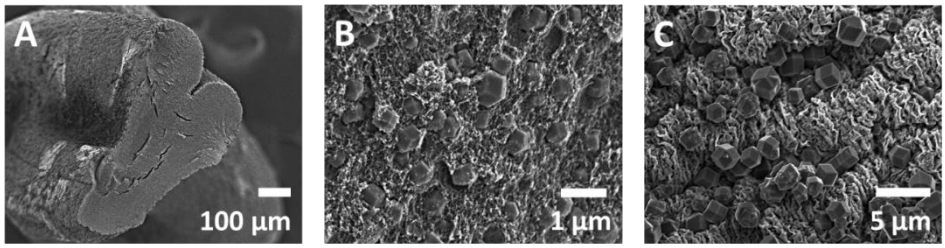

Figure S7-4. SEM images of ZIF-8-alginate composites. A) Overall view of the fiber-like composite. B) Cross-section of the fiber-like composite. C) Surface of the fiber-like composite.

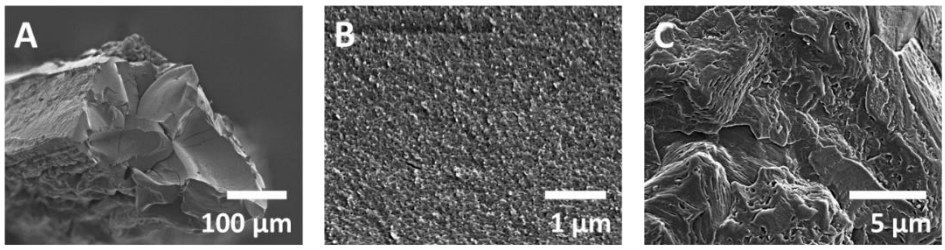

Figure S7-5. SEM images of MIL-100-alginate composites. A) Overall view of the fiber-like composite. B) Cross-section of the fiber-like composite. C) Surface of the fiber-like composite.

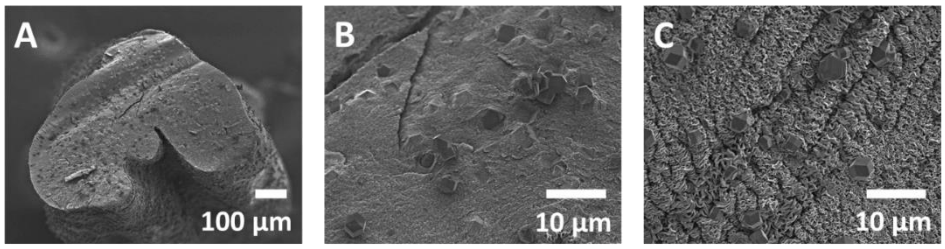

Figure S7-6. SEM images of ZIF-67-alginate composites. A) Overall view of the fiber-like composite. B) Cross-section of the fiber-like composite. C) Surface of the fiber-like composite.

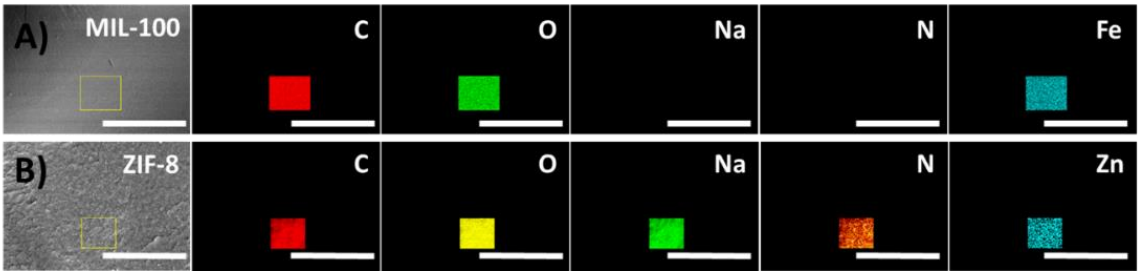

Figure S7-7. Cross-section back-scattered electron images of (A) MIL100- and (B) ZIF-8-alginate composites and their corresponding EDX elemental maps (Scale bar 60 μm).

Table S7-2. BET surface areas of MOF-alginate composites.

	HKUST-1	MIL-100[a]	ZIF-8	ZIF-67
BET surface Area (m^2 g^{-1})	19	N/A	563	317

[a] The surface area of MIL-100 was too low to be detected accurately.

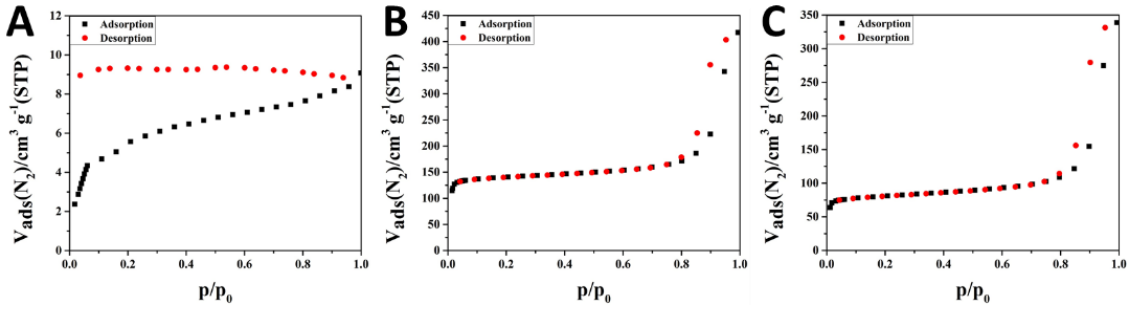

Figure S7-8. Nitrogen isotherms of A) HKUST-1-, B) ZIF-8-, and C) ZIF-67-alginate composites.

8 MAJOR CONTRIBUTIONS AND RECOMMENDATIONS FOR FUTURE WORK

In this chapter, the major contributions made in this doctoral study are summarized. Some recommendations on possible future research directions are also offered, based on the accumulated knowledge and experience.

8.1 Major contributions

The theme of this study was to use MOF particles as building blocks to construct complex architectures. Four top-down and one bottom-up methods were developed to prepare 0D and 3D MOF architectures. The major achievements are as follows:

- ZIF-8 nanocrystals were found to be a good stabilizer for the dispersion polymerization of PS. PVP was crucial in bridging ZIF-8 and PS particle together. The prepared raspberry-like structure could be further developed into PS@ZIF-8 core-shell structure.

- UiO-66 nanocrystals were found to be able to assemble into multilayer colloidosomes through a transient Pickering emulsion technique. The obtained MOFsomes could encapsulate dye molecules and release the encapsulated molecules under alkaline conditions due to the decomposition of UiO-66. It was also found the UiO-66 based MOFsomes could be used as a general platform to prepare multicomponent colloidosomes.

- UiO-66 nanocrystals were found to be able to stabilize oil-in-water high internal phase emulsions with internal oil volume phase up to 90%. Two different kinds of free-standing hierarchical porous monoliths were obtained from the UiO-66 stabilized Pickering HIPE. The obtained 3D UiO-66 monoliths showed ultralow densities (as low as 12 mg mL^{-1}), which were able to stand on a dandelion flower.

- UiO-66, ZIF-8, and MIL-100(Fe) were found to be able to assemble into 3D flexible porous aerogels assisted by CNCs and CMCs. The hybrid aerogels were prepared through a straightforward sol-gel process, followed by freeze-drying. The combination of MOFs, cross-linked clusters, and freeze drying, yielded hybrid aerogels with hierarchical pores that remained intact under compression. MOF loading could be controlled by varying the initial ratio of different components. MOFs retained their crystallinity, porosity and accessibility in the aerogel format, making them ideal absorbents for water purification and other separations applications.

- HKUST-1, ZIF-8, MIL-100(Fe), and ZIF-67 could be incorporated into alginate hydrogels through an *in-situ* growth approach. The metal ion cross-linked alginate hydrogels provided a general and shapeable platform for MOF growth. Various shaped MOF-alginate composites were prepared by manipulating the corresponding metal ion cross-linked alginate hydrogels. The obtained composite was demonstrated to be an effective absorbent for water purification.

8.2 Recommendations for future work

In this study, we explored five different processing methods in order to construct MOF complex architectures. We primarily emphasized on the processing strategies rather than potential applications. The continuous work in this area could be directed into: 1) development of new approaches to assemble MOFs, and 2) assessment of potential applications of these obtained complex architectures.

8.2.1 Development of new approaches to assemble MOFs

This thesis focused on the development of strategies to constructing 0D and 3D MOF architectures, while the preparation of 1D and 2D MOF architectures is also of great importance. Generally, the top-down methods are far less explored than the bottom-up methods, which is due to the more difficult manipulation of pre-synthesized MOF particles than that of MOF precursor solutions. However, the development of top-down methods is rather significant, especially when it comes to the cases when harsh conditions are required in preparing MOF particles, where bottom-up methods are not applicable. Future work should focus on developing strategies to assemble MOFs in a more general way, that is to say, one strategy can be used to assemble different MOFs or one strategy can be applied to assemble MOFs into different architectures.

8.2.2 Applications of complex architectures

The porous structures, the abundant choices of metal ion and organic ligand, and the designable functionalities give MOFs various properties, which can be exploited in different applications. Construction of MOFs into materials with different dimensions can introduce new properties in addition to the inherent features of MOFs. For example, 0D

MOF hollow spheres can be used as carrier to deliver different molecules, or can be used as size-selective shell to protect encapsulated catalysts. 1D MOF arrays may find applications in photonics, optoelectronics, magnetic devices, sensing and biotechnology. 2D MOF membranes and films are excellent candidates for separation and sensing devices. 3D MOF monoliths have advantages in fast diffusion, which can be applied in adsorption and catalysis. Therefore, future works should also focus on evaluation of the prepared MOF complex architectures in different applications.